AB INITIO STUDY OF INTERFACE STATES AT METAL CONTACTS TO III-V SEMICONDUCTORS

THÈSE N^{O} 2890 (2003)

PRÉSENTÉE À LA FACULTÉ SCIENCES DE BASE

Institut de théorie des phénomènes physiques

SECTION DE PHYSIQUE

ÉCOLE POLYTECHNIQUE FÉDÉRALE DE LAUSANNE

POUR L'OBTENTION DU GRADE DE DOCTEUR ÈS SCIENCES

PAR

Thomas MAXISCH

Diplom-Physiker, Philipps-Universität, Marburg, Allemagne
et de nationalité allemande

acceptée sur proposition du jury:

Prof. A. Baldereschi, directeur de thèse
Prof. H. Beck, rapporteur
Prof. H. Brune, rapporteur
Prof. S. Massidda, rapporteur

Lausanne, EPFL
2003

Version abrégée

Nous présentons une étude théorique des caractéristiques physiques des jonctions métal/semi-conducteur. En utilisant des méthodes de calcul *ab initio* basées sur les pseudo-potentiels atomiques, nous avons étudié la structure des états électroniques dont les énergies se situent dans la bande interdite pour un choix représentatif de semi-conducteurs III-V présentant des interfaces abruptes et sans défauts, ainsi qu' une couche terminale formée d'anions. Nous nous sommes notamment concentrés sur les interfaces de l'Al avec GaAs(001), AlAs(001) et GaN(001) dans sa phase cubique, de même que sur les interfaces de Al, Au et Cu avec GaN(001).

Des progrès récents, concernant les barrières de Schottky, mettent l'accent sur des relations possibles entre les états d'interface et la formation de ces barrières. Notre objectif est de cerner les mécanismes responsables, à l'échelle atomique, de la nature des états d'interface aussi bien que du rôle qu'ils jouent dans les processus de formation des barrières de Schottky.

Pour les jonctions Al/GaAs(001) et Al/AlAs(001) avec des couches terminales de As, des états d'interface résonnants et localisés apparaissent au point **J** de la zone de Brillouin bidimensionnelle de l'interface. Ces états possèdent des énergies voisines du niveau de Fermi, dans la bande interdite du semi-conducteur. Ils correspondent à des liaisons intermétalliques entre les cations les plus extérieurs du semi-conducteur et les atomes du métal proche de l'interface. Ces états proviennent d'une interaction entre des états de surface d'Al(001) et les états de conduction du semi-conducteur par l'intermédiaire d'états localisés à la surface (001) non reconstruite du semi-conducteur. Nos résultats indiquent que ces états d'interface peuvent jouer un rôle important dans les propriétés de transport des jonctions métal/$Al_xGa_{1-x}As$.

Nous avons aussi examiné la structure électronique des jonctions entre Al, Au et Cu et GaN(001) cubique de couche terminale N. L'état localisé d'interface dans le cas des jonctions Al/$Al_xGa_{1-x}As$ apparaît également pour les interfaces métal/GaN à condition que les atomes du métal qui sont près de l'interface soient situés en face des cations les plus extérieurs du semi-conducteur. Cela indique que le mécanisme de formation de ces états est très général. Contrairement aux jonctions Al/$Al_xGa_{1-x}As$, ces états apparaissent à des énergies bien supérieures à E_F pour les contacts métal/GaN. Ainsi, on ne s'attend pas à ce qu'ils contribuent de manière significative au transport électronique au travers de l'interface. Néanmoins, plusieurs états d'interface associés aux orbitales d apparaissent dans un vaste domaine d'énergie, incluant E_F, aux jonctions entre des métaux nobles et GaN.

Zusammenfassung

Wir stellen hier eine theoretische Studie der physikalischen Eigenschaften von Metall-Halbleiter Kontakten vor. Unter dem Einsatz selbstkonsistenter *ab initio* Pseudopotentialrechnungen untersuchen wir die Struktur elektronischer Zustände mit einer Energie innerhalb der optischen Bandlücke von Halbleitern an einer repräsentativen Auswahl idealer, abrupter, defektfreier Grenzflächen zwischen Metallen und anionisch begrenzten Halbleitern. Dabei konzentrieren wir uns insbesondere sowohl auf Al Kontakte zu GaAs(001), AlAs(001) und kubischem GaN(001) als auch auf Übergänge zwischen Al, Au und Cu zu kubischem GaN(001).

Neuere Entwicklungen auf dem Gebiet der Schottky-Barrieren betonen den möglichen Zusammenhang zwischen Grenzflächenzuständen und der Entstehung der Schottky-Barriere. Unser Ziel ist es, die Mechanismen, welche für die Ausbildung von Grenzflächenzuständen verantwortlich sind, auf atomarer Ebene zu verstehen und deren Rolle beim Enstehungsprozess der Schottky-Barriere zu erörtern.

Inmitten der Halbleiterbandlücke As-terminierter Al/GaAs- und Al/AlAs(001)-Übergänge treten am **J**-Punkt der zweidimensionalen Brillouin-Zone und nahe der Fermi-Energie sowohl resonante als auch lokalisierte Grenzflächenzustände auf. Sie entsprechen intermetallischen Bindungen zwischen dem äußersten Kation des Halbleiters und dem Grenzflächenatom des Metalls. Diese Zustände resultieren aus einer Wechselwirkung zwischen lokalisierten Zuständen der Al(001)-Oberfläche und Zuständen des Halbleiterleitungsbandes unter Einwirkung lokalisierter Zustände der nichtrekonstruierten, As-terminierten (001)-Halbleiteroberfläche. Unsere Ergebnisse deuten darauf hin, dass Grenzflächenzustände vom Typ einer intermetallischen Bindung eine wichtige Rolle innerhalb der Transporteigenschaften vom Metall-$Al_xGa_{1-x}As$-Übergängen einnehmen.

Wir haben weiterhin die elektronischen Eigenschaften an Al-, Au- und Cu-Kontakten zu kubischem, N-terminiertem GaN(001) untersucht. Die bereits für As–terminierte Al/GaAs(001)- und Al/AlAs(001)-Übergänge dokumentierten lokalisierten Grenzflächenzustände treten unter der Bedingung, dass sich die Metallatome an der Grenzfläche gegenüber des äußersten Halbleiterkations befinden, ebenfalls an Metall-GaN(001)-Übergängen auf. Dies deutet darauf hin, dass der Entstehungsprozess dieses Zustandes von allgemeiner Natur ist. Solche Zustände treten an Kontakten zu GaN jedoch im Gegensatz zu den $Al/Al_xGa_{1-x}As$-Übergängen nur bei Energien weit oberhalb des Fermi-Niveaus auf. Daher wird nicht erwartet dass diese Zustände wesentlich zu den Transporteigenschaften beitragen. An Kontakten zwischen Edelmetallen und GaN treten über einen großen Energiebereich, einschließlich E_F, eine grosse Anzahl von Grenzflächenzuständen, welche atomaren *d*-Orbitalen zugeordnet sind, auf.

Abstract

We present a theoretical study of the physical characteristics of metal/semiconductor junctions. Using first principle pseudopotential calculations, we have investigated the nature of electronic states with energies within the semiconductor band gap of representative abrupt, defect-free, anion-terminated metal/III-V interfaces. Namely, we focused on Al contacts to GaAs(001), AlAs(001) and cubic GaN(001) as well as on Al, Au and Cu junctions to cubic GaN(001).

Recent advances in Schottky barrier concepts emphasize the possible relationship between interface states and the formation of the Schottky barrier. We aim at understanding the atomic-scale mechanisms responsible for interface states as well as their role in the Schottky barrier formation process.

At As-terminated Al/GaAs(001) and Al/AlAs(001) junctions, resonant and localized interface states occur at the **J** point of the interface 2D Brillouin zone near the Fermi energy in the semiconductor midgap region. They correspond to intermetallic bonds between the outermost cation atoms of the semiconductor and the interfacial Al atoms of the metal. These interface states derive from an interaction between localized states of the Al(001) surface and semiconductor conduction band states, mediated by localized states of the unreconstructed, As-terminated semiconductor (001) surface. Our results indicate that interface states of the intermetallic, bonding-like kind could play an important role in the transport properties of metal/$Al_xGa_{1-x}As$ junctions.

We have also investigated the electronic structure of Al, Au and Cu junctions to cubic, N-terminated GaN(001). The localized interface state reported for As-terminated Al/GaAs(001) and Al/AlAs(001) junctions occurs also at metal/GaN interfaces under the condition that atoms on the outermost atomic plane of the metal are placed in front of the outermost semiconductor cation. This indicates that the formation mechanism of this state is a very general one. In contrast to Al/$Al_xGa_{1-x}As$ junctions, these states occur at energy much larger than E_F for the contacts to GaN. Thus, they are not expected to contribute significantly to the electronic transport of the latter interfaces. However, a large number of interface states attributed to *d*-type orbitals occur over a wide energy range including E_F at contacts of noble metals to GaN.

Contents

1 Introduction **1**

1.1 Experimental evidence on metal/semiconductor interfaces 2
1.1.1 Experimental techniques 2
1.1.2 Barrier heights and Fermi-level pinning 4
1.2 Models of metal/semiconductor interfaces 5
1.3 *Ab initio* electronic structure calculations 9
1.4 Overview of this work 11

2 Methodology **13**

2.1 *Ab initio* calculations 13
2.1.1 Adiabatic approximation 13
2.2 Density Functional Theory 14
2.2.1 Hohenberg-Kohn variational principle 15
2.2.2 Single particle Kohn-Sham equations 15
2.2.3 Local density approximation 17
2.2.4 Discussion 18
2.3 Application to metal/semiconductor contacts 19
2.3.1 Plane wave expansion 19
2.3.2 Pseudopotential approximation 20
2.3.3 Brillouin zone integration 22
2.3.4 Supercell technique 23
2.3.5 Band structure alignment and Schottky barriers 23

3 Interface states at the Al/GaAs(001) contact **25**

3.1 Interface structure 25
3.2 Brillouin zone 28
3.3 Numerical parameters and precision 30
3.4 Interface states 31
3.5 The Al(001) and GaAs(001) surfaces 35
3.6 Evolution from surface to interface states 41
3.7 GaAs conduction band edge states 44
3.8 Discussion 45

4 Interface states at the Al/AlAs(001) junction **47**
4.1 Interface states in the semiconductor gap 48
4.2 Surface states of AlAs(001) 52
4.3 Discussion 56

5 Interface states at metal contacts to cubic GaN(001) **57**
5.1 Bulk c-GaN and the GaN(001) surface 57
5.1.1 Pseudopotentials and the role of $3d$ electrons 58
5.1.2 Bulk c-GaN 59
5.1.3 The GaN(001) surface 60
5.2 The Al/GaN(001) interface 64
5.2.1 Interface structure 64
5.2.2 Electronic states 66
5.2.3 The Al(001) surface under strain 72
5.2.4 Discussion 73
5.3 The Au/GaN(001) interface 75
5.3.1 Electronic states 76
5.3.2 The Au(001) surface under strain 87
5.3.3 Discussion 89
5.4 The Cu/GaN(001) interface 90
5.4.1 The Cu(001) surface under strain 95
5.4.2 Discussion 97

6 Conclusions **99**

References **103**

1 Introduction

Metallic contacts to semiconductors are an essential part of most modern electronic and optoelectronic devices. The electronic structure of metal/semiconductor (MS) interfaces plays a fundamental role in the transport properties of these junctions. One of the most relevant parameters of MS junctions is its Schottky barrier height (SBH), which is a measure of the energy mismatch across the interface between the Fermi energy of the metal and the majority carrier band edge of the semiconductor. For ohmic contacts, a vanishing SBH is desirable while the larger the value of the SBH is, the more rectifying is the contact. Independent on the application, a control of the SBH is sought; in most cases an ohmic contact is wanted.

Due to their technological importance, MS contacts and their SBH have been the subject of numerous investigations [1, 2]. Despite the enormous progress in solid state physics and semiconductor device physics, in particular, the factors controlling the SBH are still not yet fully understood. Recent advances in Schottky barrier concepts have shown the importance of the occurrence of localized states at the interface.

This work aims at studying the existence, nature and formation mechanisms of interface states at metal contacts to GaAs, AlAs and GaN, three semiconductors which have raised considerable interest for optoelectronic applications.

1.1 Experimental evidence on metal/semiconductor interfaces

In this section we shortly present the most important experimental techniques which are used to study the properties of metal/semiconductor junctions and the kind of information that these techniques can provide. A much more extensive and detailed discussion of these techniques can be found in numerous textbooks and review articles, e.g. [3–9].

1.1.1 Experimental techniques

F. Braun reported in 1874 in his pioneering work on the rectifying properties of metal contacts to metal sulfides [10]. Rectifiers and early MS diodes were fabricated by pressing fine metal wires and plates on semiconducting crystals and were mostly used in broadcasting technologies in the 20's. Given their technical importance, an extensive work on metal contacts to several sulfides was carried out by Schottky [11]. Historically, metal/semiconductor interfaces have been characterized by $I-V$ and $C-V$ measurements [12–15]. In these cases, the conductance and the capacitance of the junction are measured as a function of the applied voltage. In general, barrier heights obtained from $I-V$ are more reliable [6] than those deduced from $C-V$ results, since in the latter case the boundary layer may introduce important corrections. However, $C-V$ measurements, which are best suited for junctions exhibiting poor rectification [16], are widely used since the experiments are essentially electrostatic measurements of equilibrium charge distributions versus position and are almost free from transport effects. The weakness of both approaches is that the SBH is derived from the measured curves using rather simplified models of the interface. With continuous improvements in epitaxy and spectroscopic techniques, these measurements have nowadays reached a precision of the order of 0.05 eV [17, 18].

In addition to the classic transport techniques mentioned above, optical and electron spectroscopy and photoemission techniques have become alternative approaches which can also provide additional interface properties such as, for example, atomic positions and energies of interface electron states. Most of these experiments are performed on devices with thin overlayers or quantum wells. A common difficulty of these techniques is their weak lateral resolution which is an important issue in semiconductor interface research. A widely used technique to overcome this drawback is the ballistic- electron emission microscopy (BEEM) [19] which is based on scanning tunneling microscopy (STM). Thereby, an STM tip is used to inject electrons into a thin metal overlayer grown on top of a semiconductor substrate.

A fraction of these electrons reaches ballistically the interface region and contributes to the current when the voltage of the tip is higher than the SBH. BEEM allows to probe the electronic transport with a lateral resolution of about 20 Å [4, 20, 21].

Electronic and optical techniques which are most commonly used for characterizing semiconductor surfaces and interfaces are listed in Tab. 1.1 together with the kind of information that they provide.

Technique	Information
Auger electron spectroscopy (AES)	Surface chemical composition, depth distribution
X-ray photoemission spectroscopy (XPS)	Surface chemical composition and bonding
UV photoemission spectroscopy	Fermi levcl with respect to band edges, work function, valence-band states
Soft X-ray photoemission spectroscopy (SXPS)	Surface chemical composition and bonding, Fermi level with respect to hand edges, valence-band state
Constant initial (CIS) and final (CFS) state spectroscopies	Empty states above Fermi level
Angle-resolved photoemission spectroscopy(ARPES)	Atomic bonding symmetry, Brillouin zone dispersion
Surface extended X-ray absorption fine structure (SEXAFS)	Local surface bonding coordination
Inverse photoemission spectroscopy	Unoccupied surface state and conduction-band states
Laser-excited photoemission spectroscopy (LAPS)	Band gap states
Low-energy electron (LEED) and positron (LEPD) diffraction	Surface atomic geometry
X-ray diffraction	Bulk atomic geometry
Total external X-ray diffraction (TEXRD)	Interface lattice structure, interface strain
Low-energy electron-loss spectroscopy (LELS,EELS)	Interface reactions, electronic and atomic excitations
Surface photovoltage spectroscopy (SPS)	Band gap states. work function, band bending
Infrared absorption spectroscopy (IR)	Band gap states, atomic bonding and coordination
Cathodoluminescence spectroscopy (CLS)	Surface states within band gap, buried interface states, new compound band gap energies
Photoluminescence spectroscopy	Surface chemical compounds, states within band gap
Surface reflectance spectroscopy (SRS)	Surface dielectric response
Ellipsometry	Surface or interface dielectric response
Surface photoconductivity spectroscopy	States within band gap
Raman scattering spectroscopy	Interface compounds and bonding, hand bending
Rutherford backscattering spectroscopy (RBS)	Surface atomic geometry, depth distribution
Secondary ion mass spectroscopy (SIMS)	Interface chemical composition, depth distribution
He beam scattering	Energy transfer dynamics, surface charge density
Scanning tunneling microscopy (STM)	Surface atomic geometry, surface morphology, filled- and empty-state geometries
Atomic force microscopy (AFM)	Surface electrostatic forces, magnetic polarization
Scanning tunneling spectroscopy (STS)	Band gap states, heterojunction band offsets
Ballistic electron energy microscopy (BEEM)	Barrier heights, heterojunction hand offsets, barrier height lateral inhomogeneity
Field ion microscopy (FIM)	Surface atomic motion, atomic geometry
High-resolution transmission electron microscopy (HRTEM)	Interface lattice structure
Low-energy electron microscopy (LEEM)	Surface morphology, diffusion, phase transformations, grain boundary motion
Electron paramagnetic resonance (EPR)	Unpaired electron spins

Table 1.1: Electronic and optical techniques for characterizing semiconductor surfaces and interfaces and the corresponding information they can provide (from [22]).

1.1.2 Barrier heights and Fermi-level pinning

The term "Fermi level pinning"is often used in the literature to describe the insensitivity of the SBH on the metal work function and metal coverage. This term is actually borrowed from the field of semiconductor surfaces and semiconductor-insulator interfaces, where the Fermi level is pinned at the interface, independently of the semiconductor doping. However, the term is widely used for metal/semiconductor contacts and, in the following, the expression Fermi level pinning will denote the insensitivity of the SBH on the metal work function.

We investigate in this work metal contacts to polar, cubic III-V semiconductors. Historically, the most investigated III-V semiconductors have been GaAs and AlGaAs alloys. More recently, GaN has gained considerable interest due to its large band gap and its application to blue and violet laser diodes.

An extensive study of the Schottky barrier heights for a range of metals on (001) surfaces of n- and p-type GaAs crystals has been carried out by Waldrop [18, 23]. The results are shown in Fig. 1.1. From these data no correlation is immediately apparent between the SBH and the metal work function. Generally, the variation of the SBH is smaller than that of the metal work function, leading to the generally accepted statement that Fermi level pinning occurs at metal contacts to GaAs. Furthermore, in most cases the sum of the n-type and the p-type SBHs $\phi_n + \phi_p$ closely reproduces the band gap (1.43 eV). A study on single crystal Al layers with two different orientations on the GaAs(001) surface confirmed the result for the Al contact and showed further that the SBH is weakly dependent on the surface stoichiometry of GaAs [24].

Studies of metal contacts to III-V compound alloys have been increasing recently due to the importance of these systems in optoelectronics. Especially the $Al_xGa_{1-x}As$ alloy is extremely important in the design of red and infrared laser diodes. For this system contradictory results exist for Al and Au contacts [25–28], but it turns out that ϕ_n is constant at least up to values of $x \simeq 0.4$, where the alloy changes from a direct to an indirect gap semiconductor. On the contrary, data for $Ga_xIn_{1-x}As(001)$ do not indicate Fermi level pinning [29] since the SBH depends strongly on the metal work function. The dependence of the Fermi level position on x is still controversial for this system [29–31].

Even more controversial are the existing results for wide band gap semiconductors like GaN. No generally accepted conclusion exists on whether metal contacts to GaN exhibit Fermi level pinning or not. For some metals, the contact to GaN is ohmic, while for other metals, the contact is rectifying [32–36]. An additional challenge concerning nitrides is that epitaxial parameters, annealing procedures and substrate surface passivation have significant effects on the electronic properties of the corresponding metal contacts.

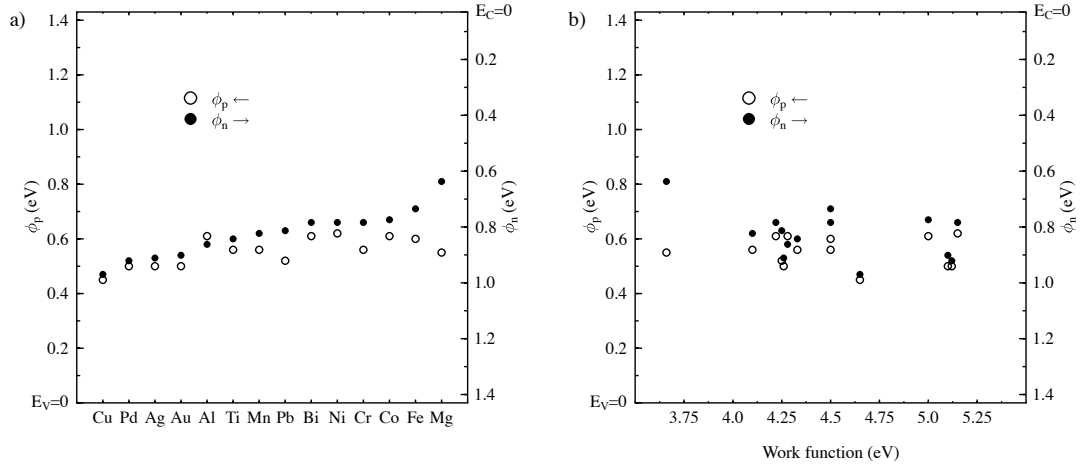

Figure 1.1: SBH of metal contacts to GaAs(001) as measured by the $I-V$ method (taken from [18]). Solid circles provide n-type contacts (right-hand scale), open circles p-type contacts (left-hand scale). Panel **b)** shows the same SBH data as panel **a)** but as a function of the metal work function.

1.2 Models of metal/semiconductor interfaces

More than 60 years after the pioneering experiments by Braun and the experimental developments by Schottky and Deutschmann [11], a first model of the barrier formation was proposed independently in 1938 by Schottky [37] and Mott [38] (see also [39, 40]). Fig 1.2 illustrates the band diagram of Schottky's *Gedankenexperiment* illustrating the formation of a Schottky barrier. The metal and the semiconductor are supposed to be electrically neutral, separated from each other and without any surface charge. We consider the most important case of an n-type semiconductor with an electron affinity χ_s and a work function ϕ_s which is smaller than the work function ϕ_m of the metal.

When the metal and the semiconductor come in electrical contact, the two Fermi levels are forced to coincide and electrons pass from the semiconductor into the metal. The result is an excess of negative charge on the metal surface and a negative charge depletion zone in the semiconductor near its surface. These excess charges form an interface dipole and produce an electric field, directed from the semiconductor to the metal. By bringing the metal and the semiconductor closer together, the gap between the two materials vanishes and the electric field corresponds now to a gradient of the electron potential in the depletion layer, resulting in the well known band-bending regime.

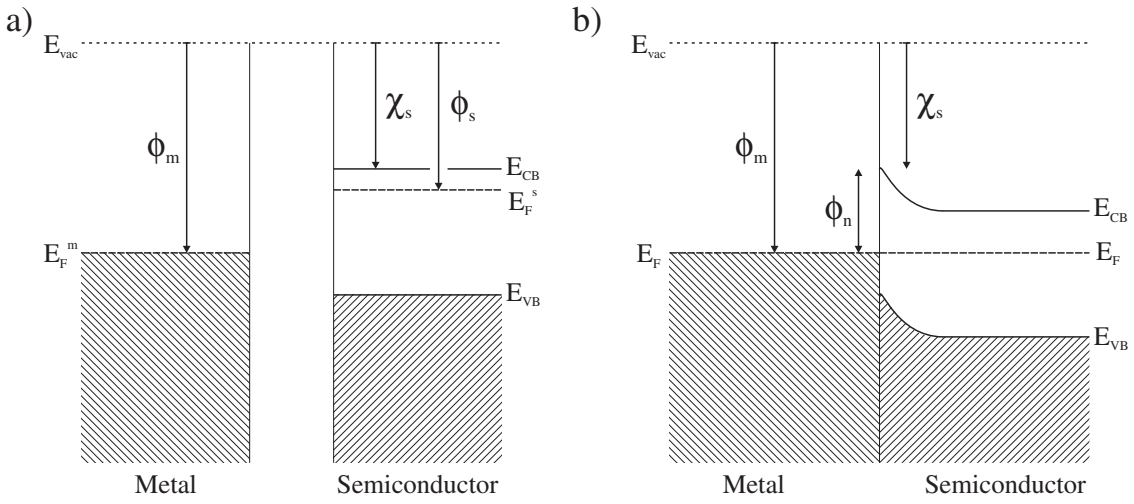

Figure 1.2: Schematic band diagram of band bending according to the Schottky model for the MS interface. **a)** Before contact, **b)** after the contact formation. An n-type semiconductor is assumed.

The Schottky-Mott model leads to a n-type SBH ϕ_n given by

$$\phi_n = \phi_m - \chi_S, \tag{1.1}$$

and therefore depending linearly on the metal work function. However, experimental results as those presented in Fig. 1.1 for GaAs do not confirm this relationship since the SBH depends only weakly on the metal work function. Deviation from the Schottky-Mott behavior are very often measured in terms of the slope parameter,

$$S = \frac{d\phi_n}{d\phi_m}, \tag{1.2}$$

first introduced by Kurtin *et al.* [41] and describing the dependence of the SBH on the metal work function. According to the Schottky-Mott model S should be equal to 1, while it is of the order of 0.1 for metal contacts to GaAs [41, 42].

An important limitation of the Schottky-Mott model is the neglect of surface states. This prompted Bardeen [43] to propose in 1947 a different model: he assumed that intrinsic surface states whose energy is in the semiconductor gap, as discussed by Tamm [44, 45] and Shockley [46], are pinning the metal Fermi level as shown in Fig. 1.3. In this extreme case, the SBH does not depend at all on the metal work function, i.e. $S = 0$ when surface states are present. All models of MS interfaces proposed afterwards are essentially generalizations of these two basic models.

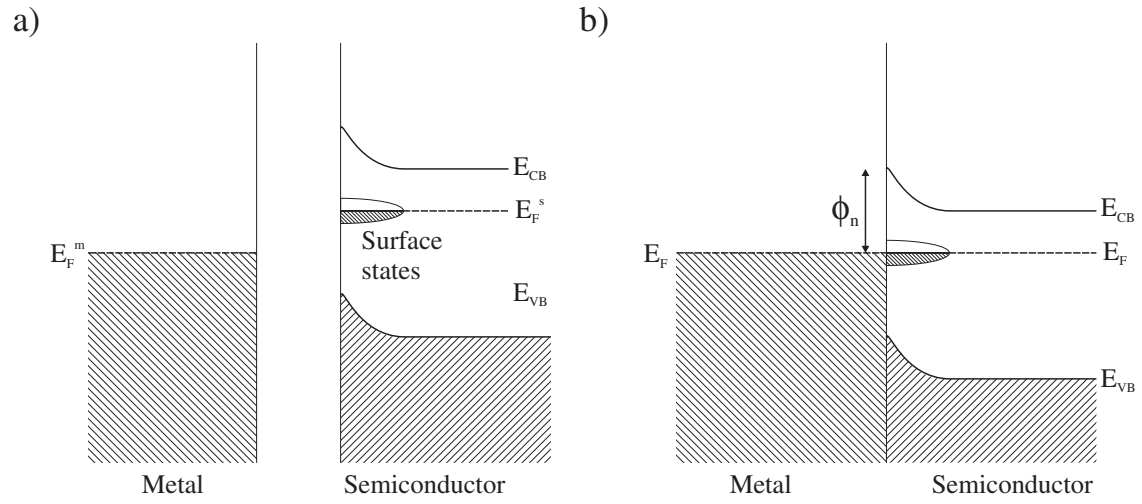

Figure 1.3: Schematic band diagram of band bending according to the Bardeen model for the MS interface. **a)** Before contact, **b)** after the contact formation. The Fermi level is pinned by a high density of surface states of the semiconductor.

Following Bardeen's ideas, Cowley and Sze [47] included a continuum of interface states leading to a phenomenological formula for the n-SBH:

$$\phi_n = S(\phi_m - \chi_s) + (1 - S)\phi_0, \tag{1.3}$$

where S is the slope factor and ϕ_0 is the barrier height when the charge neutrality level of the continuum of interface states coincides with the Fermi level at the interface.

At the same time Heine [48] made a proposal for the physical origin of interface states at MS junctions introducing the concept of metal-induced gap states (MIGS). He argued that surface states of the semiconductor cannot exist in presence of the metal. He used a matching scheme for electron wavefunctions at the junction and concluded that bulk states of the metal with energy in the optical gap of the semiconductor have exponentially decaying wavefunction tails extending into the semiconductor. The MIGS model has been refined by several groups [49–53] by introducing the concept of the charge neutrality level. Thereby, it is assumed that the semiconductor behaves locally near the interface like a metal. For locally neutral interfaces, the charge neutrality level of the semiconductor separates the occupied electron levels from the unoccupied ones. At equilibrium, its is aligned with the metal Fermi level via the formation of interface dipoles.

The neutrality level has been calculated with an empirical model by Tersoff [54]. Using simple considerations of local charge neutrality and a Green's function matching scheme, he proposed that the Fermi level in the semiconductor is pinned near an effective gap center identified by a branch point where the gap states cross over from valence- to conduction-band character. This model met good success and is still widely used.

Spicer et al. [55] and other authors [56–58] have suggested that also the electronic states of native defects generated during the early stages of interface formation, e.g. vacancies or antisites, can contribute to pinning the Fermi level in MS junctions if their energy is in the semiconductor gap. Hasegawa [59] pointed out, that also disorder may induce electron states with energy in the gap of the semiconductor.

Alternatively, it has been proposed that micro-clusters may form at the interface due to chemical interactions during metallization [60–62]. The Schottky barrier is then determined, independently of the metal, by the interphase which is formed at the interface.

Recently, Tung [2, 63, 64] has reviewed the existing theoretical models of SBH formation. In this work, he proposes that chemical bonding is likely the primary mechanism responsible for the observed Fermi level pinning at MS interfaces having an excellent crystalline quality.

In summary, there have been many proposals to explain the experimentally observed values of the SBH and their dependence on the metal work function. In particular, the low values of the slope parameter S for various systems have been attributed to the presence of electron states of different nature in the band gap of the semiconductor. Up to now, however, no generally accepted model applicable to all systems exists.

1.3 Ab initio electronic structure calculations

Besides experimental measurements and the development of empirical models, the physical properties of MS interfaces have been the subject of numerical calculations at the atomic scale in order to help the interpretation of experimental data, verify model predictions or to obtain physical quantities when experiments cannot be easily performed.

The numerical solution of the quantum mechanical equations determining the physical properties of a solid-state system at the atomic scale is a complex task. Only the availability of powerful computers has made it possible since a few decades to solve such problems of solid-state physics numerically. In practice, empirical, semi-empirical and first principle schemes are used. The latter ones, also known as *ab initio* (lat.:'from the beginning') methods, use exclusively the chemical formula and the atomic positions of the system as input. In contrast, empirical or semi-empirical approaches require models of the interatomic interactions to be supplied. The parameters of these models are usually derived by fitting the outcome of computations to experimental data and the predictive capability of these schemes is limited. *Ab initio* techniques have greater predictive capability but their high computational costs limit the application of these methods to systems composed by a relatively small number of atoms.

Historically, *ab initio* calculations have first been carried out for bulk materials. With increasing computer ressources, more complex systems such as surfaces at first and interfaces later on, have been accessible. In the following, we provide a brief overview of the relevant *ab initio* calculations which have been performed for metal/semiconductor interfaces.

Pioneering self-consistent calculations of the electronic structure of metal/semiconductor junctions have been carried out in the 70's by the group of Cohen and Louie [65–73]. In these early quantum simulations, the metal was modelled as a homogeneous jellium with the appropriate density while empirical pseudopotentials were used for the atomic-scale description of the semiconductor. These calculations have provided the first theoretical values of the p-type SBH for Al contacts to Si, Ge, GaAs, ZnSe and ZnS.

Both numerical techniques and quality of pseudopotentials have been improved considerably in later works and the calculations carried out in the 80's model the interface more realistically. In particular, a pseudopotential description has been used also for the metal atoms and atomic relaxations have been taken into account in the interface region [74, 75].

Most of the *ab initio* activity has been dedicated in the past to the calculation of the value of the SBH and of its variation as a function of several physical parameters. In the 90's, for example, *ab initio* calculations have been used to investigate trends of the SBH as a function of structure and semiconductor composition [76–78], interface morphology [79, 80] and external applied pressure [81].

In line with the works of Bardeen [43], Heine [48] and Tersoff [54], interface states in the context of metal-induced gap states have been the subject of several *ab initio* investigations [82–86]. Despite their importance, detailed *ab initio* investigations of interface states, their localization and their nature have been done for a few systems only. Intrinsic localized interface states with energies within the semiconductor band gap have been reported theoretically for Au/GaAs(001) [87] and several silicide-silicon [88, 89] interfaces. Recently, *ab initio* calculations of the electronic and structural properties of metal/GaN interfaces have been performed [90–95].

1.4 Overview of this work

This work aims at studying the electronic properties of metal/semiconductor contacts using state-of-the-art *ab-initio* pseudopotential calculations based on the local density approximation (LDA) to density functional theory (DFT). We investigate the nature of the electronic states with energy within the semiconductor band gap in abrupt, defect-free, anion-terminated metal contacts to cubic III-V semiconductors. The formation mechanisms of interface states will be studied by a series of numerical calculations where the metal and the semiconductor constituents are progressively separated. A continuous monitoring of energy levels and wavefunctions of interface states will allow us to connect the electron states of the two free-standing surfaces with the interface states occurring at the contact in equilibrium.

We shall address the existence and nature of localized interface states at Al contacts to anion-terminated GaAs(001), AlAs(001) and cubic GaN(001). This will allow us to investigate the influence of the semiconductor ionicity and energy band gap on the Schottky barrier formation. A study of the surface states of the unreconstructed (001) surfaces of the three semiconductors will permit us to understand the role, if any, of surface states of both the metal and the semiconductor in the formation of the interface and how these surface states evolve as a function of semiconductor ionicity.

We shall also perform a comparative study of Al, Au and Cu contacts to N-terminated, cubic GaN(001). We shall examine the effect of the interface atomic structure and of the metal work function on the existence and nature of interface states for these systems.

Finally, we shall discuss whether interface states contribute to the formation of the Schottky barrier and whether these states could give a contribution to Fermi level pinning.

In the following chapter, we present briefly the numerical methods used in this work. Chapter 3 is dedicated to the study of the electron structure of Al/GaAs(001) junctions. In chapter 4, we compare the electron structure of the Al/AlAs(001) interface to that of Al/GaAs(001). Chapter 5 is devoted to the investigation of Al, Au and Cu contacts to N-terminated, cubic GaN(001). The last chapter summarizes the main results obtained in this work.

2 Methodology

In this chapter, we provide a short review of a state-of-the-art approach that allows one to calculate efficiently structural and electronic properties of metals and semiconductors. It is based on Density Functional Theory (DFT). In particular, we present a plane wave implementation, using norm-conserving pseudopotentials within the local density approximation (LDA). Furthermore, we discuss the reciprocal space formalism with the use of special **k**-points, a level broadening technique and the supercell technique for non-periodic systems. A more extensive and detailed discussion of the fundamental techniques and their details can be found in a huge number of textbooks and review articles, e.g. [96–100].

2.1 Ab initio calculations

The objective of *ab initio* methods is the calculation of physical properties of materials without using any experimental input. These calculations from first principles provide the macroscopic properties of a given physical system just from the knowledge of the type and position of the constituent atoms. In particular, using the atomic structure as the only input, the electronic, mechanical, magnetic and optical properties of a condensed matter system can be obtained.

2.1.1 Adiabatic approximation

The starting point of the theoretical description is the stationary Hamiltonian of the system. We describe a solid as an ensemble of electrons (e) and nuclei (n) which are coupled by Coulomb interactions. Denoting the nuclear and coordinates by $\mathbf{R} := \{\mathbf{R}_I | I = 1, \dots N_n\}$, the electronic ones by $\mathbf{r} := \{(\mathbf{r}_i) | i = 1, \dots N_e\}$ and the conjugated momenta $\mathbf{P}$ and $\mathbf{p}$, the Hamiltonian of the system can be written as

$$H = T_n(\mathbf{P}) + T_e(\mathbf{p}) + V_{nn}(\mathbf{R}) + V_{ee}(\mathbf{r}) + V_{ne}(\mathbf{R}, \mathbf{r}), \tag{2.1}$$

where the *Ts* and *Vs* correspond to the kinetic and the Coulomb interaction operators, respectively.

The exact solution of the stationary Schrödinger equation

$$H\Psi(\mathbf{r},\mathbf{R}) = E\Psi(\mathbf{r},\mathbf{R}) \tag{2.2}$$

is extremely difficult even with the actually available computer resources. A first approximation is justified by the fact, that the nuclei are more than three orders of magnitude heavier than the electrons. As a consequence, the timescale of the nuclear motion is orders of magnitude larger than that of the electronic motion. Thus, it can be assumed that the electrons are always in their instantaneous ground state determined by the external potential of the nuclei, and that the forces acting on the nuclei are determined by the instantaneous electronic distribution and the nuclear positions of the system. The electrons are considered to be dependent merely on the nuclear positions and not on their velocities. This assumption, first introduced by Born and Oppenheimer [101], is known as the adiabatic approximation. Therein, the ionic momenta are assumed to be vanishingly small and the ionic positions are taken as fixed external parameters and the ionic part of the Hamiltonian is represented by a fixed external potential:

$$V_{ext}(\mathbf{r}) = \tfrac{1}{N_e} V_{nn}(\mathbf{R}) + V_{ne}(\mathbf{R},\mathbf{r}), \tag{2.3}$$

which leads to the following Hamiltonian for the electron system:

$$H_e(\mathbf{r}) = -\frac{\hbar^2}{2m}\sum_{i=1}^{N_e}\nabla_i^2 + \frac{1}{2}\sum_{i\neq j}\frac{e^2}{|\mathbf{r}_i-\mathbf{r}_j|} + \sum_{i=1}^{N_e} V_{ext}(\mathbf{r}_i). \tag{2.4}$$

The separation mentioned above between electronic and ionic degrees of freedom is very advantageous since it allows one to treat the ionic degrees of freedom classically while the electrons are to be treated quantum mechanically.

2.2 Density Functional Theory

The objective of DFT is the calculation of the ground state properties of an interacting many-electron system in an external potential using the ground state electron density $n(\mathbf{r})$ as the only variable. Dealing with non-magnetic materials, we neglect spin polarization. Moreover, considering only light elements we will also neglect the spin-orbit interaction, which can be included later on in perturbation theory. In the following section, we present briefly the fundamental concepts of DFT. For a more extensive treatment, see for example [99, 100].

2.2.1 Hohenberg-Kohn variational principle

In solids, N_e in (2.4) is of the order of the Avogadro constant and an exact solution of the Hamiltonian (2.4) is generally an intractable task. Since we are interested in the determination of physical ground state properties and not directly in the calculation of the many-body wavefunctions, we follow Hohenberg and Kohn [102] who demonstrated that the ground state wavefunction and therefore the ground state properties are defined uniquely by the electron density n_0 in the ground state. Furthermore, they proposed that this density and the ground state energy E_0 can be determined by minimizing the energy functional

$$E[n(\mathbf{r})] = F[n(\mathbf{r})] + \int V_{ext}(\mathbf{r}')n(\mathbf{r}')\mathbf{dr}', \tag{2.5}$$

which is minimal if and only if the charge density $n(\mathbf{r})$ is the exact ground state density $n_0(\mathbf{r})$. $F[n(\mathbf{r})]$ is independent on the external potential and therefore *universal* but, unfortunately, not known. The Hohenberg-Kohn theorem solely proves the existence of $F[n(\mathbf{r})]$ without giving any guidelines for determining it. However, in principle, all physical ground state properties of the system can be obtained by minimizing this functional.

2.2.2 Single particle Kohn-Sham equations

All usual implementations of DFT are based on a proposal by Kohn and Sham [103]. They rewrote the functional $F[n(\mathbf{r})]$ in the following form:

$$F[n] = T_0[n] + \frac{1}{2}\int n(\mathbf{r})V_H(\mathbf{r})\mathbf{dr} + E_{xc}[n], \tag{2.6}$$

where $T_0[n]$ is the kinetic energy of a non-interacting electron gas with density $n(\mathbf{r})$ and V_H is the Hartree potential given by

$$V_H(\mathbf{r}) = e^2 \int \frac{n(\mathbf{r}')}{|\mathbf{r}-\mathbf{r}'|}\mathbf{dr}'. \tag{2.7}$$

The new functional $E_{xc}[n]$, defined by (2.6), includes the all-electron corrections, the so-called exchange and correlation term.

Formally, the solution is still given by the minimization of (2.5). Under the assumption of particle conservation, the problem can be transformed into a set of single-particle Schrödinger equations:

$$\left[-\frac{\hbar^2}{2m}\nabla^2 + V_{ext}(\mathbf{r}) + V_H(\mathbf{r}) + V_{xc}(\mathbf{r})\right]\psi_i(\mathbf{r}) = \epsilon_i\psi_i(\mathbf{r}), \tag{2.8}$$

where ϵ_i is the i-th Kohn-Sham eigenvalue and V_{xc} is the so-called exchange-correlation potential, defined through

$$V_{xc}(\mathbf{r}) = \frac{\delta E_{xc}[n(\mathbf{r})]}{\delta n(\mathbf{r})}. \tag{2.9}$$

The Kohn-Sham equations (2.8) have to be solved self-consistently since V_H and V_{xc} depend explicitly on the charge density $n(\mathbf{r})$, given by the eigenstates ψ_i which in turn are determined by these potentials. In order to turn this into practice, an initial guess, e.g. a superposition of atomic charges, is used. On the basis of the eigenfunctions of (2.8), the new charge density is obtained by summing over the occupied Kohn-Sham orbitals ψ_i. Afterwards, the Hartree and exchange-correlation potentials are then constructed. This process has to be repeated until convergence is reached. In practice, the new charge density is mixed with the previous one in order to avoid numerical instabilities. Fig. 2.1. gives a schematic overview of the iterative algorithm.

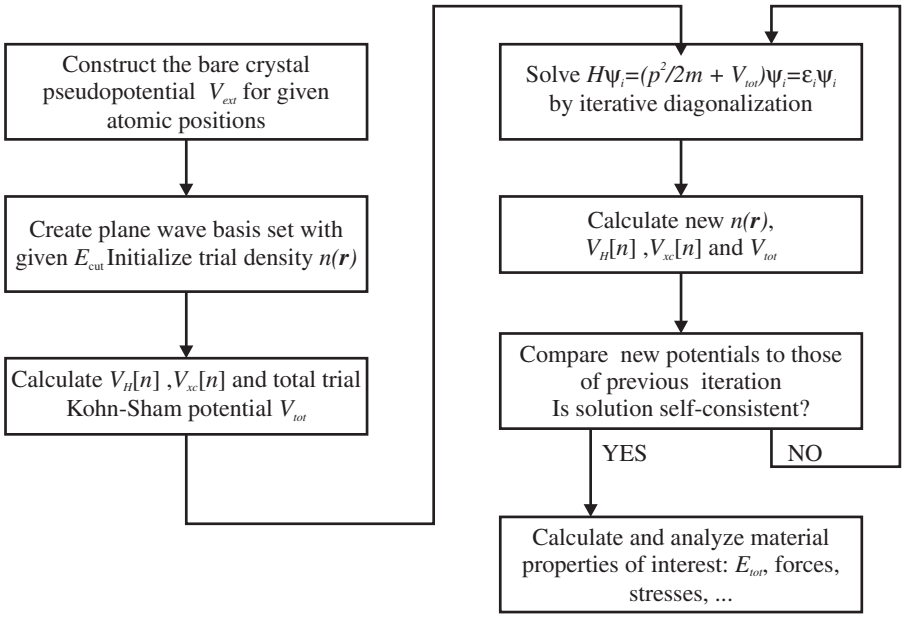

Figure 2.1: Flowchart of self-consistent Kohn-Sham calculations.

When self-consistency of the electronic potential is achieved, ions can be optionally moved towards their classical equilibrium position using the effective forces acting on the ions which can be obtained with the theorem of Hellmann and Feynman.

In order to determine the unit cell size, repeated calculations with varying lattice parameters have to be done. The equilibrium values can be obtained by minimizing the total energy or, equivalently by looking for a vanishing external stress tensor.

2.2.3 Local density approximation

The exchange-correlation potential V_{xc} has still to be defined explicitly in order to solve the problem. Since the functional $F[n]$ is not known, one has to introduce some approximations. The most popular approach is the Local Density Approximation (LDA) [103], where the exchange-correlation energy $E_{xc}[n]$ is constructed under the assumption that it is locally given by the exchange-correlation energy of a homogeneous electron gas with the same local density:

$$E_{xc}^{LDA}[n(\mathbf{r})] = \int n(\mathbf{r})\epsilon_{xc}^{hom}[n(\mathbf{r})]\mathbf{dr}. \tag{2.10}$$

The exchange-correlation energy $\epsilon_{xc}^{hom}[n(\mathbf{r})]$ of a homogeneous electron gas has been calculated by Ceperley and Alder [104] for various densities using quantum Monte-Carlo simulations. Perdew and Zunger [105] have parameterized their results in order to approximate ϵ_{xc}^{hom} over a wide range of densities. This procedure is exact if and only if the density $n(\mathbf{r})$ is constant. If $n(\mathbf{r})$ varies slowly over distances of the order of the Fermi wavelength, LDA can be expected to provide a good approximation. On the other hand, at crystalline surfaces or for atoms and molecules, where the electronic density varies rapidly, the validity of LDA appears to be very questionable. Practice shows however, that LDA yields adequate ground-state properties even for strongly inhomogeneous systems.

2.2.4 Discussion

At this point we want to stress, that DFT is a ground state theory and that the Kohn-Sham eigenvalues ϵ_i have strictly speaking no physical signification and in particular they do not coincide with quasi-particle excitation energies of the real system. However, it has become standard practice to interpret the ϵ_i as estimates of quasi-particle energies and compare them in solids with experimental band structures. In order to obtain better approximations of excitation energies, e.g. semiconductor band gaps, a Green's function based approach, which is known as the GW approximation, is generally used [106, 107]. Concerning LDA, we mention that it has some systematic errors. Specifically, it underestimates semiconductor and insulator band gaps. Furthermore the description of cohesive energies, weak bonds and of the exchange-correlation potential in the vacuum region outside surfaces, are generally qualitatively not very accurate. An improvement over LDA is the semi-local Generalized Gradient Approximation (GGA) [108, 109] which not only considers the charge density n, but also its gradient ∇n. Moreover, it uses non-local exchange-correlation functionals. In this work we solely use the LDA parameterization since we are mostly dealing with systems for which LDA has been shown to be a sufficiently valid approximation [110].

2.3 Application to metal/semiconductor contacts

In the following, we provide a brief overview of the method generally used to solve the Kohn-Sham equations for condensed matter systems. For crystalline systems, it is highly beneficial to consider periodic boundary conditions which allow one to expand the problem into a plane wave basis set, which is highly efficient for a numerical solution. At first sight, this seems not applicable to surfaces or interfaces, where the three-dimensional bulk symmetry is broken in one spatial direction. However, as we will discuss later in this section interfaces and surfaces can be investigated with the supercell technique without loosing the advantages of the plane wave approach.

2.3.1 Plane wave expansion

Using the Bloch theorem [111, 112], we represent the eigenfunctions $\psi_{n,\mathbf{k}}(\mathbf{r})$ of the Kohn-Sham equations as a product of a lattice periodic function $u_{n,\mathbf{k}}(\mathbf{r})$ and a plane wave with a wave vector $\mathbf{k}$ belonging to the first Brillouin zone (BZ):

$$\psi_{n,\mathbf{k}}(\mathbf{r}) = u_{n,\mathbf{k}}(\mathbf{r}) e^{i\mathbf{kr}}, \tag{2.11}$$

where n is the band index. Since the $u_{n,\mathbf{k}}(\mathbf{r})$ are by definition lattice periodic, they can be expanded into plane waves:

$$u_{n,\mathbf{k}}(\mathbf{r}) = \sum_{\mathbf{G}'} \varphi_{n,\mathbf{k}}(\mathbf{G}') e^{i\mathbf{G}'\mathbf{r}} \tag{2.12}$$

where the $\mathbf{G}$' are the reciprocal lattice vectors. For practical purposes the sum in (2.12) is restricted to plane waves with kinetic energy below a given cutoff energy E_{cut}. Thus, defining the set $\Omega(\mathbf{G})$:

$$\Omega(\mathbf{G}) := \left\{ \mathbf{G} \middle| \, \tfrac{\hbar^2}{2m} |\mathbf{k} + \mathbf{G}|^2 \leq E_{cut} \right\}, \tag{2.13}$$

we obtain the following expansion of the Kohn-Sham wavefunctions:

$$\psi_{n,\mathbf{k}}(\mathbf{r}) = \sum_{\mathbf{G} \in \Omega(\mathbf{G})} \varphi_{n,\mathbf{k}}(\mathbf{G}) e^{i(\mathbf{G} + \mathbf{r})}. \tag{2.14}$$

The cutoff energy E_{cut} controls the numerical convergence relative to the completeness of the basis set. It depends strongly on the elements which are present in the system under investigation. The plane wave expansion allows a very efficient momentum space formalism [66].

The Fourier coefficients $\varphi_{n,\mathbf{k}}(\mathbf{G})$, obtained by the diagonalization of the Hamiltonian matrix, contain all relevant information and allow one to calculate all physical properties of interest, as e.g. the total energy, the Hellmann-Feynman [113, 114] forces and the stresses [115, 116]. Also the Poisson equation, which defines the Hartree potential, can be easily solved in reciprocal space.

2.3.2 Pseudopotential approximation

Plane waves, which are a convenient and efficient basis set for the diagonalization of the Hamiltonian, have an essential drawback: they are very efficient in representing slowly varying functions, but they are not suitable to describe the fast oscillations of electron wave functions in the core region. In order to overcome this problem the pseudopotential approximation [100, 117–119] is often used in conjunction with the plane wave expansion. It exploits the fact that core electrons belonging to closed inner shells are tightly localized around their nucleus and do not contribute to interatomic chemical interactions. Apart from some exceptions that we will discuss later (see [120–124]), only valence electrons are influenced by neighboring atoms. Consequently, they determine the chemical properties. This feature is the basis of the frozen core approximation used in quantum chemistry. In the pseudopotential approximation, the influence of core electrons on the valence states is described by an effective potential. The reduction to the description of only valence electrons is an essential prerequisite in order to describe large systems containing several hundred atoms.

Many different schemes have been proposed for constructing pseudopotentials. An extensive review can be found in Ref. [100]. In this work, we will use the norm-conserving, *ab initio* pseudopotentials proposed by Troullier and Martins [125, 126]. They fulfill the following properties:

1. The lowest energy valence pseudo wavefunctions generated from the pseudopotential do not contain nodes.

2. The eigenvalues associated with the exact and the pseudo wavefunction are equal.

3. Beyond a certain cutoff radius r_c, the atomic pseudo wavefunctions coincide with the exact wave functions obtained by an atomic calculation, where all electrons are taken into account.

4. The charge of the pseudo wavefunctions contained in a sphere of radius r_c equals that of the exact wavefunction.

The quality and transferability, i.e. the independence of the pseudopotential on the given system, are controlled by the choice of the cutoff radius. A small value of r_c corresponds to a high transferability but requires a high energy cutoff to obtain a sufficient numerical convergence. However, r_c has to be larger than the outermost node of all core electron wavefunctions in order to fulfill the norm-conserving criterion 3. In general, the generation of "good"pseudopotentials, i.e. a good compromise between a sufficient smoothness of wavefunctions and a good transferability, is a time demanding task. The Troullier-Martins pseudopotentials V^{TM} used in this work can be separated into a local part V^{loc}, i.e. solely dependent on the distance r, and a non-local part V_l^{nloc} which depends on the orbital momenta l of the electronic pseudo wavefunctions:

$$V^{TM}(r) = V^{loc}(r) + \sum_{l,m} |Y_{lm}\rangle V_l^{nloc}(r)\langle Y_{lm}|, \tag{2.15}$$

where Y_{lm} are the spherical harmonics. In the plane wave expansion with N plane waves, the matrix elements thus depend on $\mathbf{G}$ and $\mathbf{G}$' and their evaluation therefore scales as N^2. Kleinman and Bylander [127] proposed to transform the non-local components into a form which allows one to factorize entirely the plane wave integrals:

$$V^{KB} = V^{loc} + \sum_{l,m} \frac{|\delta V_l \Phi_{lm}^0\rangle\langle\Phi_{lm}^0 \delta V_l|}{\langle\Phi_{lm}^0|\delta V_l|\Phi_{lm}^0\rangle}, \tag{2.16}$$

where $\delta V_l = V^{loc} - V_l^{nloc}$ and Φ_{lm}^0 are the pseudo wavefunctions obtained for V^{TM}. In this form, the evaluation of the matrix elements scales as N and not as N^2 as in the original form which is a significant improvement for large systems. However, the non-locality can give rise to *ghost* states [128] which have no physical meaning. By a convenient choice of the local part, the occurrence of ghost states can be avoided [129].

2.3.3 Brillouin zone integration

The fundamental variable in DFT is the electronic charge density. In order to calculate it for periodic systems an integration over the entire Brillouin zone is necessary. We use the uniform **k**-point grids proposed by Monkhorst and Pack [130], who expanded the idea of the unique mean-value point first proposed by Baldereschi [131–133]:

$$\mathbf{k}_{i_1,i_2,i_3} = \sum_{j=1}^{3} \frac{i_j + s_j}{n_j} \mathbf{b}_j, \tag{2.17}$$

where n_j's are the number of special points in the jth direction in reciprocal space, $i_j = 0, 1, ..., n_j - 1$; $\mathbf{b}_j$ are the base vectors of the reciprocal unit cell and s_j allow a shift of the grid from the origin. In this work we use **s**= (1/2, 1/2, 1/2). In order to minimize the computational effort, the crystal symmetry is taken into account and a relatively small number of inequivalent **k**-points in the so-called irreducible Brillouin zone (IBZ) is used. The charge density is thus approximated by a sum over a small number of occupied states:

$$n(\mathbf{r}) = \sum_{n} \int_{BZ} |\psi_{n,\mathbf{k}}(\mathbf{r})|^2 \simeq \sum_{n,l} w_l |\psi_{n,\mathbf{k}_l}(\mathbf{r})|^2. \tag{2.18}$$

For semiconductors, the evaluation of (2.18) is straightforward since electronic bands are either fully occupied or not. In metallic systems, bands near the Fermi level are partially filled. Due to the complicated shape of the Fermi surface in reciprocal space, a huge amount of **k**-points is generally necessary for accurate results. In order to improve the convergence and to position the Fermi level accurately, we use a Gaussian broadening scheme [134] where the discrete calculated electronic levels $\varepsilon^n_{\mathbf{k}_l}$ are replaced by Gaussian distributions centered at these energy levels:

$$\delta(E - \varepsilon^n_{\mathbf{k}_l}) \Rightarrow \frac{1}{\sqrt{2\pi\sigma}} \exp\left(-\frac{(E - \varepsilon^n_{\mathbf{k}_l})^2}{2\sigma^2}\right), \tag{2.19}$$

where σ is a broadening parameter, which in this work is set equal 0.01 Ry for metallic systems. As a consequence, even if using uniform **k**-point grids, we have a continuous density of states and we calculate the Fermi energy by setting the correct number of valence electrons below the Fermi level. It has been shown within DFT that the Kohn-Sham Fermi energy matches exactly the quasi-particle Fermi energy of the interacting electron system at zero temperature [135].

2.3.4 Supercell technique

The formalism sketched above is very efficient for calculating the electronic properties of periodic systems. The systems investigated in this work, i.e. interfaces and surfaces, lack periodicity in one direction. This drawback can be overcome considering periodically repeated thin slabs of alternating materials, i.e. artificial superlattices whose unit cells are called supercells [136]. Depending on the materials and on the physical properties of interest, these supercells can reach large sizes and contain up to several hundred atoms. The supercell defines a unit cell with one axis perpendicular to the interface or surface of interest.

The periodic repetition of the supercell leads to an artificial superlattice which allows one to model an interface if the slabs are sufficiently thick. The required thickness depends on the two materials forming the interface and on the physical quantities under investigation, i.e. the interaction between the two slab interfaces has to be sufficiently small. For each property we are interested in, as for example the Schottky barrier or the spatial distributions of interface states, the convergence has to be tested through several calculations with an increasing number of atomic layers in the slabs. Features related particularly to the finite slab thickness are known as quantum size effects. In this work we normally use 13 atomic layers for the semiconductor and up to 23 atomic layers for the metal, or vacuum, in the case of surfaces, respectively.

2.3.5 Band structure alignment and Schottky barriers

With the supercell technique it is in general not possible to recover the bulk properties of the constituent materials due to the limited slab thickness. However, the physical properties we are interested in, i.e. interface quantities, can be obtained by using the supercell results to align the band structures obtained from high precision bulk calculations. In this work, we choose the supercell electrostatic potential as a reference. It consists of the local part of the pseudopotential and the electronic Hartree potential:

$$V(\mathbf{r}) = -\sum_i \frac{Z_i e^2}{|\mathbf{r} - \mathbf{R}_i|} + e^2 \int \frac{n(\mathbf{r}')}{|\mathbf{r} - \mathbf{r}'|} \mathbf{dr}'. \tag{2.20}$$

As we are mainly interested in the spatial dependence of a physical property $f(\mathbf{r})$ in the growth direction (z-axis), it is convenient to introduce the planar average $\bar{f}(z) = \frac{1}{S}\int_S f(\mathbf{r})dxdy$. In order to get rid of the atomic-scale oscillations of $\bar{f}(z)$ and to extract interface specific features, we follow Ref. [137, 138] and define the macroscopic average of $\bar{\bar{f}}(z)$ over a convenient length α centered at z, as

$$\bar{\bar{f}}(z) = \frac{1}{\alpha}\int_{z-\alpha/2}^{z+\alpha/2} \bar{f}(z')dz'. \tag{2.21}$$

In the case of a junction between two different materials, a useful procedure is to perform a convolution of two filter functions with length α_1 and α_2.

The average electrostatic potential of an infinite periodic crystal is ill-defined since (2.20) contains an arbitrary constant [139]. On the contrary, the lineup ΔV between two semi-infinite solids is well defined. With z_1 and z_2 as the coordinates of the center of the two slabs, the potential lineup ΔV is defined in terms of the electrostatic potential $V(\mathbf{r})$ of the superlattice as $\Delta V = \overline{\overline{V}}(z_1) - \overline{\overline{V}}(z_2)$. With the use of the electrostatic potential lineup, the p-type Schottky barrier can be written as

$$\phi_p = \Delta E_p + \Delta V, \tag{2.22}$$

where the band term, $\Delta E_p = E_f - \mathrm{VBM}_{sc}$ is the difference between the Fermi level of the metal and the valence band maximum (VBM) of the semiconductor, each measured with respect to the average electrostatic potential $\overline{\overline{V}}$ in the corresponding bulk.

The potential lineup obtained in the supercell calculation is also an essential quantity for the alignment of the projected bulk band structures of the two materials forming an interface.

3 Intermetallic bonds and midgap interface states at epitaxial Al/GaAs(001) junctions

The recent progress in epitaxial growth technology has made possible the fabrication of very high quality metal/semiconductor structures. The almost perfect lattice match between Al and GaAs provides ideal conditions to examine the electronic properties of these contacts from first principles. In this chapter, we present the results of our calculations for the ideal abrupt epitaxial Al/GaAs(001) interface and provide a detailed analysis of electronic states [140]. In particular we focus on the interface states with energy in the optical semiconductor band gap.

In the first section, we provide the equilibrium interface geometry. Afterwards, we discuss the symmetry properties of the interface and the freestanding GaAs(001) and Al(001) surfaces of the two slabs forming the contact. In section 3.4 we show that localized interface states occur and investigate their structure. In order to understand the formation mechanism of these states, we analyze the surface states of the freestanding GaAs(001) and Al(001) surfaces (see section 3.5). Starting from a large value of the interfacial distance, we reduce it down to the equilibrium value and follow the energies of interface states at the **J** point. In section 3.7, we show that also GaAs bulk states at the conduction band edge interact with the interface states.

3.1 Interface structure

The arsenic-terminated Al/GaAs(001) interface is modelled using a slab geometry in a supercell containing 13 atomic layers of GaAs and 23 atomic layers of Al, i.e., a total of 59 atoms and 191 electrons. The Al fcc lattice is rotated by 45° about the [001] growth axis with respect to the cubic lattice of GaAs (see Fig. 3.2) in order to satisfy the epitaxial condition $a_{\mathrm{Al},\parallel} = a_{\mathrm{GaAs}}/\sqrt{2}$, where a_{GaAs} and $a_{\mathrm{Al},\parallel}$ are the GaAs bulk equilibrium and Al in-plane lattice constants, respectively.

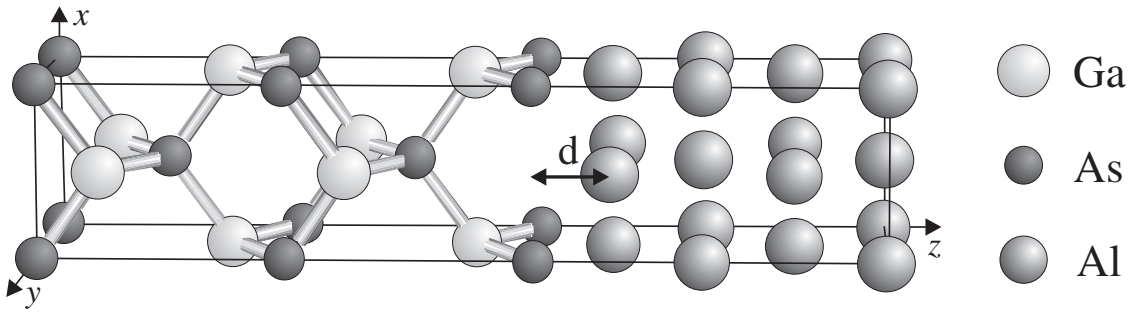

Figure 3.1: Atomic structure of the abrupt, As-terminated Al/GaAs(001) interface. The x and y axes are rotated by 45° with respect to the conventional cubic axis of the semiconductor. The interfacial distance d measures the spacing between the As and Al layers at the junction.

A similar epitaxial geometry was used previously to model Al/$Ga_xAl_{1-x}As$(001) junctions [78,87,141], and is known to correspond to experimentally observed quasi-epitaxial Al/GaAs(001) structures [142, 143]. Experimentally (and also in the *ab initio* calculations), the bulk equilibrium lattice constant of Al is about 1% larger than $a_{\mathrm{GaAs}}/\sqrt{2}$. Following macroscopic elasticity theory (MET) [144, 145], the Al in-plane compressive strain is accommodated by a 2% expansion of the Al overlayer along the growth direction in pseudomorphic structures.

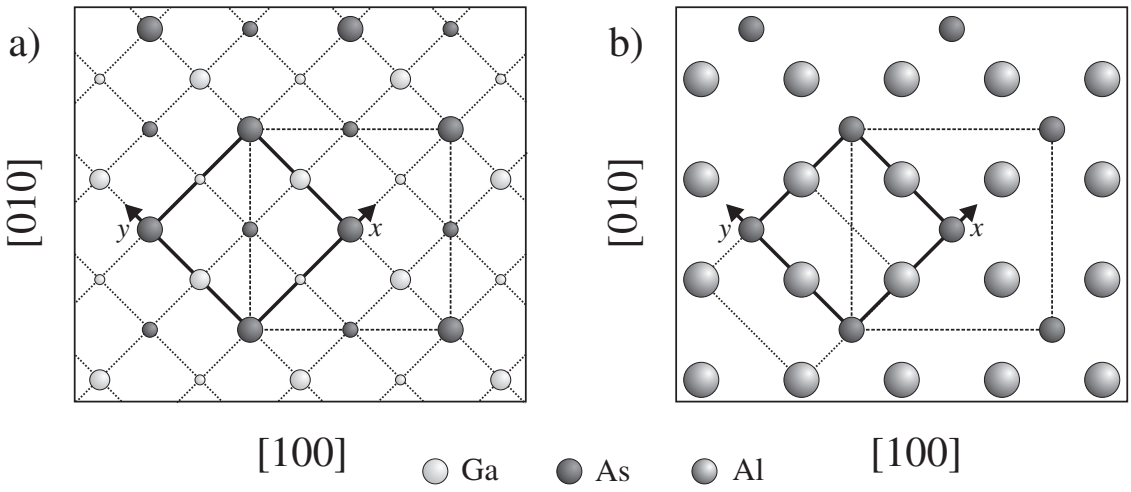

Figure 3.2: a) Topmost surface layers and the following three layers of the GaAs(001) zincblende lattice. **b)** Outermost interface layers of the As-terminated Al/GaAs(001) junction. The dotted lines shows the Al fcc unit cell. The dashed line indicates the GaAs zincblende unit cell. Solid lines show the tetragonal unit cell used for the interface calculations. The $x(y)$ axis is parallel to the [110]([1$\bar{1}$0]) crystal direction.

In this study, we use the theoretical value of the GaAs equilibrium lattice constant $a_{\mathrm{GaAs}} = 5.52$ Å, which is obtained from our high precision bulk calculations. It is 2% smaller than the experimental value of 5.65 Å. This difference is mainly attributed to the treatment of the Ga $3d$ as frozen core states [120–124] in the Ga pseudopotential (see 3.3) and to the use of the LDA approximation. Following MET, we use $a_{\mathrm{Al},\perp} = 4.06$ Å for the strained Al slab ($a_{\mathrm{Al,eq}} = 3.98$ Å).

The resulting atomic structure of the abrupt As-terminated interface considered in this chapter is illustrated in Fig. 3.1. It corresponds to the lowest energy configuration obtained by translating the Al slab parallel to the GaAs slab surface [78]. The equilibrium interfacial distance is $d_0 = 1.7$ Å (see Fig. 3.1). The corresponding volume of the supercell is $\Omega_0 = 6657\ a_0^3$.

3.2 Brillouin zone

The symmetry point group of both the Al/GaAs(001) interface and the unreconstructed GaAs(001) surface is C_{2v}, [146,147] and the space group is symmorphic. It consists of two reflections σ_{1v} and σ_{2v}, through planes perpendicular to one another, e.g. the xz and the yz planes, and the rotation C_2 around the line of the intersection of the planes. The character table of its irreducible representations is shown in Table 3.1. While GaAs has a zincblende geometry, Al has a face-centered cubic (fcc) structure and therefore, the Al(001) surface has higher symmetry than the GaAs(001) surface. Its symmetry point group is C_{4v}. Besides the symmetry operations of C_{2v}, it contains the rotations C_4 and $C_{\overline{4}}$ and two additional reflections σ_{1d} and σ_{2d} in the planes through the z axis, and the diagonals of the xy plane (see also Table 3.2).

The two-dimensional Brillouin zone (BZ) of the interface is shown in Fig. 3.3 where, for comparison, we also show the BZ's of the GaAs(001), Al(001) c2x2 and Al(001) 1x1 surfaces. The latter one (one atom per unit cell) corresponds to the common description of the Al(001) surface, while the Al(001) c2x2 configuration (two atoms per unit cell) is the relevant one in our interface study. We note that the BZ of the periodic superlattice used in this study to model the interface, is three-dimensional. However its dimension along the k_z axis is very small in view of the large size of the supercell in this direction. Therefore the electronic structure in the basal plane ($k_z = 0$) of the three-dimensional BZ of the supercell provides a good description of the electronic structure in the whole BZ.

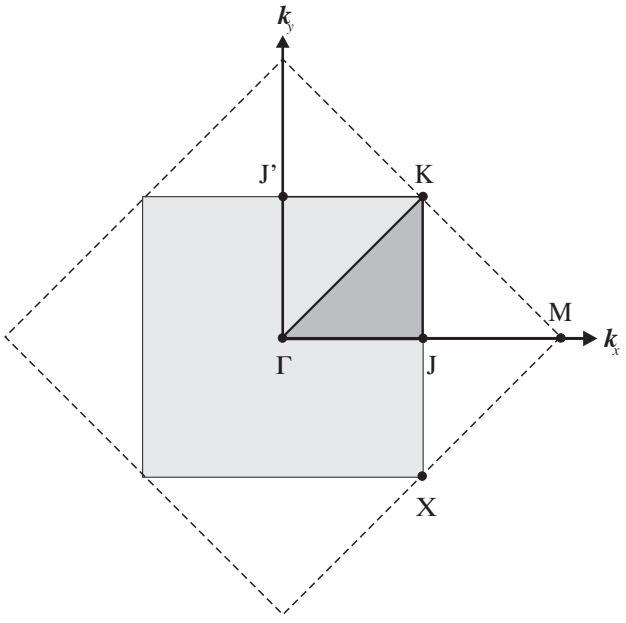

Figure 3.3: Brillouin zone of the Al/GaAs(001) interface (gray square) and of the Al(001) 1x1 surface (dashed lines). The gray square is also the BZ of the isolated GaAs(001) and Al(001) c2x2 surfaces. The irreducible part of the supercell BZ in the basal plane ($k_z = 0$) is indicated by the dark triangle.

In the supercell, the two As-terminated semiconductor surfaces of the slab are equivalent to each other through a reflection with respect to the middle plane of the GaAs slab, followed by a 90° rotation around the [001] axis ($x \to -y, y \to x$, $z \to -z$). This additional symmetry of the supercell, which does not apply to the isolated interface, reduces the irreducible part of the supercell BZ in the basal plane to one half that of the 2D-BZ of the isolated interface. In particular, **J** is folded onto **J′** in the numerical simulations. By choosing one of the two interfaces in the supercell as reference and by direct inspection of the wavefunctions, it is possible to distinguish interface state attributed to the **J** point from those of **J′**.

C_{2v}	E	C_2	σ_{1v}	σ_{2v}
Γ_1	1	1	1	1
Γ_2	1	-1	1	-1
Γ_3	1	1	-1	-1
Γ_4	1	-1	-1	1

Table 3.1: Character table of the symmetry point group C_{2v}.

C_{4v}	E	$2C_4$	C_2	$2\sigma_v$	$2\sigma_d$
Δ_1	1	1	1	1	1
Δ_2	1	-1	1	-1	-1
Δ_3	1	1	1	1	-1
Δ_4	1	-1	1	-1	1
Δ_5	2	0	-2	0	0

Table 3.2: Character table of the symmetry point group C_{4v}.

3.3 Numerical parameters and precision

The pseudopotentials of Al, Ga and As are generated from the ground-state configuration of atoms with spin unpolarized electrons. The atomic configurations, their local parts used for the nonlocal KB form and their cutoff radii of Al, Ga and As are given in Tab. 3.3. In this chapter, we treat the Ga $3d$-electrons as core electrons.

atom	configuration	local part KB	r_c^s	r_c^p	r_c^d	r_c^f
Al	$3s^2 3p^1 4d^0 4f^0$	d	2.20	2.20	2.20	–
Ga	$4s^2 4p^1 3d^0 4f^0$	f	2.20	2.20	2.70	2.70
As	$3s^2 3p^3 3d^0 4f^0$	f	2.20	2.20	2.70	2.70

Table 3.3: Parameters of the Troullier-Martins pseudopotentials in the Kleinman-Bylander form.

The supercell calculations are performed with a kinetic energy cutoff of 16 Ry for the plane-wave basis and using a (6,6,2) Monkhorst-Pack (MP) k-point grid. Bulk computations for Al and GaAs are performed using a 4-atom tetragonal unit cell with a kinetic energy cutoff of 40 Ry and a (16,16,16) MP grid. The Fermi energy, E_F, of the metallic systems is determined using a Gaussian electronic-level broadening scheme with a standard deviation of 0.01 Ry.

With these parameters, the numerical convergence of the electronic energies is about 0.05 eV. The overall uncertainty on the interface-state energies relative to E_F, which is mainly attributed to the neglect of many-body effects within the LDA, is estimated as ~ 0.1 eV.

3.4 Interface states in the semiconductor optical gap

We have examined the probability density of electronic states with energy in the range [E_F−1.5 eV, E_F+1.5 eV]. For energies near the GaAs valence band edge, i.e. about 1 eV below the Fermi energy, we find bonding-like, evanescent states at the interface. Conversely, at energies of about E_F + 1 eV, i.e., near the conduction band edge, evanescent anti-bonding-like states occur. The behavior of such states is generally consistent with Tersoff's model description of the metal induced gap states [54, 148–152].

In the midgap region, instead, the electronic states are of a different nature. In Fig. 3.4 we display, in the plane containing the neighboring, interfacial Al and As atoms, the contour plot of the integrated probability density of all electronic states with energy in the range [E_F − 0.25 eV, E_F + 0.25 eV]. They amount to 11.15 electrons per supercell. The probability density assumes particularly large values near the interfacial Al atom as well as near the Ga cation closest to the interface (second semiconductor layer from the metal) indicating a Ga–Al intermetallic bonding structure. The probability density is also high on the As atom terminating the semiconductor slab, where the contours are similar to those of a dangling-bond surface state. The behavior of the probability density in the midgap region does not correspond to that expected for semiconductor bonding or anti-bonding states, which are predicted by Tersoff's model. Rather, it indicates the existence of interface states of a different type.

Investigation of the single-state contributions to the integrated probability density shown in Fig. 3.4, which derives from different regions of the BZ, indicates that the intermetallic bonding feature at the interface is mostly attributed to electronic states near the **J**-point of the BZ. Inspection of the charge density of individual electronic states at **J** reveals an interface state with energy E_F − 0.2 eV which is fully localized at the junction.

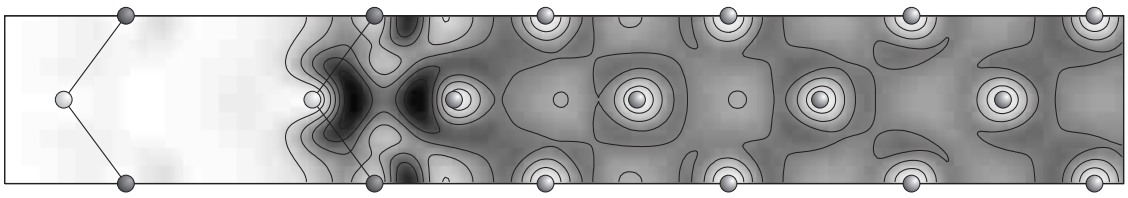

Figure 3.4: Contour plot, in the basal plane including interfacial Ga, As and Al atoms, of the integrated probability density of all electronic states with energy in the range [E_F-0.25 eV, E_F+0.25 eV]. Contour spacing is $3 \cdot 10^{-3} e/a_0^3$.

The contour plot of the probability density of this state is displayed in Fig. 3.5. It shows an Al–Ga intermetallic bonding structure which is clearly related to the high-probability-density feature observed at the interface (see Fig. 3.4). We note that the bond length of this structure is about 3 Å, which is remarkable since it is almost a factor two larger than the average interatomic bond length in covalent solids. Furthermore, the distribution of the probability density at the outermost As-atoms reveals a structure very similar to that of dangling bond surface states.

In Fig. 3.6, we show the Al/GaAs(001) interface band structure calculated in the supercell ($k_z = 0$), along the high symmetry lines **Γ**-**J**-**K** of the BZ. The electronic bands are displayed in an energy window covering the GaAs band gap. The bulk PBSs of GaAs and of Al (strained) are also shown in this figure. Both bulk PBS's are aligned with respect to the electron energies of the interface in accordance with macroscopic average of the electrostatic potential. The resulting Schottky barrier $\phi_p = 0.63$ eV is consistent with previous results [78,87,153] obtained from *ab initio* LDA-calculations.

At 11.7 eV and 8.3 eV below the Fermi energy occur around the **K** point electron states which are neither degenerate with bulk GaAs nor with bulk Al states. The lower one corresponds to an As 4*s* which feels a more attractive potential than other As states in the semiconductor. Thus, it is shifted down in energy below the bulk As 4*s* bands. The higher one corresponds to a Ga 4*s* which is shifted downwards below bulk Ga bands. These states cannot propagate into the two bulk materials and decay exponentially on both sides of the junction, which confirms the results provided in [154].

The Al PBS fills up almost entirely the semiconductor gap region, leaving only a small common gap near the **J** point for energies in the range from $E_F - 0.7$ eV to $E_F - 1.3$ eV. The localized interface state at **J** occurs at higher energy, and is indicated by the solid point in Fig. 3.6. This state is clearly degenerate with electronic states of bulk Al. Its localization derives from the fact that it has different symmetry (Γ_1) with respect to the Al bulk continuum states of the same energy and it does not interact with these states.

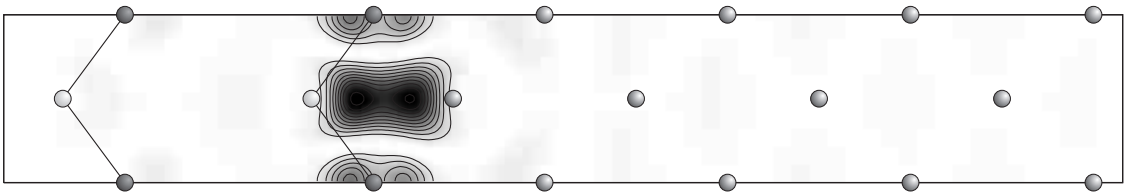

Figure 3.5: Contour plot of the probability density of the localized interface state at the **J** point of the 2D-BZ. Same plane and contour spacing as in Fig. 3.4.

We note that such a situation is actually known [155–157] to occur in the case of the surface state of Al(001) for energies in the range from $E_F - 0.5$ eV to $E_F - 1$ eV. In our case we find that, as in the case of the Al(001) surface state in [155–157], the localized state at **J** is even with respect to the σ_{1v} reflection in the xz plane (see Fig. 3.7), whereas Al bulk states with the same energy at **J** are odd with respect to σ_{1v} (see Fig. 3.7). Thus, similarly to the case of the Al surface state, the Al/GaAs interface state cannot mix with electronic states of the Al bulk continuum and remains localized. The above similarities, together with the As dangling-bond surface structure appearing in the probability density of Fig. 3.4, suggest that localized states of the isolated Al(001) and GaAs(001) surface might be relevant for understanding the nature of the Al/GaAs(001) interface state.

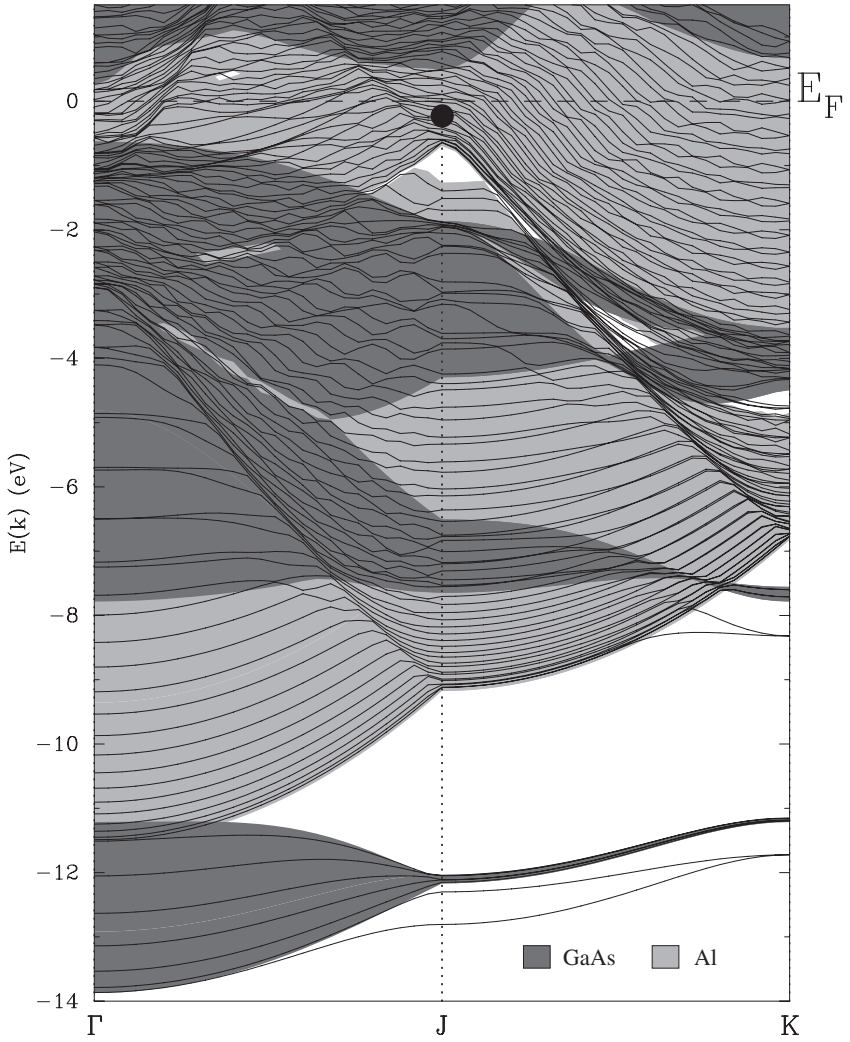

Figure 3.6: Electron band structure of the Al/GaAs(001) interface. The solid point indicates the localized interface state at **J**. The projected band structures of bulk GaAs (dark grey) and of epitaxially strained bulk Al (light grey) on GaAs(001)are also indicated.

In order to better understand the metal and semiconductor surface contributions to the localized interface state, we have studied the energies of the electronic states in the supercell as a function of the interfacial distance d, from its equilibrium value d_0 up to the value $d = 15\ a_0$, where the Al and GaAs surfaces are essentially non interacting. This allows us to identify unambiguously the dominant metal and semiconductor contributions as well as the interaction mechanism responsible for the formation of the interface state. As mentioned before, the atomic configurations of the Al and GaAs slabs are kept frozen while increasing d, i.e., for large values of d we obtain an artificial unreconstructed GaAs slab and a strained metallic Al slab with their (001) surfaces. As a first step, we decided to study the electronic structure of such frozen slab surfaces.

3.5 The Al(001) and GaAs(001) surfaces

The surface of the strained Al(001) slab was studied using a supercell including 41 layers of Al and 9 equivalent vacuum layers. Such a thick Al slab was used to ensure negligible interactions between the two slab surfaces. The Al(001) surface state is indeed characterized by a very slow decay within the bulk material (decay length of $\sim$ 20 Å) [156]. The Al slab calculations were carried out with a 32 Ry cutoff and using a (6,6,2) MP grid. Fig. 3.7 shows the PBS of the strained Al bulk along the **Γ**-**J**-**M** and **Γ**-**X** high-symmetry lines of the Al 1x1 surface BZ. In this figure, we distinguish by different shadings the states which are even or odd relative to the mirror plane which is parallel to the relevant high symmetry line, i.e., the σ_v reflection along **Γ**-**J**-**M** and the σ_d reflection along **Γ**-**X**. A stomach gap is present below the Fermi energy for Al bulk states with even symmetry. At **J** the gap extends from $E_F-1.2$ eV to E_F. In the stomach gap we show the dispersion of the Al(001) Shockley surface state with Δ_1 symmetry (see Table 3.2). Along the **J**-**M** line, the surface state becomes degenerate with Al bulk states with odd symmetry. As it cannot interact with such states, the surface state remains localized along **J**-**M** below the Fermi energy until it enters the continuum of bulk states with even symmetry. We note that at **J** the energy of the localized surface state of strained Al(001) is about $E_F-1.0$ eV, i.e. $\sim$ 0.8 eV below the energy of the Al/GaAs(001) interface state with respect to the interface Fermi level.

In the middle of the **J**-**M** line, a stomach gap of bulk states with even symmetry occurs. Therein we found another localized surface state with even symmetry and a similar structure compared to the one reported at **J**. We note, that we have studied the symmetry properties of the electron states for bulk Al and the Al(001) surface in the (1×1) geometry with one atom at the origin of the unit cell.

In order to investigate the effect of the applied strain on the electronic structure of the Al(001) surface, we calculated the surface states and projected band structures of Al(001) surface without applied strain. We can conclude that the applied strain has a negligible effect on the electronic structure since the shifts of bulk and surface energies are negligibly small.

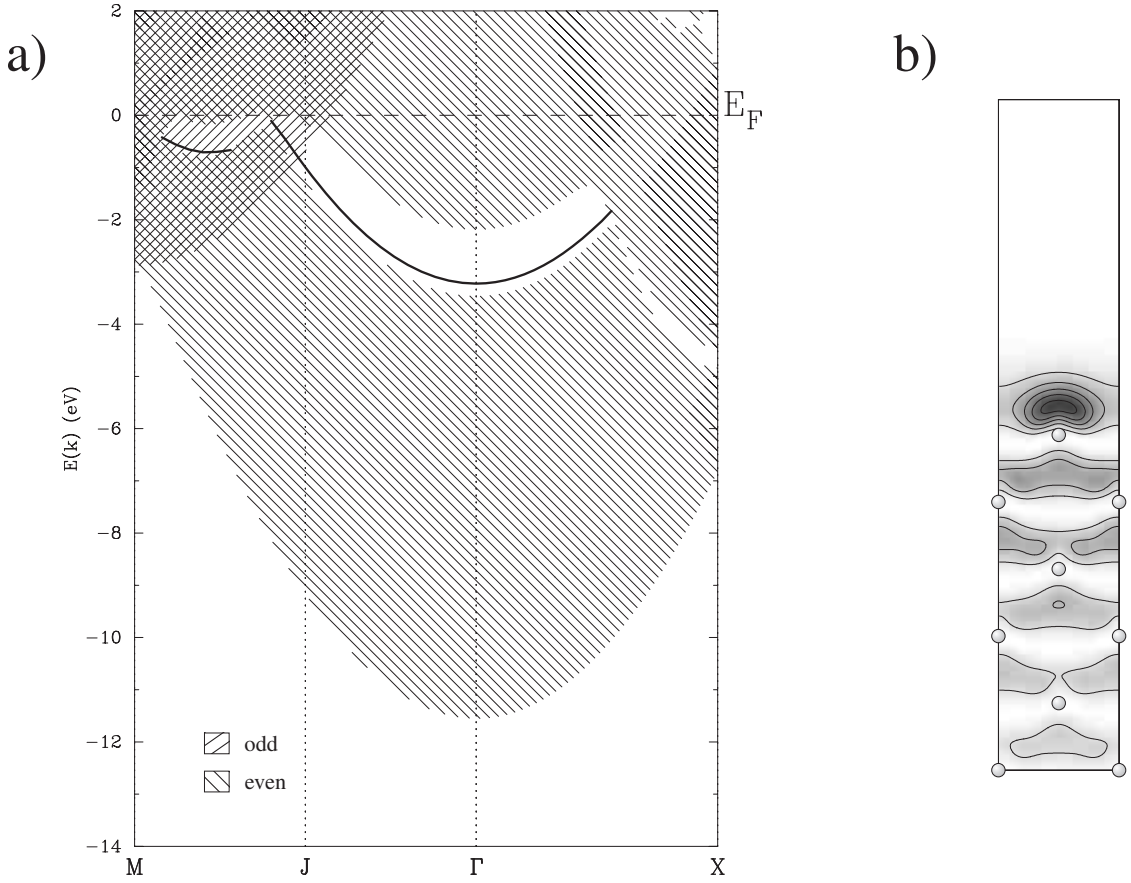

Figure 3.7: a) Dispersion of the localized surface states of the epitaxial strained Al(001) surface along high-symmetry lines of the surface BZ. The left(right)-hatched area shows the projection of epitaxially strained Al bulk states which are even(odd) with respect to the mirror plane parallel to the relevant high-symmetry line and orthogonal to the surface. **b)** Contour plot of the surface state at **J**.

The isolated, As-terminated GaAs(001) slab is artificial since the ideal, unreconstructed (001) surface of GaAs is metallic and unstable against surface reconstructions [158,159]. For this system, we obtain surface states with energies comparable to those obtained in previous work [160,161]. The projected band structure of bulk GaAs with the dispersions of the surface states of the unreconstructed GaAs(001) surface along the lines of high symmetry are shown in Fig. 3.8. In particular, the path **Γ**-**J**-**K**-**J′**-**Γ** represents the border of the square IBZ of the surface. The direct band gap of bulk GaAs at **Γ** is calculated as 0.88 eV. The underestimation with respect to the experimental value of 1.52 eV [162] is very typical for LDA calculations. The Fermi level coincides in this calculation with the valence band maximum (horizontal line in Fig. 3.8).

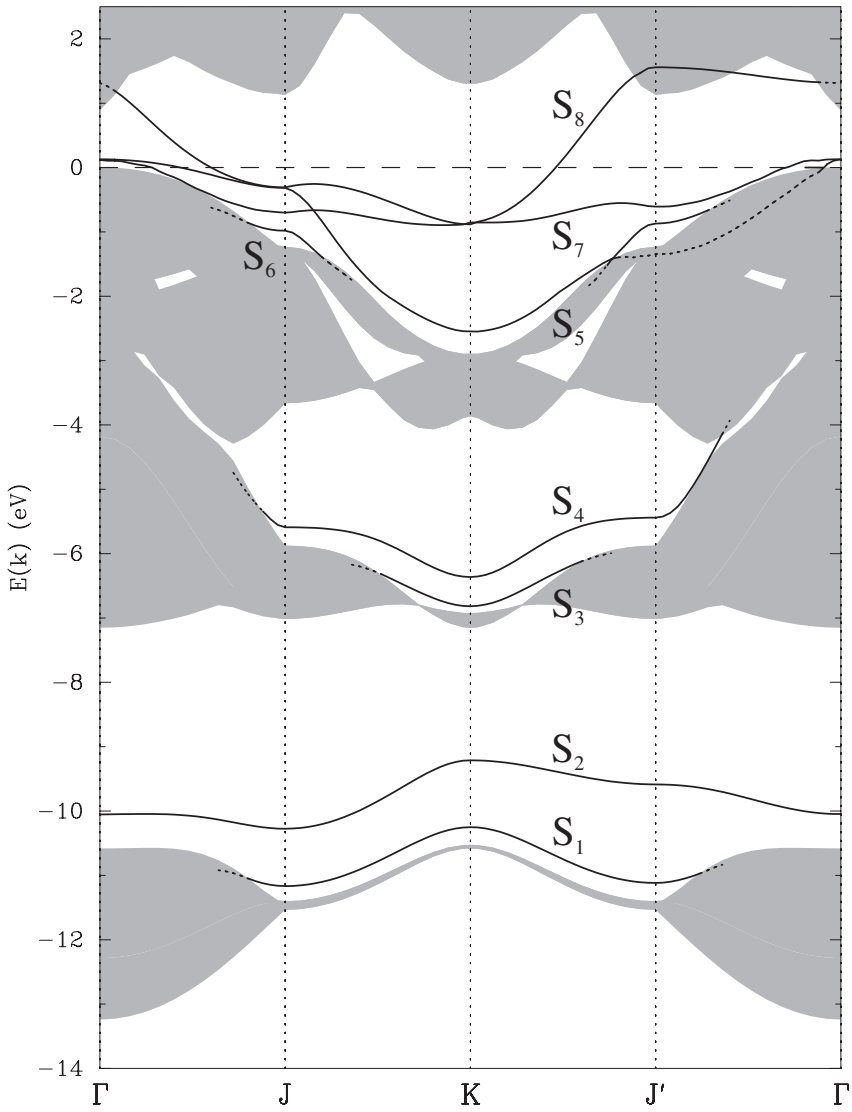

Figure 3.8: Dispersion of the localized surface states S_1 to S_8 of the unreconstructed GaAs(001) surface along high-symmetry lines of the surface BZ. The shaded areas indicate the projection of GaAs bulk states onto the basal plane of the BZ. Solid (dotted) lines indicate localized (resonant) surface states. Energies are given with respect to the valence band maximum.

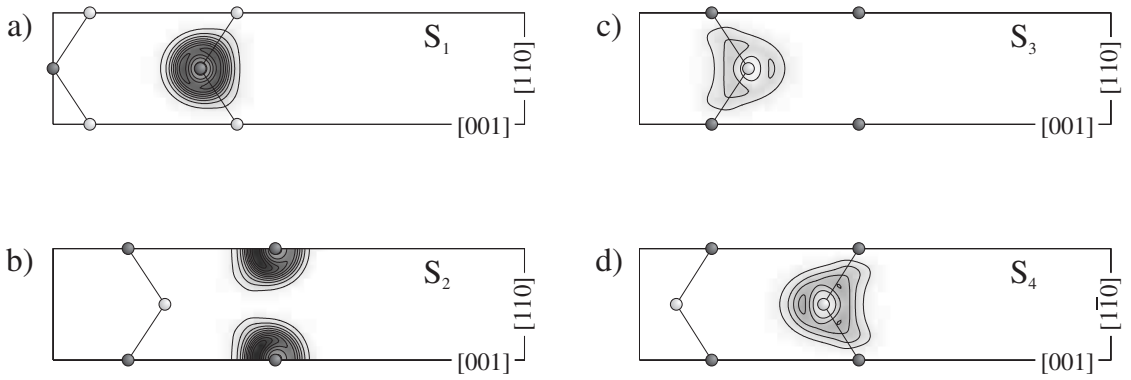

Figure 3.9: Contour plot of the surface states S_1 up to S_4 of the GaAs(001) surface at the **K** point of the BZ. The crystal directions are indicated at the right side of the plots. S_1 is shown in the central plane of the unit cell (see Fig. 3.1) while the other states are shown in border planes of the unit cell. Contour spacing is $5 \cdot 10^{-3} e/a_0^3$.

The four surface states S_1 to S_4 have energies from -11 eV up to -5 eV below the Fermi energy. Fig. 3.9 shows a contour plot of these four states at the **K** point of the BZ. S_1 and S_2 are related to 4*s*-orbitals of the As atoms while S_3 and S_4 are attributed to Ga 4*s*-orbitals. $S_1(S_2)$ has at the **K** point $\Gamma_3(\Gamma_1)$ symmetry (see Tab. 3.1). $S_3(S_4)$ has $\Gamma_4(\Gamma_2)$ symmetry. All four surfaces states can be identified as Tamm [44, 45] surface states: the surface is a perturbation of the periodic crystal potential and influences in particular the electrostatic potential of the GaAs slab near the surface. This affects the surface bands associated with atoms near the surface. In our case, the atomic levels are shifted to higher energies so that they are no longer degenerate with bulk GaAs bands. We note that the shift of the surface states to higher energy is in contrast to the energy shift of the two interface states in the lower part of the interface band structure, shown in Fig. 3.6, downwards to lower energy. As a consequence, these states become localized. Their probability density is localized around the surface atom which is very typical for Tamm surface states. In our case the effect of the surface is so strong that also the energy bands of the second Ga (S_3) and As (S_1) layers are shifted to higher energies.

The four surface states S_5 to S_8 have energies within the optical band gap. Contour plots of their probability density at the **J** point of the BZ are shown in Fig. 3.10. At this point, the energy of the S_6 and S_7 states are 1.0 eV and 0.6 eV below the Fermi energy, respectively. The states S_5 and S_8 have energies very close to each other at 0.3 eV below E_F.

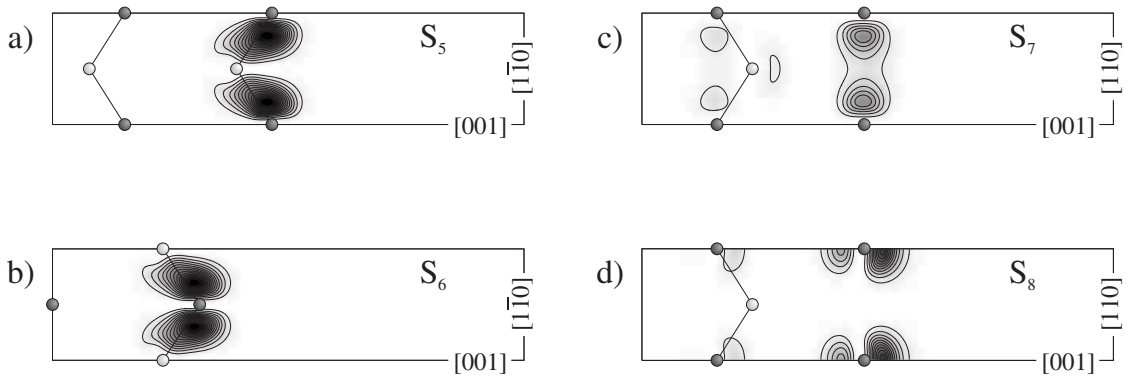

Figure 3.10: Contour plot of the surface states S_5 up to S_8 of the GaAs(001) surface at the **J** point of the BZ. The crystal directions are indicated at the right side of the plots. S_6 is shown in the central plane of the unit cell while the other states are shown in border planes of the unit cell. Contour spacing is $5 \cdot 10^{-3} e/a_0^3$.

The Tamm surface state S_5 has at **J** Γ_2 symmetry and is localized along the path **Γ**-**J**-**K**. Along the line **K**-**J′**, the state becomes degenerated with bulk states and delocalizes. However, it remains resonant along the line **J′**-**Γ** and becomes localized close to the **Γ** point. It is attributed to a $4p_y$-orbital of the interfacial As atom. The y direction is the one parallel to the atomic zigzag chain at the surface (see Fig. 3.1). The probability density shows a bonding-like structure with the Ga atom indicating that this state is a superposition of $4p_y$-orbitals of the Ga and As atoms.

The surface state S_6, very similar to S_5, is localized only in regions of the BZ which are close to **J** and **J′**. It has at **J** Γ_3 symmetry and is localized at the As atom of the second As layer. We can conclude here, that electron states corresponding to As $4p$-orbitals are also shifted to higher energies.

The origin of the two surface states S_7 and S_8 is different. The missing cation at the surface leads to a dangling bond and to a bridge bond surface state. At the **J** point, S_7 corresponds to the bridge bond state, has Γ_4 symmetry and is mainly related to the $4p_x$-orbitals of the interfacial As atoms. The bridge bonds are in the x plane, i.e. orthogonal to the atomic zigzag chain at the surface. The dangling bond surface state S_8 has at **J** Γ_1 symmetry. It derives mainly from the $4p_z$-orbitals of the interfacial As atoms, polarized towards the vacuum.

The two surface states S_7 and S_8 are localized over the whole Brillouin zone. The classification as dangling bond and bridge bond state is not straightforward: along the lines **Γ**-**J** and **K**-**J**′, where the symmetry operation σ_{1v} is not valid, these two states are both even with respect to σ_{2v}. They interact along these lines and the resulting states are superpositions of dangling bond and bridge bond surface states. At **Γ** S_7 is the dangling bond state and S_8 has the bridge bond character. In Fig. 3.8, an anti-crossing of the bands corresponding to these two surface states along the lines **Γ**-**J** and **K**-**J**′ can be observed. In Fig. 3.11 we show contour plots of the probability density of the two states along the line **Γ**-**J**. Therein we show the exchange of dangling bond and bridge bond character.

We note that S_8 is a localized surface state also at **J**′ since it has different symmetry compared to degenerate bulk GaAs states.

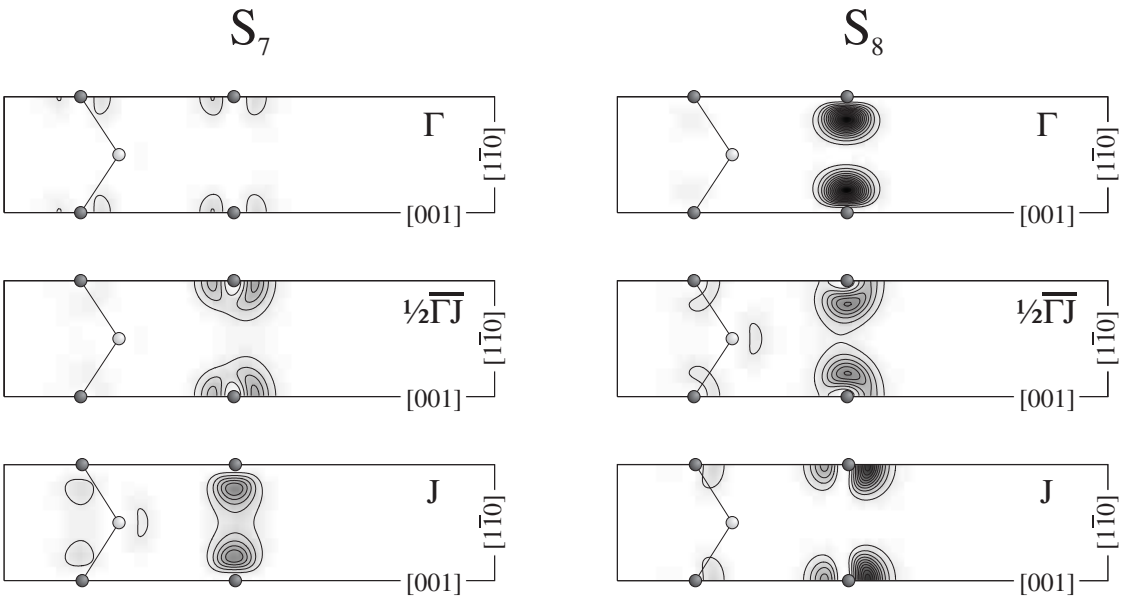

Figure 3.11: Contour plot of the surface states S_7 and S_8 of the GaAs(001) surface along the high symmetry line **Γ**-**J** of the BZ. Contour spacing is $5 \cdot 10^{-3} e/a_0^3$.

3.6 Evolution from surface to interface states

We have examined the energy band structure of the Al/GaAs(001) superlattice as a function of the interfacial distance d. Fig. 3.12 shows the energy as a function of d of those electronic states at the **J** point, which are close to the Fermi energy and have Γ_1 symmetry. The figure also indicates the calculated position of the conduction and valence PBS edges of the semiconductor as well as the stomach gap of Al bulk states with even symmetry at **J**. Solid lines indicate localized states while dotted lines indicate resonances.

For $d = 15\ a_0$, we recover the surface states of the isolated, strained Al(001) surface and of the unreconstructed, As-terminated GaAs(001) surface. The dangling-bond surface state of the latter surface occurs at E_F-0.3 eV. Furthermore, two localized Al surface states occur at about E_F-0.9 eV. It has to be noted, that the tetragonal supercell corresponds to an Al(001) $c(2\times2)$ surface, with two atoms in the unit cell, and therefore two surface states occur. Due to the finite size of the Al slab, these surface states interact and their energies split. This splitting is 0.15 eV (0.03 eV) for an Al slab consisting of 23 (41) layers.

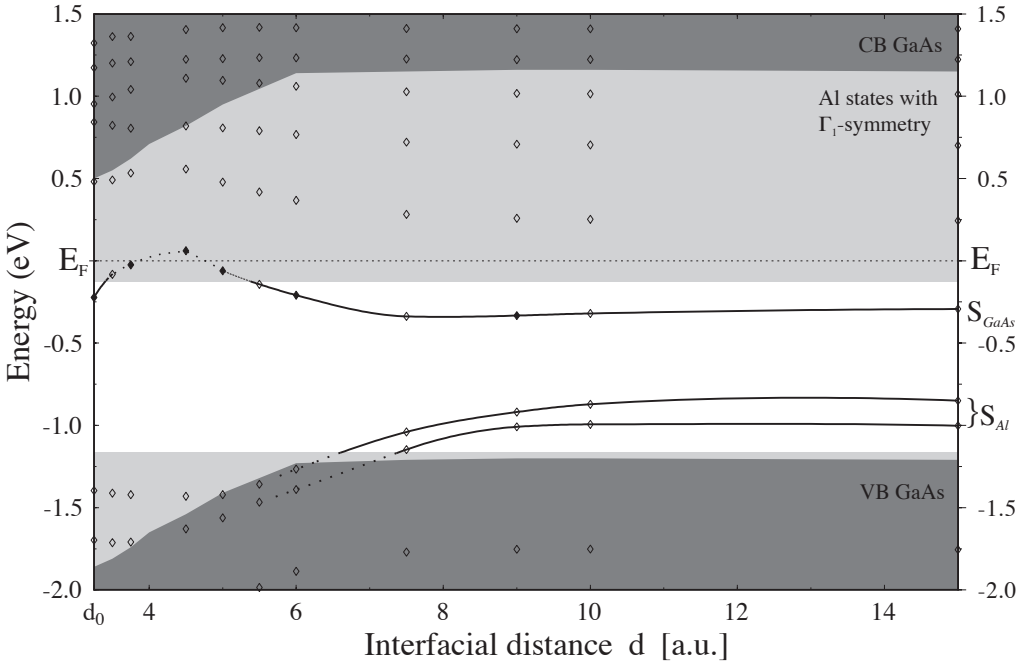

Figure 3.12: Energy levels of the electron states of the Al/GaAs(001) superlattice at the **J**-point of the Brillouin zone as a function of interfacial separation between GaAs and Al slabs. Localized (sol and resonant (dashed) states with Γ_1 symmetry are represented. Diamonds indicate calculated levels of the superlattice. Light grey areas indicate the band energies of bulk Al states with even symmetry. Dark grey areas show bulk GaAs conduction and valence band energies.

Reducing the interfacial distance, the Al surface states interact with the dangling bond surface state of the semiconductor resulting in a level repulsion. We note here, that the GaAs(001) dangling bond surface state is the only localized surface state in the optical band gap which has at **J** odd (even) symmetry with respect to the symmetry operation σ_{1v} (σ_{2v}). It is therefore the only GaAs surface state which can interact at **J** with the surface state of the Al slab. As a consequence, for interfacial distances smaller than $9a_0$, Al/GaAs interface states are a superposition of these two types of states. Decreasing further the interfacial distance to about $d = 7\ a_0$, the lower interface states leave the stomach gap of the Al bulk states with even symmetry, enter into the continuum, and delocalize.

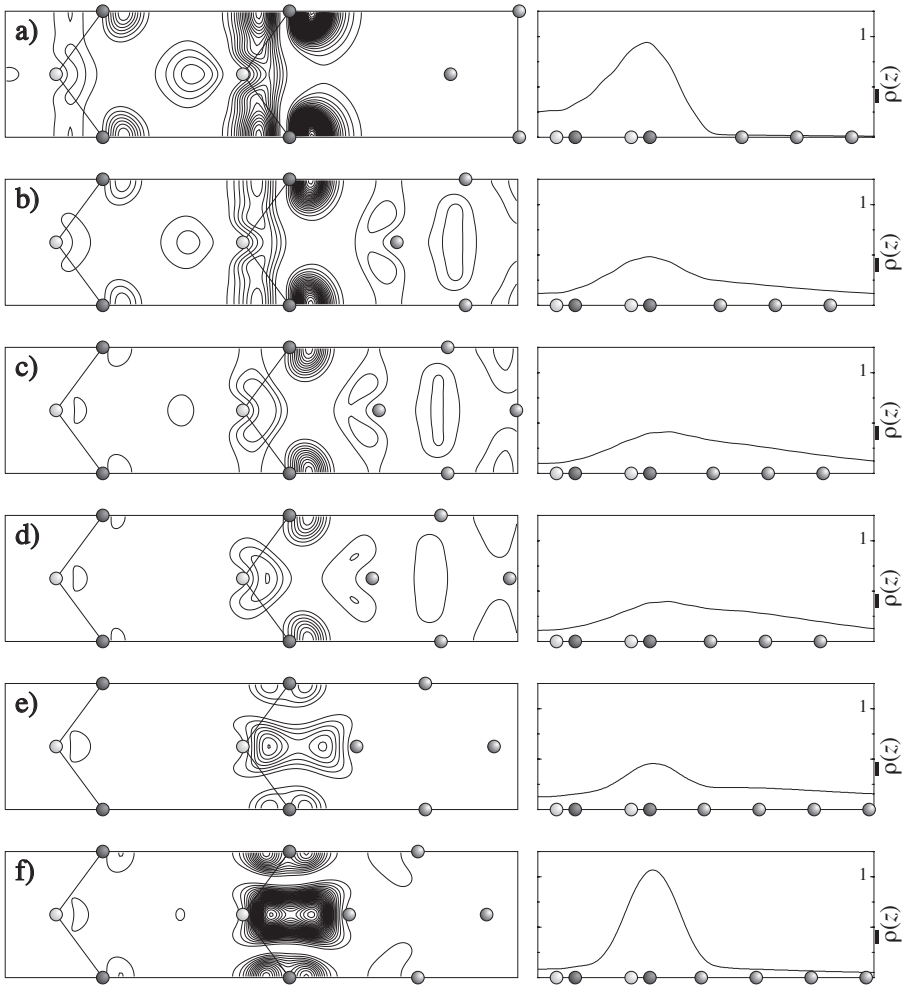

Figure 3.13: Contour plot (left panel) and macroscopic planar average $\overline{\overline{\varrho}}$ (right panel) of the probability density of the Al/GaAs(001) interface state at **J** for selected values of the interfacial distance d: $9a_0$(a), $6a_0$(b), $5a_0$(c), $4.5a_0$(d), $3.75a_0$(e) and $3.25a_0$(f). Contour spacing is $1 \cdot 10^{-3} e/a_0^3$. Units of $\overline{\overline{\varrho}}(z)$ are $1 \cdot 10^{-4} e/a_0$.

For interfacial distances less than 5.5 a_0, the upper interface state raises in energy with respect to the Fermi energy, crosses the upper edge of the stomach gap of even bulk Al states, and enters the continuum. For interfacial distances smaller than $d = 3.5\ a_0$, the upper interface state lowers in energy, re-enters the stomach gap, and re-localizes. The latter behavior is observed when the interface state is approaching the GaAs conduction PBS edge, whose energy decreases monotonously with respect to E_F for $d < 6\ a_0$. The behavior of the upper interface state for small values of d, together with the monotonic decrease of the GaAs conduction band, suggests a repulsion of the interface state from the semiconductor conduction-band edge at **J**.

The above picture, including the level repulsion, is supported by a study of the changes taking place in the probability density of the upper interface state as a function of interfacial distance. Fig. 3.13 shows contour plots of the probability density in the supercell basal plane for several values of d as well as the corresponding macroscopic average of the probability density along the growth axis, which yields a measure of the localization at the interface.

For $d \geq 9\ a_0$ (see Fig. 3.13.a), we recover the probability density of the localized dangling bond surface state of GaAs(001). For $d = 6\ a_0$ (Fig. 3.13.b), the interface state is a superposition of the GaAs dangling-bond and Al surface states. At $d = 5\ a_0$ (Fig. 3.13.c), a Ga-related feature appears with maximum probability density in the direction of the Al surface atom. The presence of this feature is ascribed to the interaction of the interface state with low-energy conduction band states of GaAs at **J** (see below). We note that the localization of the interface state at the junction reduces considerably at such intermediate distances (5 a_0 - 4.5 a_0) (Fig. 3.13.c, d), when the interface state leaves the stomach gap to enter the continuum of Al even states and becomes a resonance. The formation of the bonding-like structure between the outermost Ga cations of the semiconductor and the interfacial Al atoms for $d \leq 3.75\ a_0$ (see Fig. 3.13.e) gives rise to the dominant feature of the localized interface state found at $d = 3.25\ a_0$ (Fig. 3.13.f).

3.7 GaAs conduction band edge states

The origin of the Ga-related feature of the localized interface state at Al/GaAs(001) was further investigated by examining the probability density of the lowest GaAs conduction states that contribute to the PBS at **J**. In Fig. 3.14, we show the probability density of the GaAs bulk state with Γ_4 symmetry (in the bulk tetragonal cell), which corresponds to the minimum of the conduction PBS at **J**. This state derives from Bloch states of the **L** conduction-band minima of the bulk GaAs 3D BZ, which are projected onto **J** in two dimensions. The probability density of this state is large near the Ga atom, with a structure which is similar to that of the Ga-related feature involved in the formation of the Al–Ga intermetallic bonding structure in Fig. 3.13. We conclude thus that the decrease in energy of the interface state for small d, which corresponds to the formation of the intermetallic bonding structure, derives from an interaction with the continuum of GaAs bulk states near the conduction band minimum at **L**.

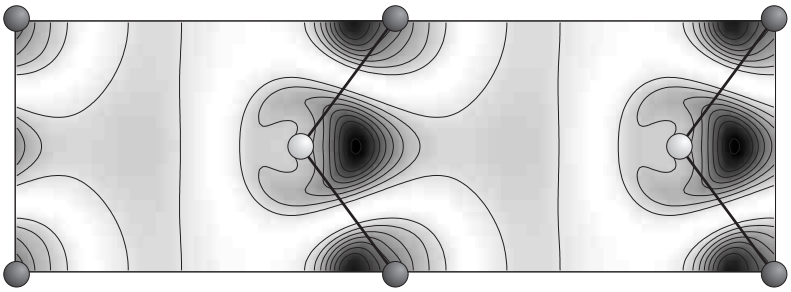

Figure 3.14: Contour plot of the probability density of the bulk GaAs state with Γ_1 symmetry which occurs at the conduction band minimum of the PBS at **J**. This state derives from GaAs Bloch states at the **L** conduction-band minima of the bulk 3D BZ. Contour spacing is $3.5{\cdot}10^{-3} e/a_0^3$.

3.8 Discussion

We have studied the nature of the electronic states with energy in the semiconductor band gap at abrupt, As-terminated, epitaxial Al/GaAs(001) junctions. The results indicate the existence of electronic states near the Fermi energy which exhibit a high probability density at the interface. In particular, we find a localized interface state at the **J**-point of the interface Brillouin zone. These states have an unexpected nature, namely an intermetallic, bonding-like character across the interface between outermost Al atoms in the metal and Ga atoms in the second atomic layer of the semiconductor.

The mechanism responsible for the formation of the localized interface state at **J** has been identified by studying the electronic energies as a function of the interfacial distance d. We have found that the interface state derives from an interaction between localized states of the isolated Al(001) surface and GaAs bulk conduction band-edge states, mediated by dangling bond surface states of the isolated, unreconstructed GaAs(001) surface. It remains now to verify whether the interaction process identified in this chapter occurs for interfaces other than Al/GaAs(001). This will be discussed in the two following chapters investigating Al/AlAs and metal/GaN junctions.

4 Midgap interface states at epitaxial Al/AlAs(001) heterojunctions

In the following chapter, we investigate whether the interface states calculated in the previous chapter for Al/GaAs occur also in other junctions. With this goal we examine the abrupt epitaxial, As-terminated Al/AlAs(001) interface [163]. AlAs is also an ideal candidate for epitaxial junctions to Al since it has approximately the same lattice constant as GaAs and the Al overlayer can be grown almost lattice matched on the AlAs substrate. A comparison of the electronic structure of the contact allows us to investigate the dependence of interface states on the electronic properties of the semiconductor. The main differences between the electronic structure of GaAs and AlAs are that AlAs is an indirect semiconductor with a larger band gap compared to GaAs. The experimental value of the indirect gap ($\mathbf{\Gamma}$-$\mathbf{X}$) is 2.24 eV [162]. The direct occurs gap at $\mathbf{\Gamma}$ and its value is 2.89 eV, while in our LDA calculations, we obtain 1.33 eV for the direct band gap at $\mathbf{\Gamma}$. Thus, bulk conduction band states are expected to occur at higher energy with respect to the Fermi level than in GaAs. Since bulk semiconductor states are supposed to play a role in the formation of localized interface states, we expect interface states at higher energy in the band gap region. If this energy is so high that the corresponding band is not in the stomach gap of even Al states (see Fig. 3.7) we expect interface states with a weaker localization.

In order to allow a direct comparison between the results for the Al/AlAs(001) interface and those obtained for the Al/GaAs(001) contact, the same supercell geometry is used in the two cases. It includes 13 atomic layers of the semiconductor, i.e. here AlAs, and 23 atomic layers of Al, corresponding to a total of 191 valence electrons. The atomic structure of the supercell in the interface region is given in Fig. 4.1a. The theoretical lattice constant of AlAs is $a_{\mathrm{AlAs}} = 5.61$ Å and therefore it is slightly larger than that of GaAs ,$a_{\mathrm{GaAs}} = 5.52$ Å. The experimental values are $a_{\mathrm{GaAs}} = 5.65$ Å and $a_{\mathrm{AlAs}} = 5.66$ Å [162].

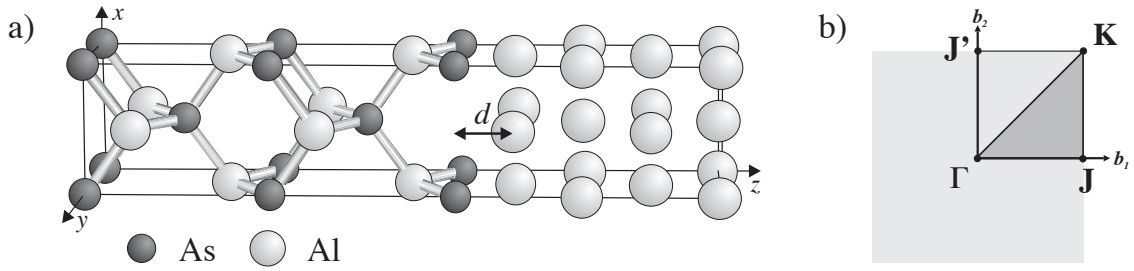

Figure 4.1: a) Atomic structure of the Al/AlAs(001) interface. The interfacial distance d measures the separation between the As and Al planes at the contact. **b)** Two-dimensional BZ of the interface and of the AlAs(001) and Al(001)$c(2\times2)$ surfaces. The basal plane of the irreducible part of the BZ of the supercell used to model the interface is indicated by the dark triangle.

The equilibrium volume of the supercell is $\Omega_s = 6854\ a_0^3$. As in the Al contact to GaAs(001), the Al(001) slab can be grown epitaxially on the AlAs substrate when the Al fcc lattice is rotated by 45° around the [001]-axis with respect to the cubic axes of the semiconductor. The lattice parameter of bulk Al has a small mismatch ($\sim$1%) to that of the substrate. Using an in-plane lattice constant $a_{\mathrm{Al},\parallel} = a_{\mathrm{AlAs}}/\sqrt{2}$ for Al and following macroscopic elastic theory, the lattice mismatch is accommodated by an expansion of the Al overlayer along the growth direction. In our study, we use the theoretical lattice parameter $a_{\mathrm{AlAs}} = 5.61$ Å; macroscopic elastic theory requires $a_{\mathrm{Al},\perp} = 3.99$ Å. The equilibrium distance between the interfacial As and Al planes is $d_0 = 1.9$ Å.

All bulk, surface and interface calculations are performed with the same numerical parameters used in the previous chapter. In particular, the same pseudopotentials, cutoff energies and **k** point grids are used. Thus, we expect for Al/AlAs(001) the same numerical uncertainty on the interface-state energies relative to $\mathrm{E_F}$ as for Al/GaAs(001).

4.1 Interface states in the semiconductor gap

We calculate the probability density of electronic states at several energies within the semiconductor gap. In Fig. 4.2.a we show, in the basal plane containing the interfacial Al and As atoms, the contour plot of the probability density of all electronic states with energy in the range [$\mathrm{E_F}$,$\mathrm{E_F}$+0.5 eV]. They amount to a total charge of 10.52 electrons per supercell.

The probability density exhibits large values near the interfacial Al atoms of the metal as well as on the outermost Al atoms of the AlAs slab indicating an intermetallic bond structure. The density is also high near the As atoms terminating the AlAs slab and the contours are similar to those of dangling bond surface states.

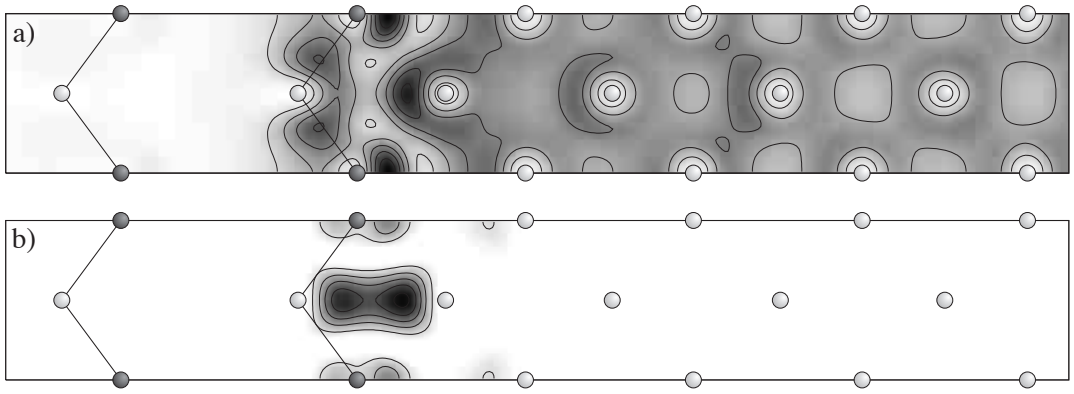

Figure 4.2: a) Contour plot, in the basal plane containing interfacial As and Al atoms, of the integrated probability density of all electronic states of the Al/AlAs(001) superlattice with energy in the interval [E_F,E_F+0.5eV]. **b)** Contour plot of the probability density of the interface state at the **J**-point with energy E_F+0.18 eV. The spacing of the contour lines is $3 \cdot 10^{-3} e/a_0^3$ in both cases.

Direct inspection of the contributions to the integrated probability density given in Fig. 4.2.a, originating from different regions of the Brillouin zone, indicates that the intermetallic Al-Al bonding features come mostly from electronic states near the **J**-point (see Fig. 4.1b). Analysis of the charge density of individual electronic states at **J** reveals one state in the midgap region with energy E_F+0.18 eV which exhibits strong localization at the interface. The contour plot of the probability density of this state at **J** is shown in Fig. 4.2.b and demonstrates an intermetallic bonding-like character between the Al cations closest to the interface and the facing Al atoms of the metal slab. The bond length of this structure is about 3 Å.

Comparison of the results obtained for the Al/GaAs interface reveals that the bonding-like state has, as expected, a higher energy as the one occurring at the Al/GaAs junction. The interface state shown in Fig. 4.2.b is not entirely localized; rather it is a resonant state, i.e. the probability density does not entirely vanish in the metallic Al slab.

The energy bands along the high symmetry lines **J**-**Γ**-**K** of the Al/AlAs superlattice are displayed in Fig. 4.3. The projected band structure (PBS) of bulk AlAs (dark grey) is also displayed and it indicates the energy dispersion of the valence and conduction band edges. The light grey area corresponds to the PBS of bulk Al which fills up the entire semiconductor gap apart from a small stomach-gap at **J** with energy around 1 eV below E_F.

Both bulk PBS's are aligned with respect to the electron energies of the interface in accordance with macroscopic average of the electrostatic potential. We obtain Schottky barrier as $\phi_p = 1.18$ eV which is in good agreement to previous results [78, 141] obtained from DFT-LDA calculations.

The interface state at **J** whose density is shown in Fig. 4.2.b occurs at higher energy than the stomach gap and is indicated by a solid point in Fig. 4.3. It is degenerate with electronic states of bulk Al and its localization is quite strong since most bulk Al states in this energy range have different symmetry. Similarly to the interface band structure of Al/GaAs, interface states, not degenerate with AlAs or Al bulk states, are present at the **K** point at around 7 eV and 11 eV below the Fermi level, respectively. Compared to the Al/GaAs system, they are much closer in energy to the projected bulk states.

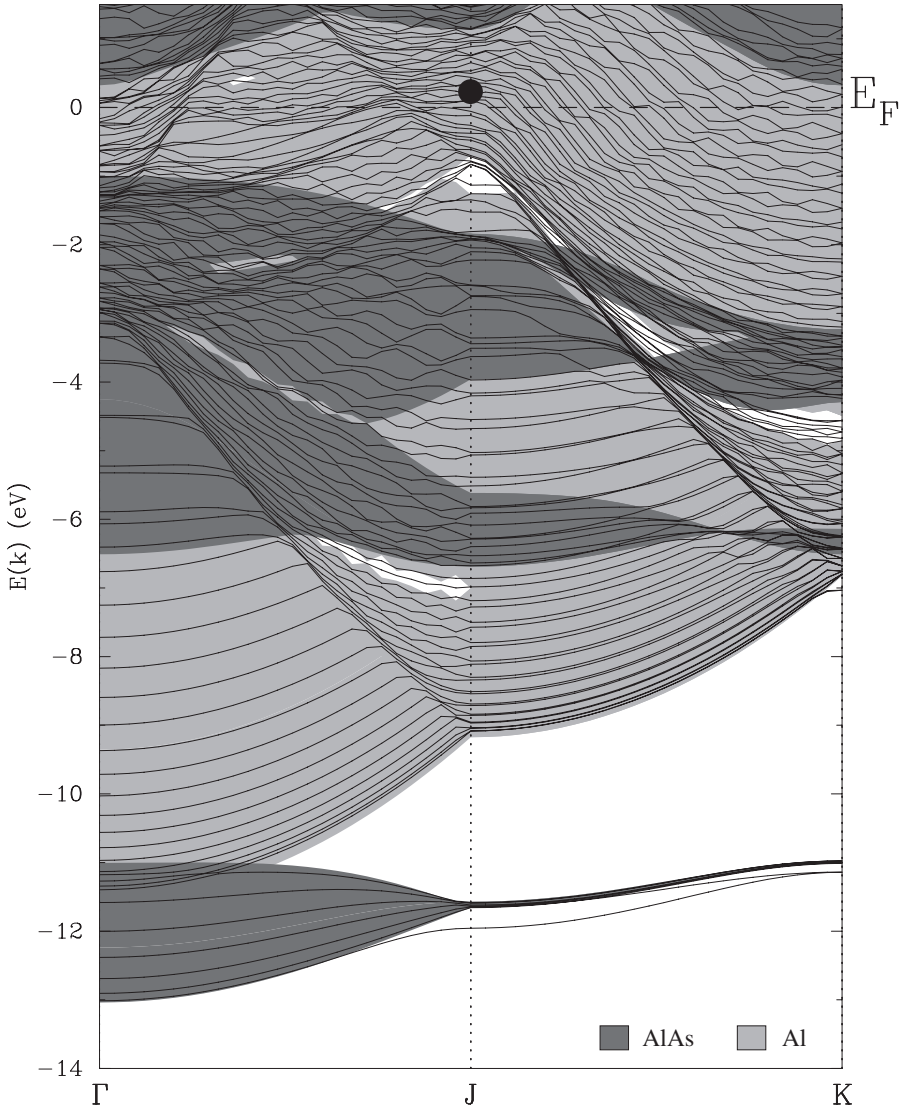

Figure 4.3: PBS of bulk Al (light grey) and bulk AlAs (dark grey). Solid lines show the calculated band energies of the Al/AlAs(001) superlattice corresponding to a 13+23 supercell. The position of the resonant interface state at **J** is indicated with the solid circle.

In order to clarify whether the metal and the semiconductor contributions to the resonant interface state are the same as for the interface state investigated for the Al/GaAs junction, we carried out the study of its energy and wavefunctions as a function of the interfacial distance d. As for the Al/GaAs interface, d is increased from the equilibrium value d_0 up to the value $d = 15a_0$, for which the Al and the AlAs slabs of the supercell are entirely separated and non-interacting. Upon increasing the interfacial distance d, the two slabs are kept frozen in their equilibrium supercell geometry. For the maximal interfacial distance $d = 15a_0$, we obtain surface states for both the strained Al(001) surface and the unreconstructed As-terminated AlAs(001) surface. Upon reducing d we observe an interaction with level repulsion between the dangling-bond surface state of the AlAs(001) and the Al(001) surface state. This produces an anti-bonding AlAs-Al interface state which in turn, at smaller values of d, interacts with low-energy conduction band states of the semiconductor and results at d_0 in the resonant interface state represented in Fig. 4.2.b.

Direct inspection of the conduction band-edge states of bulk AlAs whose symmetry is compatible with that of the interface state, shows that they have a strong charge density near the Al cation which resembles that of the semiconductor component of the Al-Al interface bonding feature.

These results are similar to those calculated for Al/GaAs(001) and confirm the formation mechanism as a robust one. Furthermore, the higher energy and weaker localization of the interface state confirm the role of bulk semiconductor states at the conduction band edge. In order to better understand the differences in the electronic structure between Al/GaAs and Al/AlAs and how they are related to the different semiconductor components of the two junctions, we investigate in the following section the freestanding, unreconstructed AlAs(001) surface and compare the results with those obtained for the GaAs(001) surface calculated in the previous chapter.

4.2 Surface states of AlAs(001)

As for GaAs(001), the isolated, As-terminated AlAs(001) slab is artificial since the ideal, unreconstructed (001) surface of AlAs is metallic and unstable against surface reconstructions [158, 159, 164, 165]. The projected band structure of bulk AlAs and the energy dispersion of the surface states of the unreconstructed, As-terminated AlAs(001) surface along the lines of high symmetry are shown in Fig. 4.4. In order to facilitate the comparison of the surface states of AlAs and GaAs, corresponding surface states of the two systems have the same labels. Since no surface state corresponds the the surface state S_3 of the GaAs(001) surface does not occur, this label is missing for AlAs(001). The Fermi level is located at 0.2 eV above the valence band maximum.

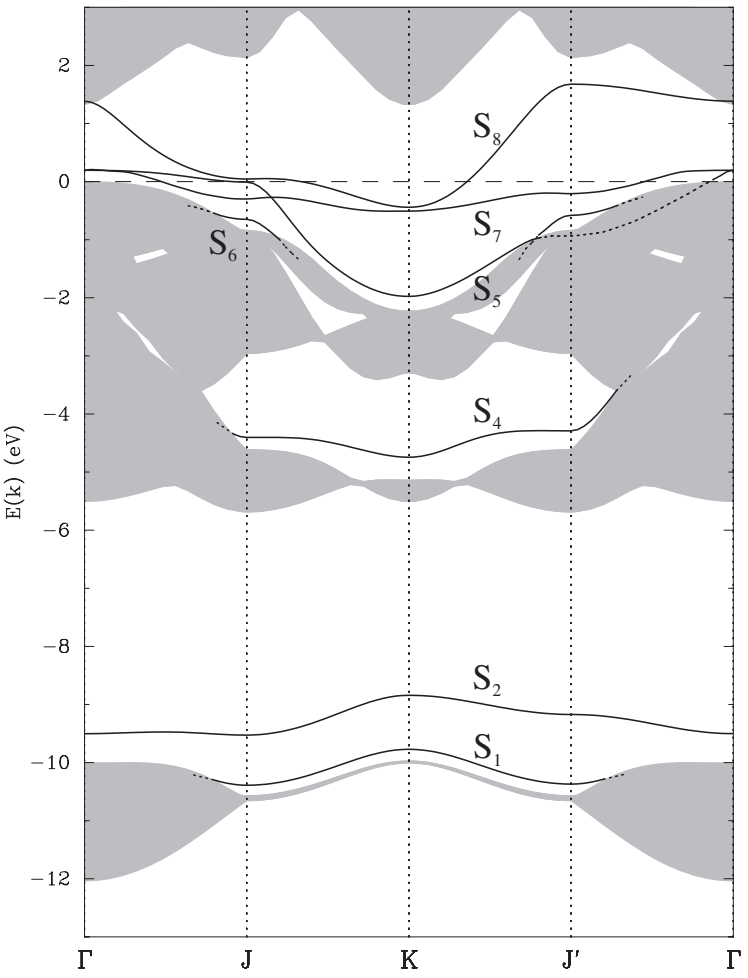

Figure 4.4: Energy dispersion of the localized surface states S_1 to S_8 (S_3 is missing) of the unreconstructed, As-terminated AlAs(001) surface along high-symmetry lines of the 2D BZ. Solid (dotted) lines indicate localized (resonant) surface states. The shaded areas indicate the projection of AlAs bulk states onto the basal plane of the BZ. Energies are given with respect to the valence band maximum which is indicated with the horizontal dashed line.

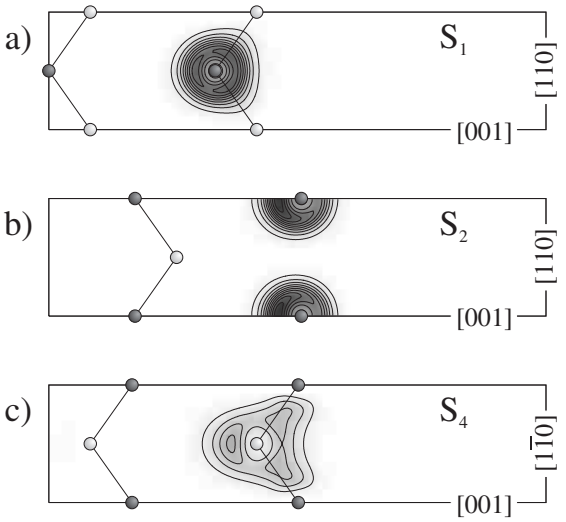

Figure 4.5: Contour plot of the surface states S_1, S_2 and S_4 of the AlAs(001) surface at the **K** point of the BZ. The crystal directions of the representation planes are indicated at the right side of the panels. S_1 is shown in the central plane of the unit cell (see Fig. 4.1.a) while S_2 and S_4 are shown in planes on the surface of the unit cell. Contour spacing is $5 \cdot 10^{-3} e/a_0^3$.

The three surface state bands S_1, S_2 and S_4 have energies ranging from -11 eV up to -4 eV below the Fermi energy. Fig. 4.5 shows a contour plot of the states of these three bands at the **K** point of the BZ. S_1 and S_2 are related to 4*s*-orbitals of the As atoms while S_4 corresponds to Al 3*s*-orbitals partly bonding with neighboring As atoms. These surfaces states are Tamm surface states. As for GaAs, the energy levels of atoms close to the surface are shifted to higher energy so that they are no longer degenerate with bulk AlAs bands. We note that the shift to higher energy of the surface states S_1 and S_2 is opposite to that of the two interface states in the lower part of the interface band structure, shown in Fig. 4.3, which is a shift downwards to lower energy.

The four surface state bands S_5 to S_8 have energies within the optical band gap. Contour plots of their probability density at the **J** point of the BZ are shown in Fig. 4.6. At this point of the BZ, the energy of the S_6 and S_7 states are 0.8 eV and 0.6 eV below the Fermi energy, respectively. The states S_5 and S_8 have energies very close to each other, close to the valence band maximum which is 0.2 eV below E_F.

The Tamm surface state S_5 has Γ_2 symmetry and is localized over a large portion of the BZ including the path **Γ**-**J**-**K**. Along the line **K**-**J′**, the state becomes degenerate with bulk states and delocalizes. However, it remains resonant along the line **J′**-**Γ** and becomes again localized close to the **Γ** point. It corresponds to a $4p_y$-orbital of the interfacial As atom. (see Fig. 4.1.a for the definition of the y direction). The probability density shows some bonding the Al atoms underneath. The surface state S_6 is similar to S_5, but it is localized only in regions of the BZ which are close to **J** and **J′**. It has Γ_3 symmetry and is localized on the As atoms of the second As layer below the surface.

The bridge-bond surface states S_7 and the dangling-bond state S_8 are localized over the whole Brillouin zone. The classification as dangling-bond and bridge-bond state as well as their symmetry properties are the same as for the corresponding states S_7 and S_8 of the GaAs(001) surface: along the lines **Γ-J** and **K-J′**, where the symmetry operation σ_{1v} is not valid, these two states have the same symmetry and in particular they are both even with respect to σ_{2v}. Therefore, they interact along these lines and the resulting states are superpositions of dangling-bond and bridge-bond surface states. At **Γ**, the dangling-bond state is S_7 while S_8 has the bridge-bond character. An anti-crossing of the bands corresponding to these two surface states occurs along the lines **Γ-J** and **K-J′**, as shown in Fig. 4.4. In Fig. 4.7, we show contour plots of the probability density of the states of the S_7 and S_8 bands at different BZ points along the line **Γ-J**. The figure shows the exchange of dangling-bond and bridge-bond character along this line.

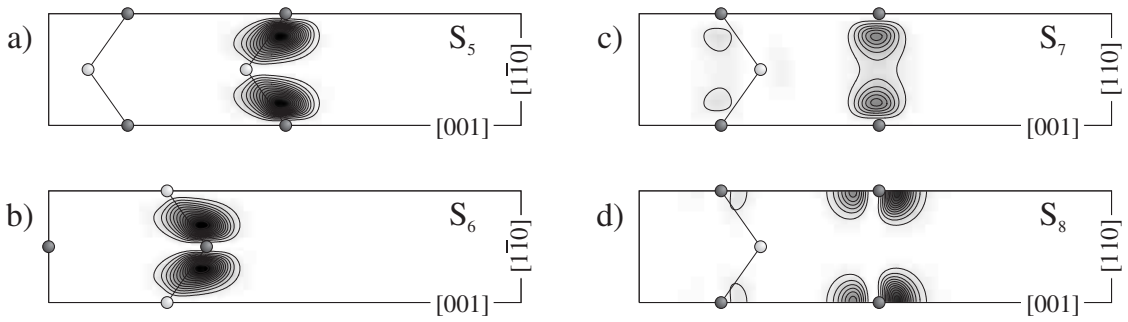

Figure 4.6: Contour plot of the surface states S_5 up to S_8 of the AlAs(001) surface at the **J** point of the BZ. The crystal directions of the representation planes are indicated at the right side of the plots. S_6 is shown in the central plane of the unit cell while the other states are shown in planes on the surface of the unit cell. Contour spacing is $5 \cdot 10^{-3} e/a_0^3$.

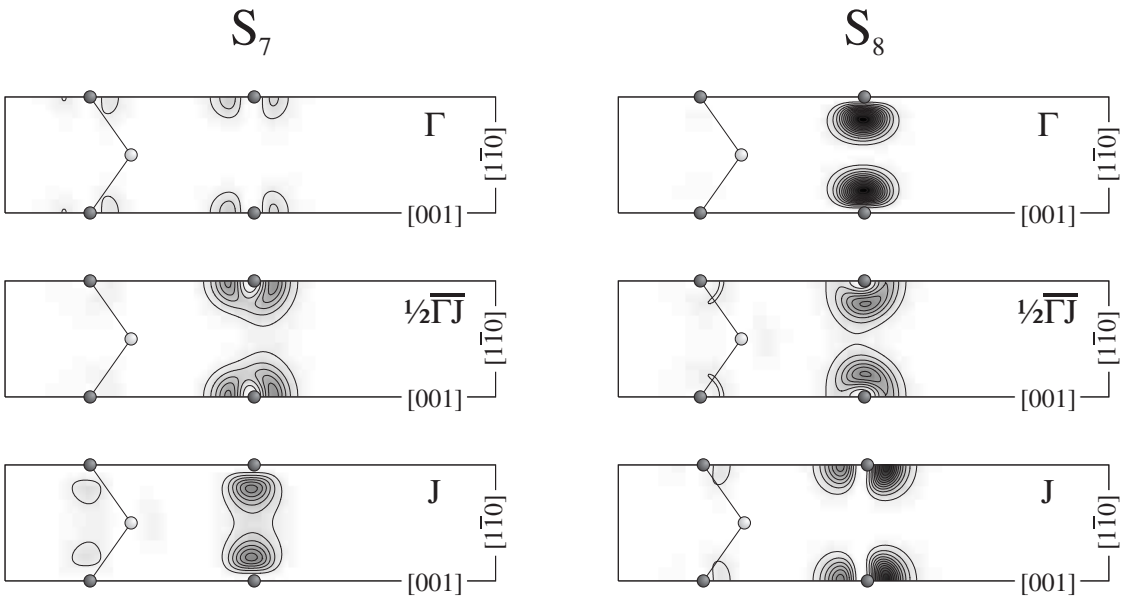

Figure 4.7: Contour plot of the surface states S_7 and S_8 of the AlAs(001) surface along the high symmetry line **Γ-J** of the BZ. Contour spacing is $5 \cdot 10^{-3} e/a_0^3$.

4.3 Discussion

We have studied the nature of the electronic states with energy in the semiconductor band gap at abrupt, As-terminated, epitaxial Al/AlAs(001) junctions. In particular, we investigated those electronic states near the Fermi energy which exhibit a high probability density at the interface. We have found a resonant interface state at the **J** point of the interface Brillouin zone, very analogous to the localized interface state at the Al/GaAs(001) junction. They form an intermetallic, bonding-like state between the interfacial Al atoms of the metal and Al atoms in the second atomic layer of the semiconductor.

The formation mechanism responsible for the resonant interface states at **J** is the same as for the Al/GaAs(001) contact. Due to the larger band gap at **J** for AlAs, the level repulsion is not as strong as in the case of GaAs. Thus, the resulting state does not occur in the stomach gap of Al bulk states with the same symmetry. As a consequence, it is not a localized interface state as for the Al/GaAs contact, but it is a resonant state with a very high probability density at the interface.

5 Interface states at metal contacts to cubic GaN(001)

In this chapter we present our results for epitaxial, abrupt Al, Au and Cu contacts to cubic, N-terminated GaN(001) [166]. The comparison of the results obtained for the Al/GaN interface with those of previous chapters allows us to investigate the effect of different semiconductor electronic properties, from GaAs to AlAs and GaN, on the electronic properties of Al contacts to these semiconductors. Additionally, comparing the results obtained for several metals, Al, Au and Cu, permits to examine the effect of different metal contacts to GaN. In particular, it is of high interest whether localized interface states occur at metal contacts to GaN and if the different metal work functions have an effect on the Schottky barrier height of the junctions we investigate.

We first discuss the structural and electronic properties of bulk *c*-GaN and the GaN(001) surface. In sections 5.2 and 5.3 we investigate the Al/GaN(001) and Au/GaN(001) contacts. Since Al and Au have lattice constants relatively close to that of GaN, we propose a similar geometry at the interface for both metals: the metal atoms continue the gallium fcc sublattice of the semiconductor. In section 5.4, we analyze the electronic properties of the Cu/GaN(001) junction which has an interface structure similar to that of Al/GaAs(001) and Al/AlAs(001) contacts. Unlike the situation for Al/GaAs and Al/AlAs where the metal can be grown almost lattice matched onto the semiconductor surface, Al, Au and Cu have a large lattice mismatch with respect to GaN. This leads to highly strained metal slabs.

5.1 Bulk c-GaN and the GaN(001) surface

In most devices GaN is present in the wurtzite structure, with space group $P6_3mc$. The wurtzite structure consists of alternating close-packed (0001) planes of Ga and N pairs in the stacking sequence ABAB. GaN in int wurtzite structure lacks reflection symmetry in a plane perpendicular to the *c*-axis, thus, crystal surfaces have either a Ga or a N-polarity [167–169].

The zincblende structure (space group F$\overline{4}3m$) of GaN can be stabilized in epitaxial films on 3C-SiC/Si(001), Si, GaP, MgO or GaAs(001) substrates [170], the latter being the most commonly employed one. In general, the heteroepitaxy of nitrides is difficult due to the lattice mismatch between GaN and the substrates, the difference in thermal expansion and the contamination of the grown films by substrate elements. In general, several annealing processes have to be applied very carefully in order to reduce the density of crystal defects.

5.1.1 Pseudopotentials and the role of $3d$ electrons

The role of the $3d$ electrons of Ga has been widely discussed in the literature [124]. In particular, the Ga $3d$ shell of GaN is not as rigid as in other Ga compounds, e.g. GaAs and GaP [121], and affects both the electronic and structural properties [120]. The treatment of the $3d$ electrons in the frozen-core approximation leads to inaccurate results which are related to the closed shell repulsion of the Ga $3d$ levels and the spatial overlap of Ga $3d$ and Ga $4s$ and $4p$ charge densities [121].

The pseudopotentials used in this chapter are generated from the ground-state configuration of the spin unpolarized atoms. The atomic configurations, the local parts used for the KB form and the cutoff radii of Al, Ga and N together with those of Au and Cu used later, are given in Tab. 5.1.

atom	configuration	local part KB	r_c^s	r_c^p	r_c^d	r_c^f
Al	$3s^2 3p^1 4d^0 4f^0$	p	1.79	1.79	1.79	–
Ga	$3d^{10} 4s^2 4p^1 4f^0$	f	1.63	1.63	1.63	2.00
N	$2s^2 2p^3 3d^0 4f^0$	p	1.42	1.42	–	–
Au	$5d^{10} 6s^1 6p^0 6f^0$	s	2.47	2.47	2.47	–
Cu	$3d^{10} 4s^1 4p^0 4f^0$	s	2.05	2.30	2.05	–

Table 5.1: Parameters of the Troullier-Martins pseudopotentials in the Kleinman-Bylander form.

The pseudopotentials used in this chapter differ from those used before (see Tab. 3.3). In chapter 3, the $3d$ electrons of Ga were treated as core states. Since a much higher energy cutoff of about 80 Ry is needed for numerical convergence, we also reduced the cutoff radius used for the generation of the pseudopotential for Al from 2.20 a_0 to 1.79 a_0 in order to have more accurate results.

With these potentials and the parameters used for all simulations reported in this chapter, the numerical convergence of the electronic energies is about 0.05 eV. The overall uncertainty on the electron energy levels relative to E_F is expected to be less than 0.1 eV.

5.1.2 Bulk c-GaN

A comparison of calculations performed with the $3d$ electrons as (i) frozen-core (ii) valence states revealed that the lattice constant for cubic GaN is significantly improved from (i) $a_0 = 4.35$ Å to (ii) $a_0 = 4.47$ Å with respect to the experimental value $a_{0,exp} = (4.49 \pm 0.02)$ Å [171, 172]. Thus, we treat the Ga $3d$ electrons as valence electrons in all GaN calculations. With the pseudopotentials given in Tab. 5.1, we obtain a band gap $E_{g,LDA}$ of 1.93 eV. The experimental value $E_{g,exp}$ is about 3.28 eV. In Fig. 5.1, we present the band structure of cubic, bulk GaN calculated with E_{cut} of 100 Ry and a (16,16,16) MP grid.

The Ga $3d$ bands occur in the valence band at about 13.5 eV below the valence band maximum (see also projected areas in Fig. 5.2), within the same energy range as the N $2s$ band. This gives rise to a spurious $s - d$ hybridization which splits the N $2s$ band into two parts, one above and one below the Ga $3d$ bands. This is in disagreement with experiments which place the $3d$ bands approximately 3 eV below the N $2s$ band [173]. Very recently, it was pointed out, that this problem can be overcome by a self-interaction correction scheme [174]. Using this scheme, the Ga $3d$ bands are positioned correctly at 3 eV below the center of the N $2s$ band.

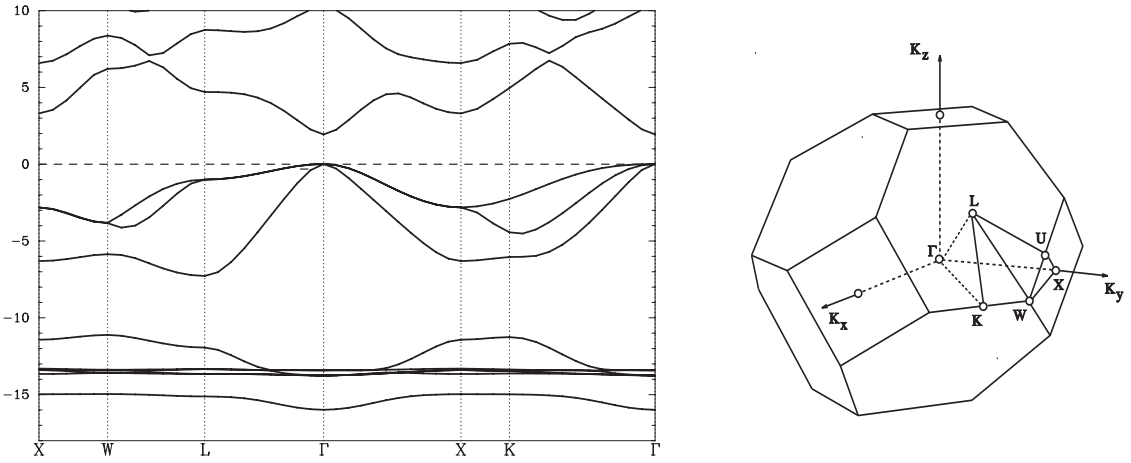

Figure 5.1: Band structure of bulk c-GaN along the lines of high symmetry in the BZ, shown in the right panel.

5.1.3 The GaN(001) surface

It is generally accepted, that the unreconstructed, N-terminated GaN(001) surface exists when the epitaxy is performed in a N-rich environment and the $c(2 \times 2)$ Ga-terminated surface exists for an excess of gallium. The (2×2) reconstruction pattern occurs when there is no excess of nitrogen or gallium [175]. However, several *ab initio* calculations indicate, in agreement with experimental findings, that the only stable GaN(001) surface is the (2×2) reconstructed, Ga-covered surface which is terminated by a half-monolayer of Ga ions [176–181].

In Fig. 5.2, we show the projected band structure of bulk GaN together with the energy bands of surface states of the N-terminated, unreconstructed GaN(001) surface along the lines of high symmetry **Γ**-**J**-**K**-**J′**-**Γ**.

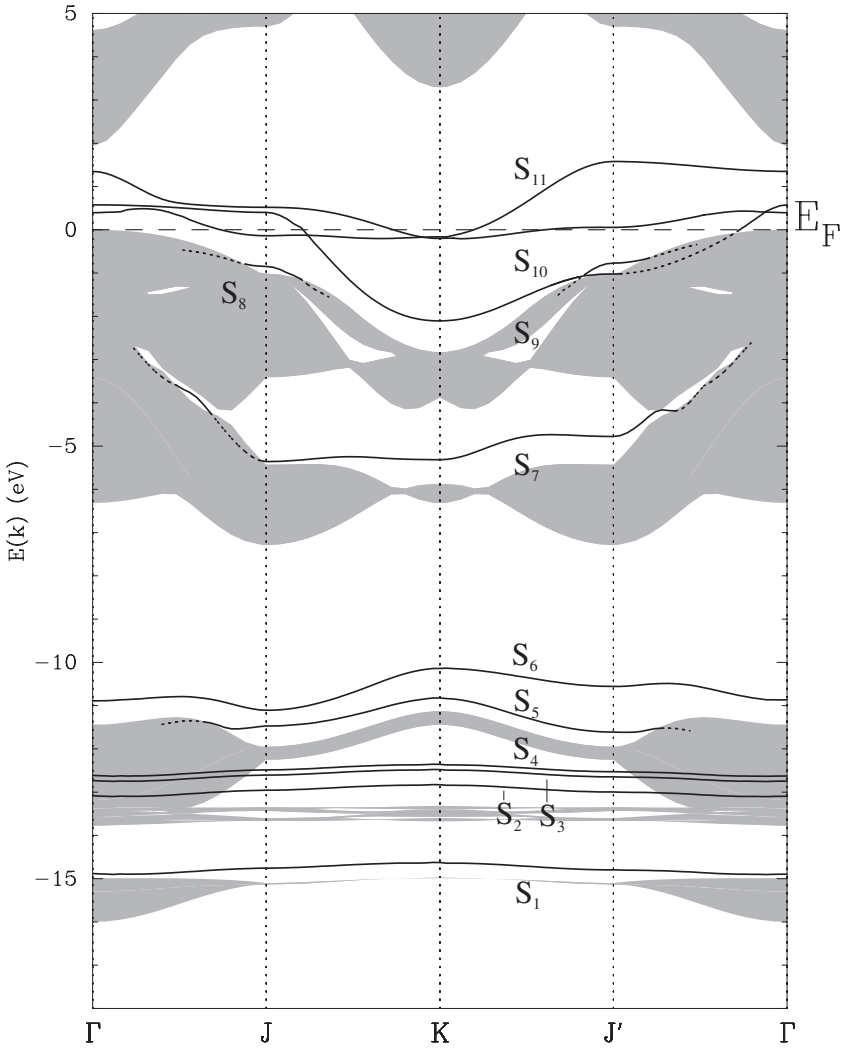

Figure 5.2: Band structure of the localized and resonant surface states of the N-terminated, unreconstructed GaN(001) surface along high-symmetry lines of the surface BZ. The shaded areas indicate the projection of GaN bulk states onto the basal plane of the BZ. Solid (dotted) lines indicate localized (resonant) surface states. Energies are given with respect to the valence band maximum.

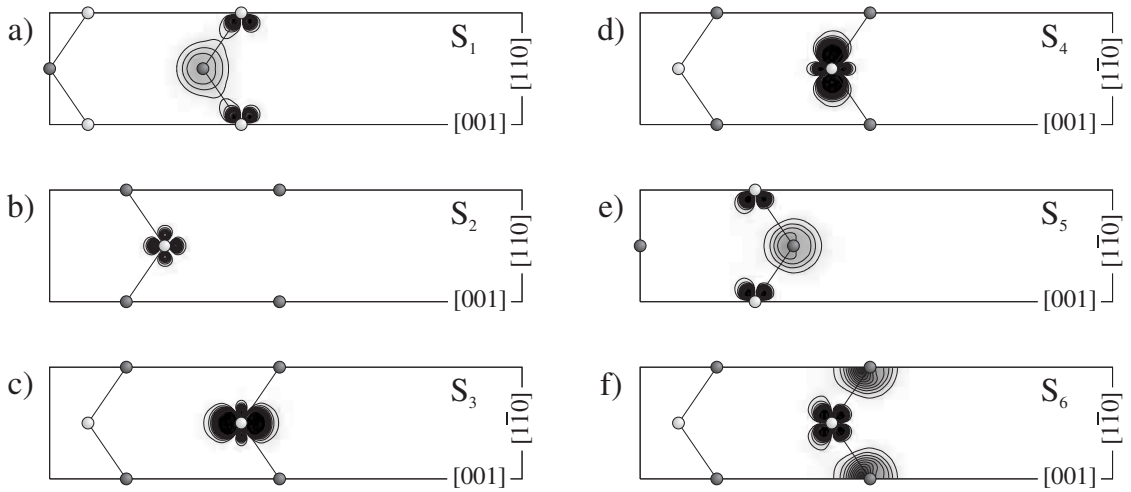

Figure 5.3: Contour plot of the surface states S_1 up to S_6 of the GaN(001) surface at the **K** point of the BZ. The crystal directions are indicated at the right side of the plots. S_1 and S_4 are shown in the central plane of the unit cell while the other states are shown in border planes of the unit cell. Contour spacing is $1 \cdot 10^{-2} e/a_0^3$.

The surface calculation is performed with an energy cutoff E_{cut} of 80 Ry and a (6,6,1) MP **k** point grid using a supercell containing 21 layers of GaN separated by 13.5 Å of vacuum. The bulk calculation is done with E_{cut}=100 Ry and a (6,6,6) MP **k** point grid. As in the case of GaAs(001) and AlAs(001), the surface is metallic and the Fermi level is located 0.13 eV above the valence band maximum. In the lower part of the valence band, at about 14 eV below the Fermi energy, the Ga 3*d* bands occur, having an almost constant energy over the whole BZ. The N 2*s* bands are split into two parts, centered at 2 eV below and above the Ga 3*d* bands. In the lower part of the valence band, i.e. below -10 eV, six surface states, S_1 to S_6, occur which are localized over the whole BZ. The contour plots of these states are shown in Fig. 5.3. S_1, shown in the xz plane in the center of the supercell, as well as S_5 and S_6 exhibit a superposition of N 2*s* and Ga 3*d* orbitals. The x (y) axis is parallel to the [110] ([1$\bar{1}$1]) crystal direction. The z axis corresponds to the [001] direction, which is also the epitaxial growth direction. The surface states S_2 up to S_4, located very close to the Ga 3*d* bands, are purely related to Ga 3*d* orbitals.

At -5 eV, in the stomach gap of the *p*-like bands, the surface state S_7 occurs. This state is a superposition of N $2p_y$ and Ga 4*p* orbitals (see Fig. 5.4).

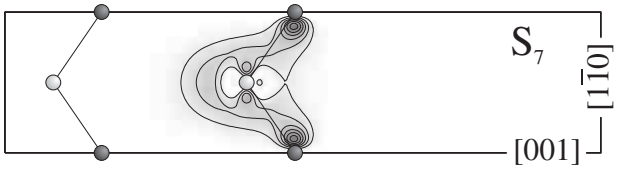

Figure 5.4: Contour plot of the surface states S_7 of the GaN(001) surface at the **K** point of the BZ. Contour spacing is $1 \cdot 10^{-2} e/a_0^3$.

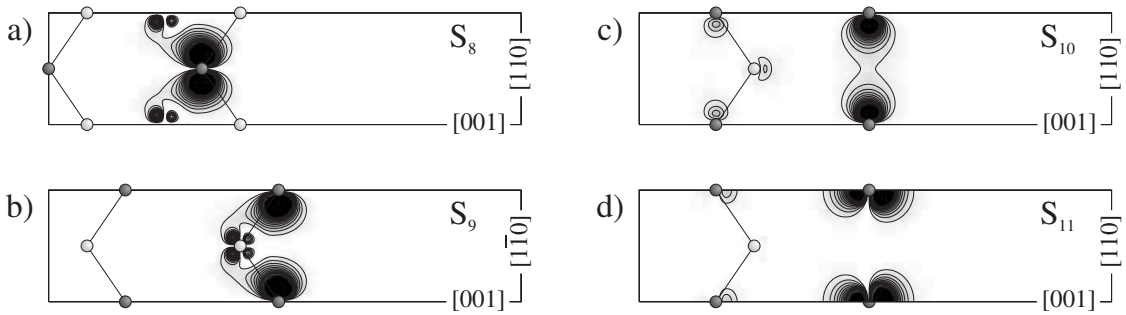

Figure 5.5: Contour plot of the surface states S_8 up to S_{11} of the GaN(001) surface at the **J** point of the BZ. The state S_8 is shown in the central plane of the unit cell while the other states are shown in border planes of the unit cell. Contour spacing is $1 \cdot 10^{-2} e/a_0^3$.

In the band gap region, four surface states occur. The contour plots of their probability density are shown in Fig. 5.5. S_8, shown in Fig. 5.5.a. in the central yz plane, is localized just around **J** and **J′**. Its probability density is localized around the N atom of the third layer from the surface. Also contributions of Ga d orbitals occur, but the main contribution is related to N p_x orbitals. S_9 has a similar structure, but it is localized at the surface layer. Along **Γ**-**J**, it is located 0.5 eV above the valence band maximum, lowers in energy down to -2 eV at **K**, enters the projected bulk continuum near **J′** at -1 eV, remains resonant along the path **J′**-**Γ** and leaves the projection of bulk states near **Γ**. Along this path S_9 has crossed the band S_8 near **J′** and the band S_{10} near **J** and near **Γ**. These crossings are possible since these states have different symmetry at these points. In particular, S_9 has Γ_2 symmetry at **J** (see Tab. 3.1).

The surface states S_{10} and S_{11} correspond to the bridge bond and dangling bond surface states. At the **J** point, S_{10} corresponds to the bridge bond state, has Γ_4 symmetry and is mainly related to the $2p_x$-orbitals of the interfacial N atoms. The bridge bonds are in the x plane, i.e. orthogonal to the atomic zigzag chain at the surface. The dangling bond surface state S_{11} has Γ_1 symmetry at **J**. It derives mainly from the $2p_z$-orbitals of the interfacial N atoms, polarized slightly towards the vacuum. The two surface states are localized over the whole Brillouin zone. The classification as dangling bond and bridge bond state is the same as for the GaAs(001) and AlAs(001) surfaces: along the lines **Γ**-**J** and **K**-**J′**, where σ_{1v} is not a conserved symmetry operation, these two states are both even with respect to σ_{2v}. They interact along these lines and the resulting states are superpositions of dangling bond and bridge bond surface states. At **Γ**, S_{10} is the dangling bond state and S_{11} has the bridge bond character.

Comparing the surface band structure of GaAs(001), shown in Fig. 3.8, with those of AlAs(001), shown in Fig. 4.4 and GaN(001), we can conclude that, apart from the significant influence of the Ga $3d$ bands, the electronic structures of all three unreconstructed anionic terminated (001) semiconductor surfaces are similar. This applies in particular to the four surface states occurring in the semiconductor band gap.

5.2 The Al/GaN(001) interface

We investigate in the following section the Al/GaN(001) interface. We will clarify, if the bonding-like interface state documented for the Al/AlAs and Al/GaAs contacts occurs also at the Al/GaN interface. Thereby, we will have the possibility to investigate the effect of band gap size and interface morphology on the formation of the interface state.

5.2.1 Interface structure

The equilibrium lattice constant of Al ($a_{\mathrm{Al,eq}} = 3.98$ Å) is about 11% smaller than that of GaN and it is thus closer to the equilibrium lattice constant of GaN $a_{GaN} = 4.47$ Å than to $a_{GaN}/\sqrt{2} = 3.16$ Å. We assume therefore a (1x1) epitaxial geometry for Al on GaN(001), where the Al atoms continue the cation fcc sublattice. The Al in-plane expansive strain is accommodated by a compression of the Al overlayer along the growth direction. Considering a_{GaN} as the in-plane lattice constant of Al, we determine the lattice constant $a_{\perp}$ orthogonal to the interface by performing several calculations and minimizing the total energy as a function of $a_{\perp}$. We obtain $a_{\perp} = 3.21$ Å, which is 19% smaller than the equilibrium lattice constant.

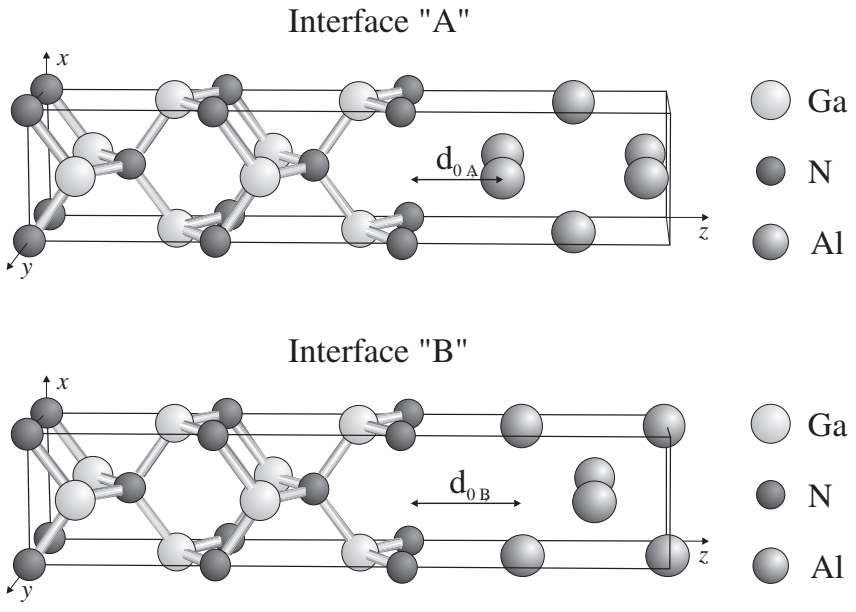

Figure 5.6: Two atomic structure of the abrupt, N-terminated Al/GaN(001) interface. The x and y axes are rotated by 45° with respect to the conventional cubic axis of the semiconductor. The interfacial distance d measures the spacing between the N and Al layers at the junction.

Such high deformations are not possible in devices, which means that Al cannot be grown epitaxially and defect-free on GaN(001). However, we investigate this highly strained system in order to clarify whether the interface state documented for the Al/GaAs(001) and Al/AlAs(001) junctions occurs also at the Al/GaN(001) interface.

The interface is modelled using a slab geometry in a supercell containing 13 atomic layers of GaN and 20 atomic layers of Al, i.e. a total of 33 atoms and 173 valence electrons. We investigate two different possible interface geometries: in the configuration "A", shown in Fig. 5.6.a, the Al atoms are positioned on the Ga fcc sites and in the configuration "B"(see Fig. 5.6.b) they occupy the interstitial sites. This means that for configuration B, the Al overlayer is displaced by a half unit cell in x and y direction. Configuration A is the favored one: the difference in the interface formation energy for geometry A with respect to B is 0.7 eV per interface atom.

The equilibrium interfacial distances are $d_{0,\mathrm{A}} = 1.1$ Å and $d_{0,\mathrm{B}} = 1.4$ Å. At equilibrium, the volume of the supercells are $\Omega_{0,\mathrm{A}} = 2029\ a_0^3$ and $\Omega_{0,\mathrm{B}} = 2065\ a_0^3$. An epitaxial geometry similar to configuration A was used previously to model the Al/GaN junction [90] using an all-electron full-potential linearized augmented plane wave (FLAPW) [182] method within DFT in the LDA. Our results structural agree very well with those of [90, 93]: these authors obtain $d_{0,\mathrm{A}} = 1.1$ Å and $a_{GaN} = 4.47$ Å.

The symmetry point group of the Al/GaN(001) interface and the unreconstructed GaN(001) surface is C_{2v}, [146, 147] (see also Table 3.2). Therefore the symmetry point groups and symmetry operations are the same as for Al/GaAs and Al/AlAs, but one has to take into account, that the orientation of the metal is now (1×1) and not $c(2 \times 2)$ with respect to the semiconductor slab.

5.2.2 Electronic states in the semiconductor optical gap

We calculate the probability density of electronic states at several energies within the semiconductor gap. In Fig. 5.7.a (Fig. 5.7.b) we show the contour plots in the supercell border planes of the probability density corresponding to all electronic states with energy in the range [E_F - 1 eV, E_F + 1 eV] for the interface configuration A (B). They amount to 8.29 (9.53) electrons per supercell. The calculations were performed with a cutoff energy E_{cut} of 80 Ry and a (6,6,1) MP **k** point grid.

For both geometries, the probability density exhibits large values near the interfacial N atoms. The plots in the left panel indicate a large contribution of dangling bond surface states for the configuration A while the right panel gives rise to a large contribution of N p_x orbitals forming a bridge-bond-like structure. In the region of the metal, the density is relatively homogeneous and does not have any exposed maximum values. In particular, no intermetallic, bonding-like feature occurs as it was the case for the Al/GaAs(001) and Al/AlAs(001) junctions.

In Fig. 5.8, we show the Al/GaN(001) interface band structure for both interface configurations calculated in the supercell ($k_z = 0$), along the high symmetry lines **Γ**-**J**-**K** of the BZ. The electronic bands are displayed in an energy range covering the GaN valence bands and the band gap. The bulk PBSs of GaN and of strained Al are also shown. They are aligned with respect to the electron energies of the interface in accordance with the macroscopic average of the electrostatic potential. The resulting Schottky barriers are $\phi_{p,A} = 1.68$ eV and $\phi_{p,B} = 1.18$ eV. Taking into account that our calculations are performed with soft pseudopotentials, our result for the Schottky barrier height $\phi_{p,A}$ is reasonably close to the theoretical value $\phi_p = 1.51$ eV obtained in the FLAPW calculations [90, 93].

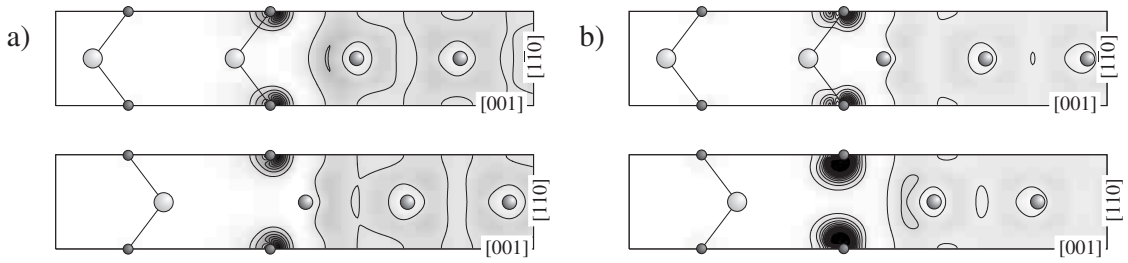

Figure 5.7: Contour plots in the supercell border planes of the summed probability density of all electronic states with energy in the range [E_F- 1 eV, E_F+ 1 eV]. **a** (**b**) shows the result for the geometry A (B) shown in Fig. 5.6. Contour spacing is 0.1 e/a_0^3.

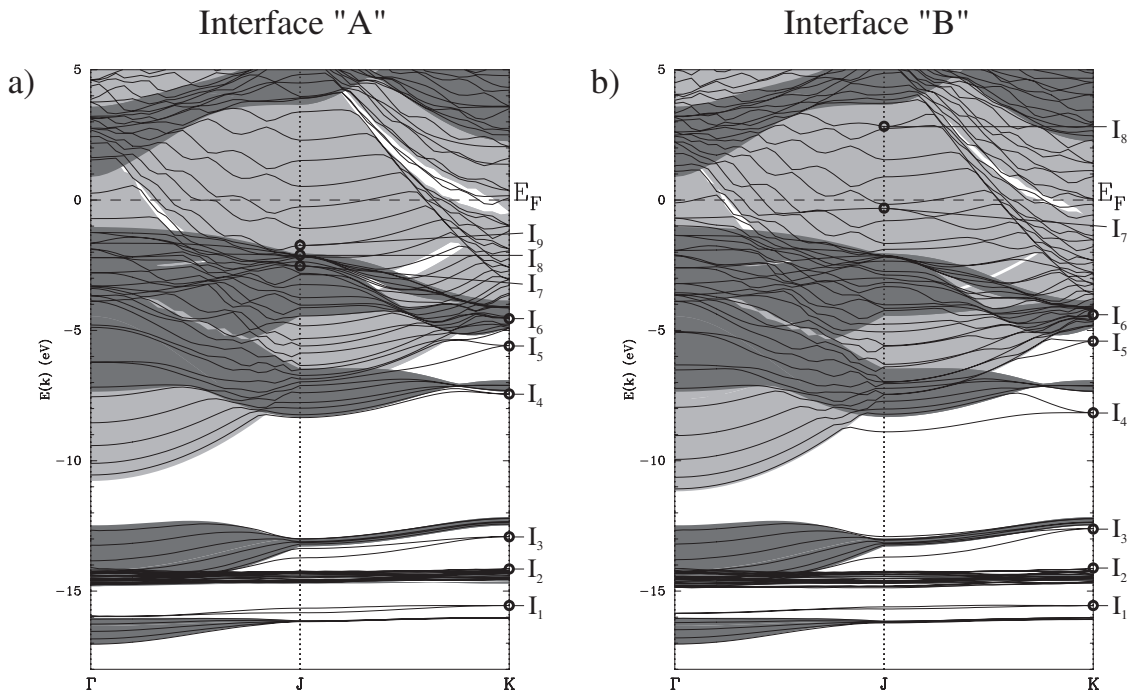

Figure 5.8: Electron band structure of the two Al/GaN(001) interfaces (see Fig. 5.6. The projected band structures of bulk GaN (dark grey) and of epitaxially strained bulk Al (light grey) on GaN(001)are shown. Circles indicate the energy position of interface states shown in Fig. 5.9 to Fig. 5.12.

In order to have a more detailed insight on the interface formation, we investigate the structure of localized and resonant interface states. The comparison of the contour plots with those of the surface state discussed in section 5.2.3 allows us to identify the contribution of the GaN(001) surface states to interface states.

In Fig. 5.9, we show the contour plots of the interface states I_1 up to I_6 for the interface configuration A at the **K** point of the BZ. Their energy positions within the interface band structure are indicated with circles in Fig. 5.8. Direct inspection of interface state I_1 reveals, that it corresponds to a bonding-like structure between N 2*s* and Ga 3*d* orbitals. Its energy position is between the lower N 2*s* band and the Ga 3*d* bands. Its structure is not exactly the same as the one of the surface state S_1 of the GaN(001) surface shown in Fig. 5.3.a, but the energy position is comparable. Interface state I_2 can directly be identified with the surface state S_2 shown in Fig. 5.3.b even though its energy is much closer to that of the Ga 3*d* bands than for S_2. The state I_3 is related to an anti-bonding-like structure between N 2*s* and Ga 3*d* orbitals. It cannot be identified with any of the GaN surface states.

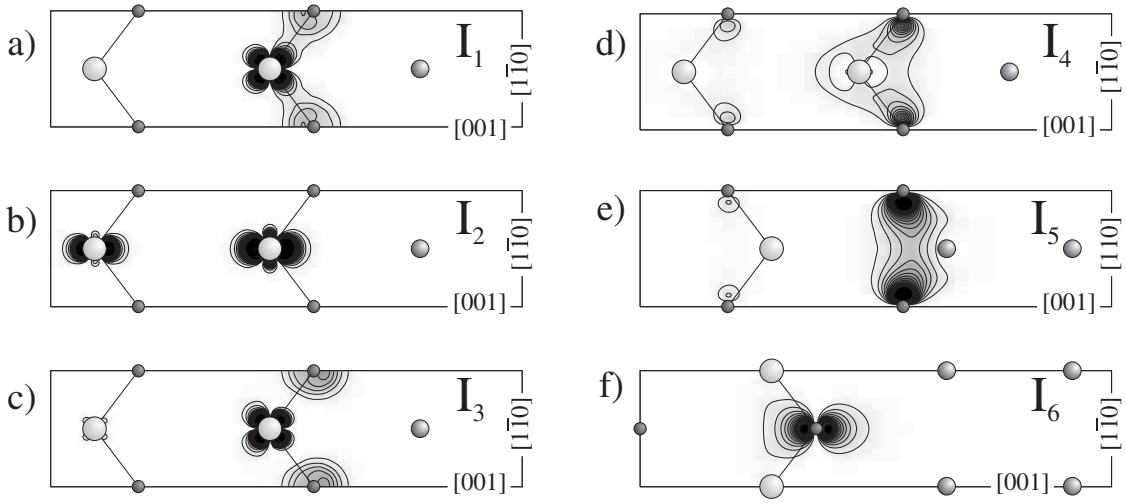

Figure 5.9: Contour plot of the interface states I_1 to I_6 of the Al/GaN(001) contact (geometry "A") at the **K** point of the BZ. The crystal directions are indicated at the right side of the plots. I_6 is shown in the central plane of the unit cell while the other states are shown in border planes of the unit cell. Contour spacing is $1 \cdot 10^{-2} e/a_0^3$.

At around 7.5 eV below E_F, the interface state I_4 occurs just below the projected p bands of Balk GaN. Its contour plot reveals that it is related to the surface state S_7 shown in Fig. 5.4 which occurs in the surface band structure above the GaN p bands. Thus, the presence of Al shifts this surface state 2 eV towards lower energy without changing its structure.

The two interface states I_5 and I_6 have no counterparts in the surface band structure. I_5 exhibits a strong contribution of N p_x orbitals, forming a bridge-bond-like structure. The state I_6, shown in a plane passing through the center of the supercell, is associated to p_y orbitals of N atoms in the third layer from the interface. It is degenerate with bulk GaN states, but it remains localized since its symmetry is different from that of degenerate GaN bulk continuum states.

In order to better compare interface states in the semiconductor band gap region, we present in Fig. 5.10 the localized and resonant interface states at the **J** point of the BZ. The localized interface state I_7 can be directly identified with the surface state S_9 shown in Fig. 5.5.b. With respect to the latter, it is shifted downwards to lower energy, even into the projection of bulk GaN states. However, it remains localized because of symmetry arguments. The two interface states I_8 and I_9 are not localized due to interactions with bulk states of GaN and Al. I_8 can be identified with the bridge bond states shown in Fig. 5.5.c.

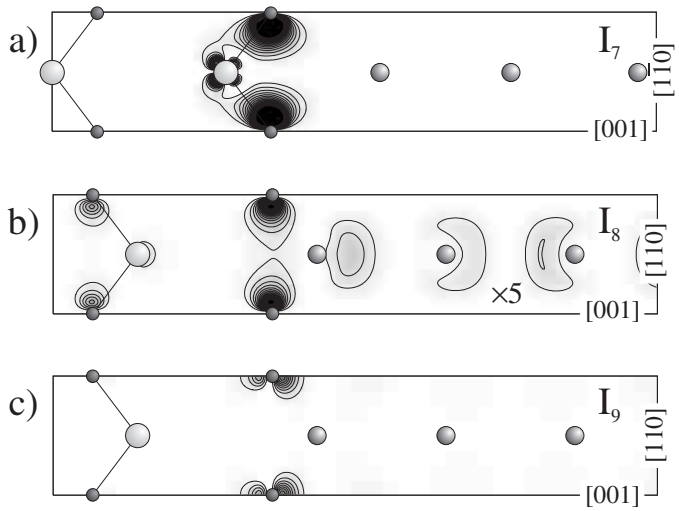

Figure 5.10: Contour plot of the interface states I_7 up to I_9 of the Al/GaN(001) contact (geometry "A") at the **J** point of the BZ. Contour spacing is $1{\cdot}10^{-2}e/a_0^3$ for I_7 and I_9 and $2 \cdot 10^{-3}e/a_0^3$ for I_8.

In order to better compare the two structures, we divided the contour spacing by a factor 5 in Fig. 5.10.b. I_9 corresponds to the dangling bond surface state shown in Fig. 5.5.d. Compared to the corresponding surface states of the free-standing GaN(001) surface, the two interface states are shifted to lower energies, very close to the valence band edge.

We conclude that for the interface geometry A the majority of interface states can be identified as GaN surface states. In general, their energies are shifted to lower values with respect to the values for the free-standing surface. In contrast to the interface state observed for the Al/GaAs and Al/AlAs contacts, no interface state exhibits a contribution of Al surface states. Contrary to the interface structure of Al/GaAs and Al/AlAs contacts, the interfacial Al atom is not facing any of the outermost Ga atom. In order to clarify whether this difference in the interface geometry is responsible for the absence of Al surface related features, we investigate in the following the alternative interface geometry B, shown in the lower panel of Fig. 5.6. For this interface geometry, the interfacial Al atoms are situated opposite to the outermost Ga atoms, as it is the case for the Al/GaAs and Al/AlAs junctions.

We perform the same analysis of interface states for the configuration B in which the Al slab is laterally displaced by a half of the basis vectors in the x and y direction. Since the results are very similar, we focus on the differences between the two interface geometries. In Fig. 5.11, we present the contour plots of the probability density of the interface states I_1 up to I_6 of the interface configuration B.

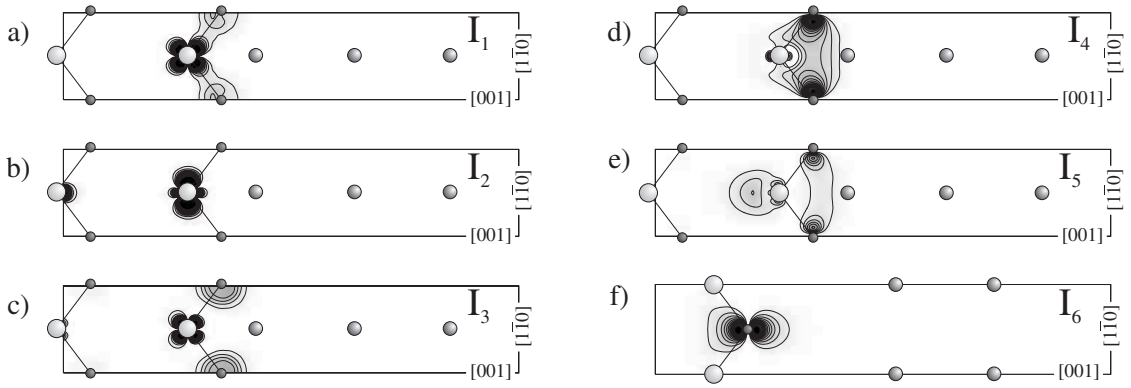

Figure 5.11: Contour plot of the interface states I_1 up to I_6 of the Al/GaN(001) contact (geometry "B") at the **K** point of the BZ. The crystal directions are indicated at the right side of the plots. I_6 is shown in the central plane of the unit cell while the other states are shown in border planes of the unit cell. Contour spacing is $1 \cdot 10^{-2} e/a_0^3$.

The different interface geometry has no effect on the interface states I_1, I_3 and I_6 since they exhibit the same energies and probability densities. For the interface state I_2 shown in Fig. 5.11.b we observe the same energy, but a different orientation of the orbital. While the interface state corresponding to configuration A exhibits an orientation of the $3d$ ($m = 0$) orbital in the z direction (see Fig. 5.9.b), for the B configuration the orbital is oriented in the y direction. The interface state I_4 corresponds to that shown in Fig. 5.9.d. In the configuration B its energy is shifted towards lower energy, i.e. farther away from bulk GaN bands, and therefore it is more localized than the corresponding state for the configuration A. The interface state I_5 has the same energy for both systems, but different orientations. For configuration B it is attributed to an anti-bonding-like structure of N p_y and Ga p_z orbitals. In summary, the structure of interface states I_1 to I_6 is very similar for the two interface configurations. Three states are equivalent, two are very similar but have different orbital orientations and one state (I_5) has another structure due to the different orientation of N p orbitals.

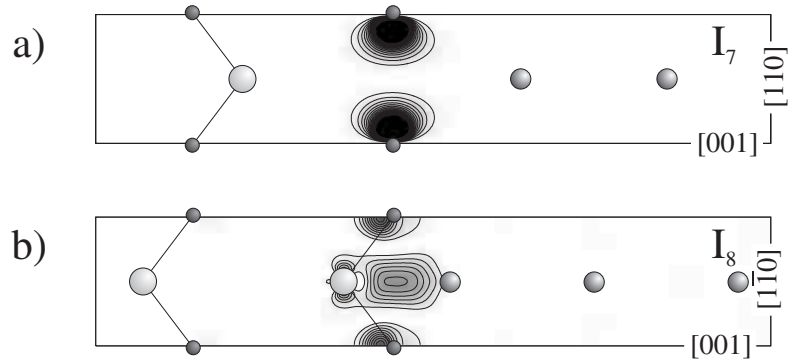

Figure 5.12: Contour plot of the interface states I_7 and I_8 of the Al/GaN(001) contact (geometry "B") at the **J** point of the BZ. Contour spacing is $1 \cdot 10^{-2} e/a_0^3$.

We focus now on the interface states occurring in the semiconductor band gap. Fig. 5.12 shows the contour plot of two localized interface states at the **J** point of the BZ. They are the only localized or resonant states that occur in the band gap region at this **k** point. In particular, in the energy range where the interface states for the configuration A occur, no resonant or localized interface state appears. The state I_7 occurs 0.4 eV below E_F and I_8 is 2.7 eV above the Fermi energy. Their energies and probability densities are very different with respect to those for configuration A shown in Fig. 5.10. I_7 corresponds clearly to N p_x orbitals forming a bridge bond structure as the surface state S_{10} shown in Fig. 5.5.c. The interface state is even more localized than the surface state. The most interesting interface state is I_8. Since its energy is much higher than E_F it is unoccupied and does not contribute to transport properties of the junction. It exhibits the same intermetallic, bonding-like structure as the localized interface state investigated for the Al/GaAs and Al/AlAs interfaces shown in Fig. 3.5 and Fig. 4.2.b.

We conclude, that the orientation of the Al slab with respect to the GaN surface affects only weakly the electronic structure in the valence band, but states in the semiconductor band gap are significantly different. In particular, for the interface configuration B, localized states attributed to GaN bridge bond surface states occur close to the Fermi level. Furthermore, an intermetallic bonding-like interface state, very similar to that reported for the Al/GaAs and Al/AlAs interfaces, occurs at 2.7 eV above E_F.

5.2.3 The Al(001) surface under strain

In order to better understand why Al surface states do not contribute significantly to the interface states, we investigate the electronic structure of the Al(001) surface in the geometry used for the interface calculations. Since Al is a relatively rigid material, we expect significant changes in the electronic structure for the strained slab. In Fig. 5.13 we compare two projected band structures of bulk Al. The left panel shows, together with the surface state bands, the PBS in the unstrained, equilibrium geometry. The right panel is calculated including the strain occurring for the interface, GaN-matched geometry. Bulk calculations are performed using E_{cut}=40 Ry and a (16,16,16) MP grid. For surface calculations, a supercell with 21 layers of Al, E_{cut} of 40 Ry and a (6,6,1) MP grid was used.

Compared to the equilibrium structure with its surface states already discussed in section 3.5, the projected bulk band structure of the strained Al slab is significantly changed. The stomach gap at **J** is entirely closed and the surface state does not occur any longer. Bulk states with odd symmetry are shifted approximately 1.5 eV towards lower energy. In the shown energy range, no surface state of the strained Al(001) surface is observed.

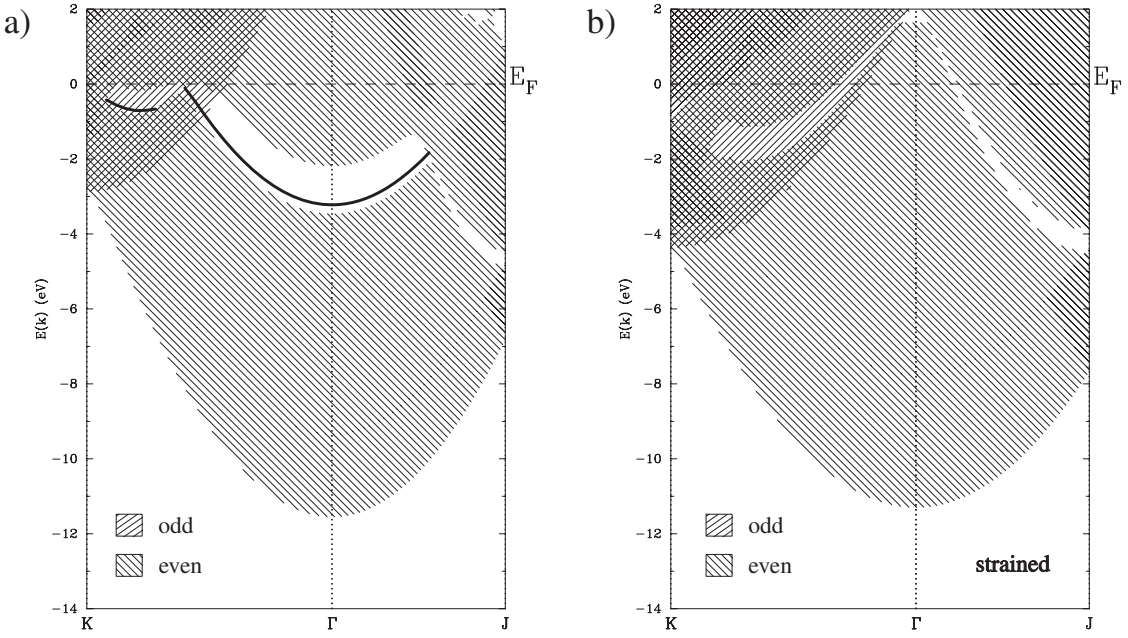

Figure 5.13: Projected band structures of epitaxial bulk Al along high-symmetry lines of the surface BZ. Panel **a)** shows the unstrained, equilibrium geometry. The solid lines show the localized surface states of the Al(001) surface. Panel **b)** represents the highly strained geometry used for the Al/GaN(001) interface. The left(right)-hatched area shows the projection of states which are even (odd) with respect to the mirror plane parallel to the relevant high-symmetry line and orthogonal to the surface.

5.2.4 Discussion

We have investigated the electronic structure of two different interface configurations for the Al/GaN(001) interface. Configuration A is predicted by total energy calculations to be more stable than configuration B. The geometry B was also investigated since it provides in the y plane an atomic structure at the interface similar to that of Al/GaAs and Al/AlAs junctions. Direct inspection of interface states for both interfaces showed, that localized states in the semiconductor valence band region are weakly affected by the atomic structure at the interface. All interface states in this energy range are attributed to GaN surface states and do not show any contribution from Al surface states.

In the semiconductor optical gap, the situation is different. While three interface states occur near the GaN valence band maximum at **J** for configuration A, two different localized interface states appear for configuration B. Notably, an intermetallic bonding-like interface state, comparable to those of the Al/GaAs and Al/AlAs junction, has been identified. This difference can be explained by two different arguments. First, the atomic structure at the interface is different and due to the missing Al atom in the position opposite to the outermost Ga atom, the bonding-like interface state cannot occur for the interface A. Secondly, by the displacement of the Al slab with respect to the GaN one, the reference planes of the reflection symmetry operations of Al is changed by half of the unit cell in x and y direction with respect to the GaN slab. In configuration A, the relevant Al bulk continuum states have the same symmetry as the dangling bond and bridge bond GaN surface states. Thus, an interaction between these states is possible and the interface states are a superposition of GaN surface and Al bulk states. In configuration B, the symmetries are different and therefore the two states shown in Fig. 5.12 are localized. This argument is confirmed by the fact, that interface state I_7 shown in Fig. 5.12.a. has the same energy with respect to E_F as the corresponding surface state S_{10} (see Fig. 5.5.c).

For the intermetallic, bonding-like interface state, which has exactly the same structure as those identified for the Al/GaAs and the Al/AlAs junctions, the formation mechanism is confirmed. Especially, the important role of states in the conduction band edge is validated by the fact, that the state is located constantly 1 eV below the conduction band edge for all three Al/semiconductor interfaces. Considering the interface configuration B, we can conclude that the intermetallic, bonding-like interface state occurs at all three Al/semiconductor contacts we have investigated.

Comparing the Schottky barrier height obtained for Al/GaAs ($\phi_p = 0.53$ eV) and Al/AlAs ($\phi_p = 0.63$ eV) to those of the Al/GaN ($\phi_{p,A} = 1.68$ eV, $\phi_{p,B} = 1.18$ eV), it turns out, that with increasing semiconductor ionicity and band gap, the p-type SBH is also increased.

5.3 The Au/GaN(001) interface

As already mentioned, the lattice mismatch between Al and GaN is about 11% and therefore the Al/GaN contact presents a highly strained Al slab. Au is known to be much softer and one could expect that it is much better suited for epitaxial contacts to GaN. Metallic Au has a fcc structure and its experimental lattice constant is 4.08 Å [183]. Thus, the lattice mismatch between Au and GaN is about 9% which is smaller compared to the lattice mismatch between Al and GaN, but it is still very large. In our calculations, we use a pseudopotential for Au with the parameters shown in Fig. 5.1. Therein, we treat the closed $5d$ electron shell as valence electrons since a treatment of these electrons as frozen core states leads to inaccurate results. Using this pseudopotential for Au, we obtain 4.08 Å as theoretical equilibrium lattice constant.

We assume the same (1x1) epitaxial geometry for Au on GaN(001) as for the Al/GaN(001) junction (see Fig. 5.14). The Au in-plane expansive strain is accommodated by a compression of the Au overlayer along the growth direction. From total energy calculations as a function of the orthogonal lattice constant $a_\perp$, we obtain $a_\perp = 3.44$ Å for the Au in the case that $a_\parallel$ is fixed to the lattice constant of GaN a_{GaN}. Since the interface geometries of the Al/GaN(001) and the Au/GaN(001) junctions are very similar, we carry out the same comparative study for the two possible interface geometries A and B. As in the case of Al/GaN, configuration A is more stable and the difference in the interface formation energy for geometry A with respect to B is 0.6 eV per interface atom.

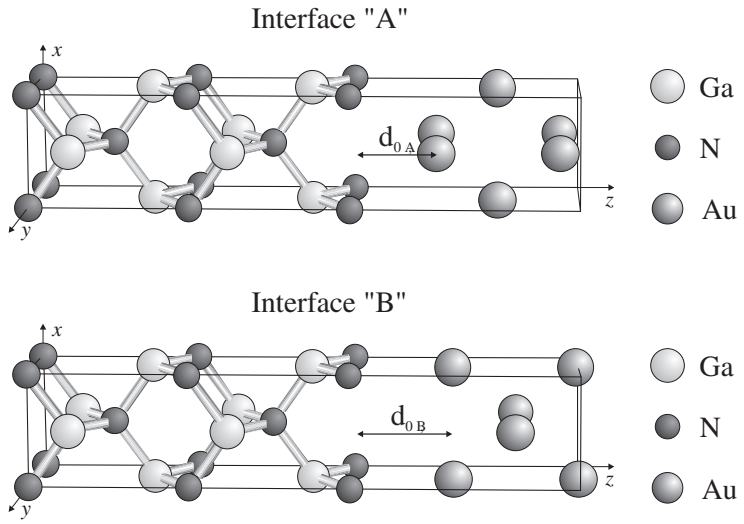

Figure 5.14: Two atomic structure of the abrupt, N-terminated Au/GaN(001) interface. The interfacial distance d measures the spacing between the N and Au layers at the junction.

The interface is modelled using a slab geometry in a supercell containing 13 atomic layers of GaN and 10 atomic layers of Au, i.e. a total of 23 atoms and 223 valence electrons. The equilibrium interfacial distances for the two configurations are $d_{0,\mathrm{A}} = 1.4$ Å and $d_{0,\mathrm{B}} = 1.7$ Å. At equilibrium, the volume of the supercells are $\Omega_{0,\mathrm{A}} = 2141\ a_0^3$ and $\Omega_{0,\mathrm{B}} = 2176\ a_0^3$. An epitaxial geometry analogous to configuration A was used previously to model this junction using an all-electron LDA-FLAPW method [93] . Our structural results agree reasonably well with the FLAPW ones: $d_{0,\mathrm{A}} = 1.34$ Å and $a_{GaN} = 4.47$ Å. The difference in the equilibrium interfacial distance can be attributed to the neglect of spin-related phenomena in our calculations. These effects are expected to be more important for heavier atoms like Au than for lighter ones like Al.

5.3.1 Electronic states in the semiconductor optical gap

We calculate the probability density of electronic states at several energies within the semiconductor gap. In Fig. 5.7.a (5.7.b) we show the contour plots in the supercell border planes of the probability density corresponding to all electronic states with energy in the range [$\mathrm{E_F}$ - 1 eV, $\mathrm{E_F}$ + 1 eV] for the interface configuration A (B). They amount to 8.01 (11.19) electrons per supercell. The calculations were performed with a cutoff energy E_{cut} of 80 Ry and a (10,10,1) MP **k** point grid.

For both geometries, the probability density exhibits large values near the interfacial N and Au atoms. The plots of the left-hand panels indicate a large contribution of dangling-bond (upper left panel) and bridge-bond (lower left panel) surface states for the configuration A. Additionally, a large contribution at the interfacial Au atoms occur (lower left panel), forming an anti-bonding-like density at the interface.

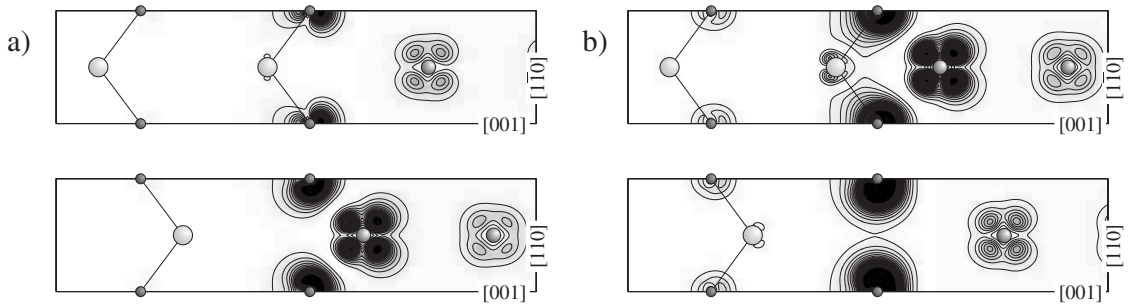

Figure 5.15: Contour plots in the supercell border planes of the summed probability density of all electronic states with energy in the range [$\mathrm{E_F}$ - 1 eV, $\mathrm{E_F}$ + 1 eV]. **a)** (**b)**) shows the result for geometry A (B) shown in Fig. 5.14. Contour spacing is 0.1 e/a_0^3.

For the geometry B, shown in the right-hand panels, the contributions of the interfacial N atoms are bridge-bond-like in both cases. In the right upper panel, where the y-plane is shown, the dominant contribution comes from anti-bonding-like states. In particular these states are anti-bonding between the outermost Ga and the interface N atoms as well as between the interfacial N and Au atoms.

In the metal region, the density is not as homogeneous as for the Al/GaN(001) contact since the $5d$ orbitals influence strongly the probability density of Au near the Fermi energy. As for the Al/GaN(001), no intermetallic bonding-like structure occurs between the outermost Ga and the interfacial Au atoms.

In the following we discuss first the results for the interface geometry A. In Fig. 5.16, the Au/GaN(001) superlattice band structure is shown along the high symmetry lines **Γ**-**J**-**K** of the BZ. The electronic bands are displayed in an energy range covering the GaN valence bands and the band gap. The bulk PBSs of GaN and of the strained Au slab are also shown as grey shaded areas. They are aligned with respect to the energy band structure of the interface in accordance with the macroscopic average of the electrostatic potentials. The resulting Schottky barrier height is $\phi_{p,A} = 0.82$ eV. This value is 0.26 eV smaller than that of [93] who obtained a theoretical value of $\phi_p = 1.08$ eV. This difference can be attributed to two reasons: the different treatment of core electrons (pseudopotentials versus all-electron potentials) and the smaller equilibrium interfacial distance between the metal and the semiconductor slab. The larger the interfacial distance between the two slabs, the smaller is the value of the SBH.

In comparison to the band structure of the Al/GaN(001) superlattice shown in Fig. 5.8, it turns out that the interface states in the deep valence band region at around 15 eV below the Fermi level are only weakly affected by the different choice of the metal. However, the band structure corresponding to the upper part of the semiconductor valence bands and in the semiconductor optical gap is significantly different to that of Al/GaN(001). The projection of Au bulk states exhibits several stomach gaps below E_F along the line **J**-**K**. Furthermore, a large stomach gap extending from -0.8 eV to 3.2 eV arises at the **J** point. Therein several bands of the superlattice, not degenerate with any projected bulk states, occur. Due to the presence of several stomach gaps, the number of localized and resonant interface states is much higher than for the Al/GaN(001) junction. Their energy positions are indicated in Fig. 5.16 with black circles.

We remind that due to the higher symmetry of the supercell, the BZ point **J** is folded onto **J′**. Thus, interface states appear twice in Fig. 5.16. However, by considering one of the two interfaces in the supercell as the reference and by direct inspection of the wavefunctions, it is possible to distinguish interface states corresponding to the **J** point from those corresponding to **J′**.

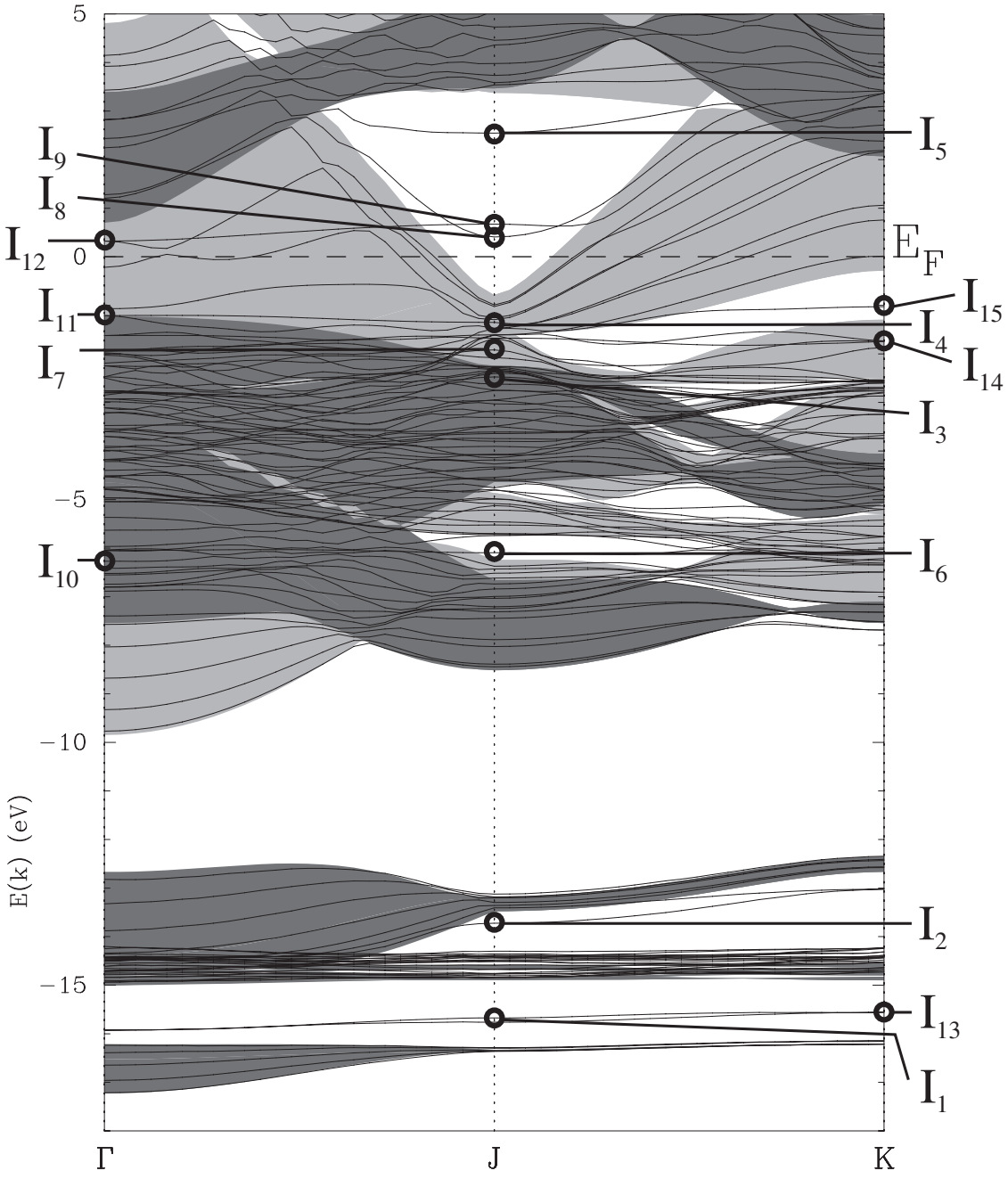

Figure 5.16: Electron band structure of the Au/GaN(001) superlattice in the configuration A (see Fig. 5.14.a). The projected band structures of bulk GaN and epitaxially strained bulk Au are shown as dark grey and light grey areas, respectively. Circles indicate the energy position of interface states.

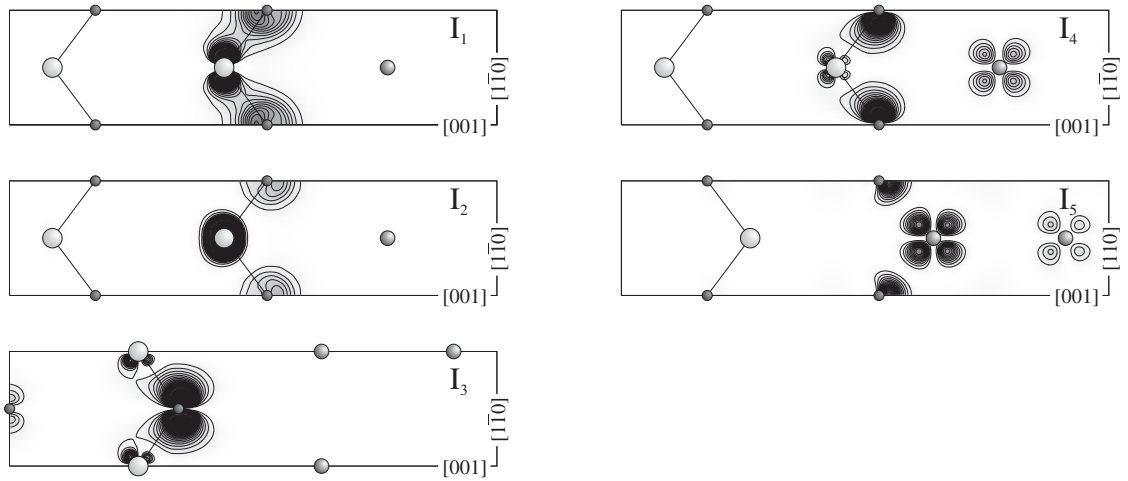

Figure 5.17: Contour plot of the interface states I_1 up to I_5 of the Au/GaN(001) contact (geometry A) at the **J** point of the BZ. I_3 is shown in the central plane of the unit cell while the other states are shown in border planes of the unit cell. Contour spacing is $1 \cdot 10^{-2} e/a_0^3$.

In Fig. 5.17, we show the contour plots of interface states at the **J** point. The two interface states I_1 and I_2 are related to GaN surface states which lie deep in the valence band and originate from N 2*s* and Ga 3*d* states. I_1 exhibits a bonding structure between the outermost N and Ga atoms while I_2 corresponds to an anti-bonding state. I_3 occurs at E_F -2.3 eV, is localized around N atoms belonging to the second layer from the interface. It corresponds to the GaN surface state S_8, shown in Fig. 5.5.b. It has exactly the same structure and a very similar energy position. Similarly, I_4 represents the GaN surface state S_9 (see Fig. 5.5.c), but in contrast to I_3, it exhibits an additional contribution of Au 5*d* orbitals. The interface state I_5 consists of a bonding structure between a GaN dangling bond surface state and 5*d* orbitals of the interfacial Au atom.

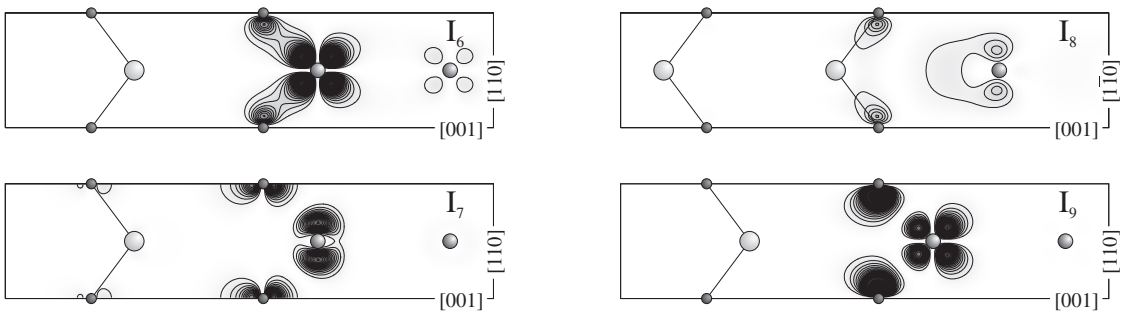

Figure 5.18: Contour plot of the interface states I_6 up to I_9 of the Au/GaN(001) contact (geometry A) at the **J'** point of the BZ. Contour spacing is $1 \cdot 10^{-2} e/a_0^3$.

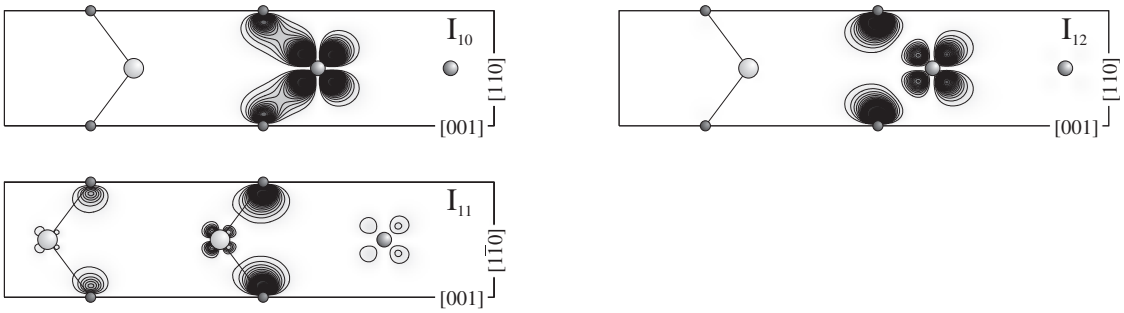

Figure 5.19: Contour plot of the interface states I_{10}, I_{11} and I_{12} of the Au/GaN(001) contact (geometry A) at the $\mathbf{\Gamma}$ point of the BZ. Contour spacing is $1 \cdot 10^{-2} e/a_0^3$.

The interface states I_6 to I_9, attributed to $\mathbf{J}'$, are shown in Fig. 5.18. All four states exhibit contributions from both GaN and Au surface states. I_6 occurs in a stomach gap of projected bulk states at 6 eV below the Fermi level. It consists of N p_x and Au d orbitals, forming a bonding interface state. I_7, appearing at -1.7 eV, represents an anti-bonding state between N p_z and Au d orbitals. I_8 occurs 0.4 eV above E_F and therefore in the stomach gap of projected Au bulk states. However, it exhibits a weak localization. I_9 is forming an anti-bonding state between N p_x and Au d orbitals.

At the $\mathbf{\Gamma}$ point of the BZ, only the interface state band which corresponds to I_1 is not degenerate with projected bulk states. However, several interface bands remain localized since degenerate bulk states have different symmetry. Fig. 5.19 shows the contour plot of the probability density of three interface state bands localized at $\mathbf{\Gamma}$. I_{10} occurs 6 eV below the Fermi level and corresponds to the same interface state bands as I_6 indicating that this interface state is localized along the path $\mathbf{J}'$-$\mathbf{\Gamma}$. Similarly, I_{11} is related to I_4 and I_{12} represents the same interface state band as I_9.

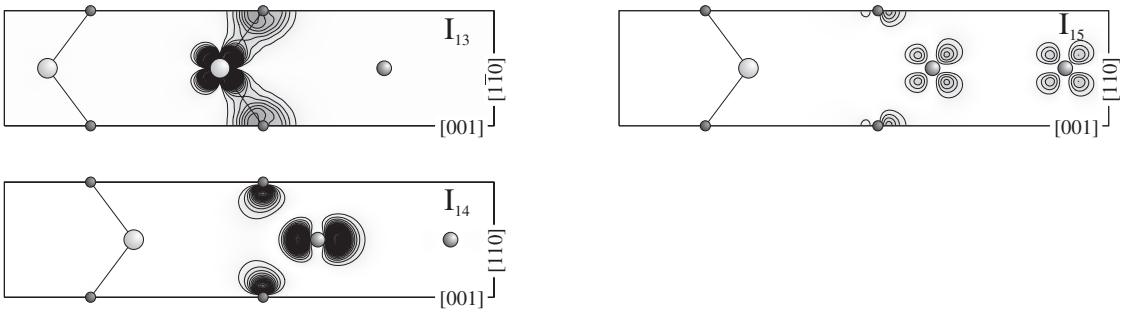

Figure 5.20: Contour plot of the interface states I_{13}, I_{14} and I_{15} of the Au/GaN(001) contact (geometry A) at the **K** point of the BZ. Contour spacing is $1 \cdot 10^{-2} e/a_0^3$.

In Fig. 5.20, we present three interface states at the **K** point. I_{13} is very similar to I_1, with a bonding structure between N s and Ga d contributions, but with a different orientation of the Ga $3d$ orbitals. I_{14} corresponds to an anti-bonding state between N p_x and Au d orbitals. I_{15} is not degenerate with Au bulk states, but it does not exhibit localization at the interface.

Summarizing the results for the configuration A, it turns out that compared to the Al/GaN(001) contact, which has the same interface geometry, more localized interface states occur. Most of these states show bonding or anti-bonding contributions of GaN and Au surface states which is not the case for the Al/GaN junction. Direct inspection of these interface states reveals that they are formed with the help of the $5d$ orbitals of Au. Al does not have d electrons and therefore we conclude that the electronic structure of MS interfaces depends highly on the electron configuration of the interfacial metal atoms.

By focussing now on the interface geometry B, we expect similar results for the interface band structure corresponding to the semiconductor valence band region, as we have previously found for Al/GaN. The interesting and open question is whether the electronic structure will show differences in the semiconductor band gap region. Especially, we want to clarify if intermetallic bonding-like interface states occur also for Au/GaN(001).

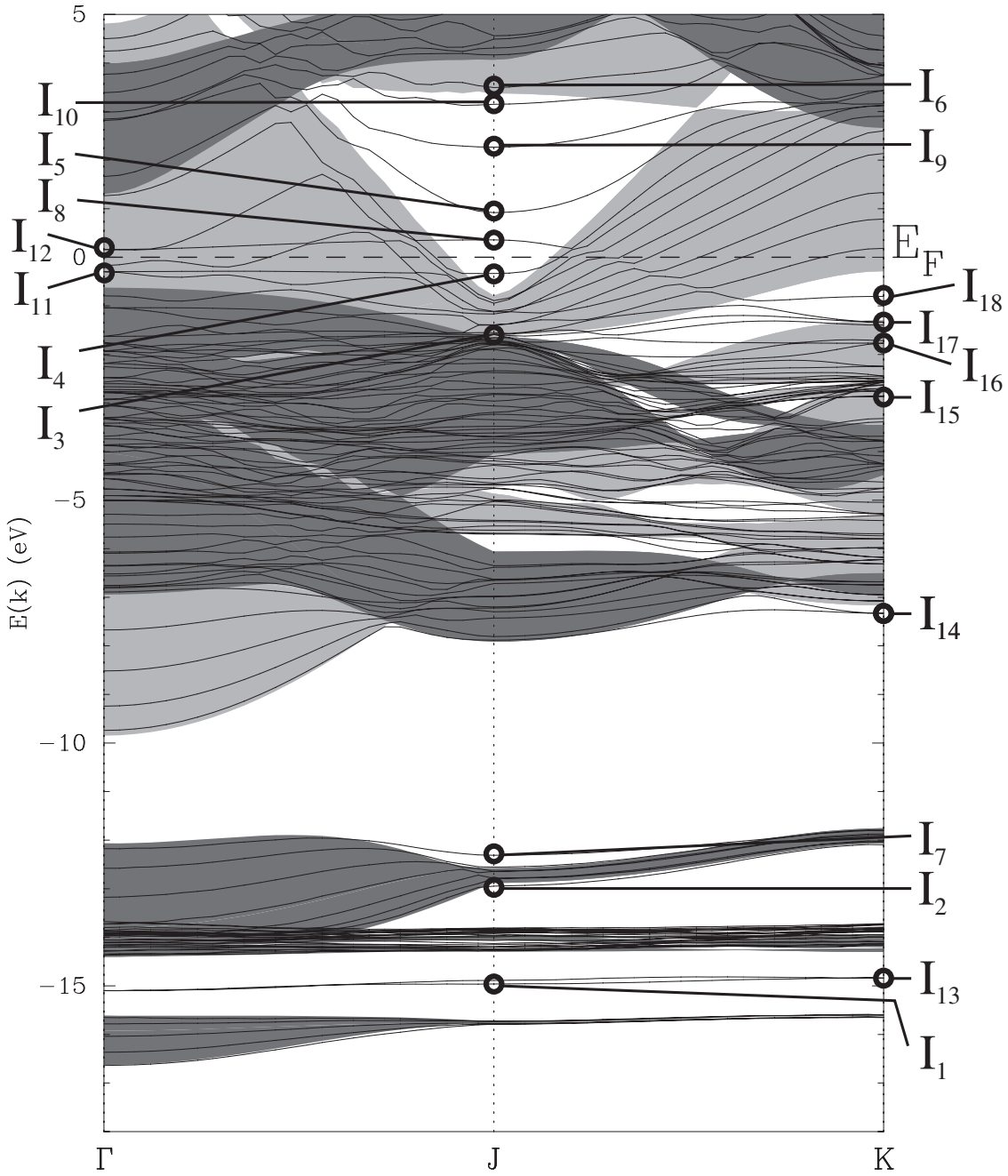

Figure 5.21: Electron band structure of the Au/GaN(001) interface (see Fig. 5.14.b) in the configuration B together with the projected band structures of bulk GaN and epitaxially strained bulk Au. Circles indicate the energy position of interface states.

Fig. 5.21 shows the Au/GaN(001) superlattice band structure for the interface geometry B along the high symmetry lines **Γ**-**J**-**K** of the BZ. Similar to Fig. 5.16, the bulk PBS's of GaN and of the strained Au slab are also shown as grey shaded areas. Numbered circles indicate the energy positions of interfaces states shown in Figs. 5.22 up to 5.25. The Schottky barrier for this interface geometry is $\phi_{p,B} = 0.66$ eV, 0.16 eV smaller than $\phi_{p,A}$ and confirming the trend that the SBH is smaller for larger interfacial distances ($d_{0,\mathrm{B}} = 1.7$ Å).

The superlattice band structure is very similar for the two Au/GaN interfaces. Compared to the interface band structure for configuration A, GaN related states, including the GaN surface states occurring at $\mathrm{E_F}$ - 12 eV, are shifted to higher energies with respect to the Fermi energy. The main differences between the two interface configurations appear in the semiconductor band gap region. While for the geometry A three interface states occur in the stomach gap at the **J** (**J**′) point, five interface states are found in the same gap for the B geometry.

In the following, we discuss briefly the structure of localized and resonant interface states for the B geometry. Most of them can be attributed to the corresponding states at the Au/GaN in the geometry A even though the atomic geometry at the interface is different.

In Fig. 5.22, we show the contour plots of interface states at the **J** point. The interface states $\mathrm{I_1}$ to $\mathrm{I_3}$ can directly be identified with the states $\mathrm{I_1}$ to $\mathrm{I_3}$ shown in Fig. 5.17. Also state $\mathrm{I_4}$ has a similar structure compared to that of geometry A, indicating, that these states are mainly determined by the GaN slab. The state $\mathrm{I_5}$ of geometry B corresponds to the state $\mathrm{I_8}$ of geometry B shown in Fig. 5.18 which is attributed to **J**′.

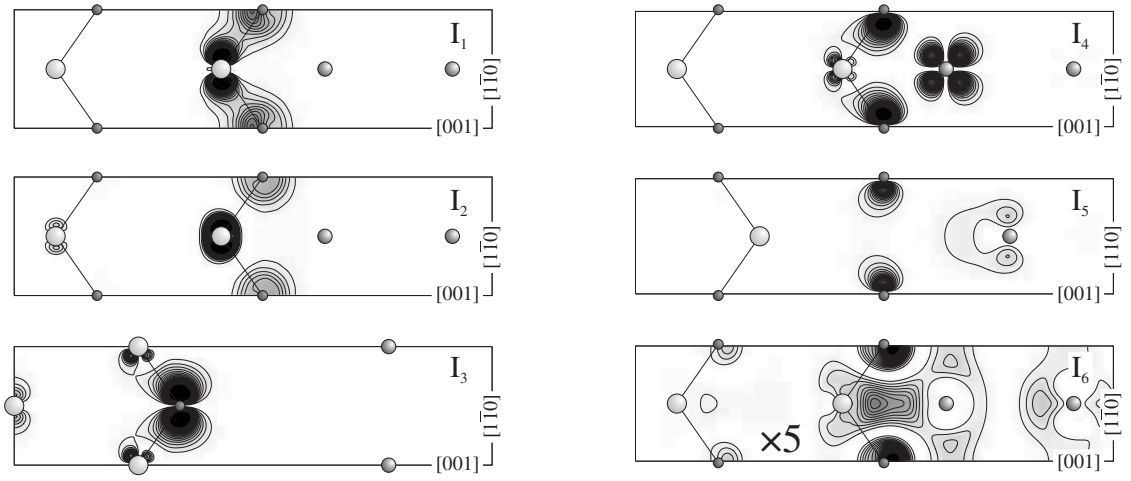

Figure 5.22: Contour plot of the interface states $\mathrm{I_1}$ up to $\mathrm{I_6}$ of the Au/GaN(001) contact (geometry B) at the **J** point of the BZ. Contour spacing is $1 \cdot 10^{-2} e/a_0^3$ ($2 \cdot 10^{-3} e/a_0^3$ for state $\mathrm{I_6}$).

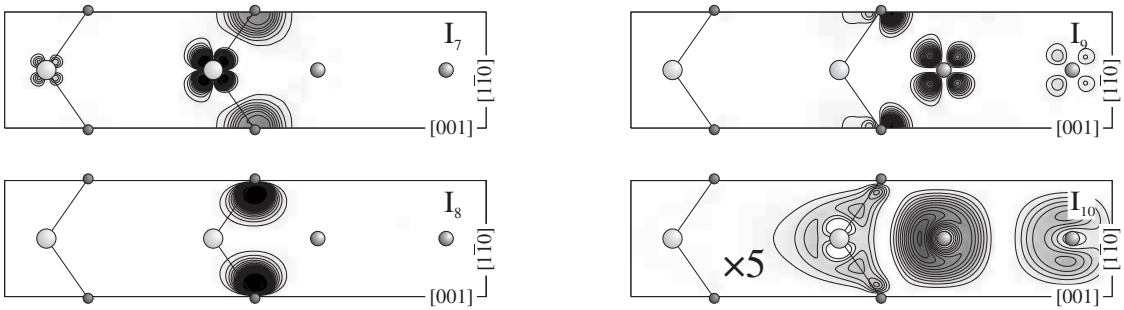

Figure 5.23: Contour plot of the interface states I_7 up to I_{10} of the Au/GaN(001) contact (geometry B) at the **J'** point of the BZ. Contour spacing is $1 \cdot 10^{-2} e/a_0^3$ for I_9 to I_9 and $2 \cdot 10^{-3} e/a_0^3$ for I_{10}.

Thus, this state is weakly dependent on the orientation of the interfacial GaN zigzag chain and essentially determined by the Au surface state. The most remarkable interface state is I_6 which exhibits the intermetallic bonding-like structure. It occurs 3.5 eV above the Fermi energy and is degenerate with Au bulk states. Due to interactions with metal bulk states, it is not localized. The contour spacing is reduced by a factor five in order to better identify its structure. As the corresponding state at the Al/GaN interface, also this state is unoccupied and does not contribute to transport properties of the junction. It turns out, that the formation mechanism of this state is quite general and it occurs also at the Au/GaN contact.

Fig. 5.23 shows the contour plots of the probability density of interface states at the $\mathbf{J}'$ point of the BZ. Therein, I_7 corresponds to the GaN surface state S_6. The interface state I_8 occurs 0.3 eV above E_F and corresponds to the GaN bridge bond surface state shown in Fig. 5.5.c. State I_9 exhibits the structure of the dangling bond GaN surface state with an additional contribution of Au 5*d* orbitals. The state I_{10} is very close to the continuum of bulk Au states and is not localized. The contour spacing is reduced by a factor five. It forms an anti-bonding interface state between Au 6*s* orbitals and N as well as Ga *p* orbitals.

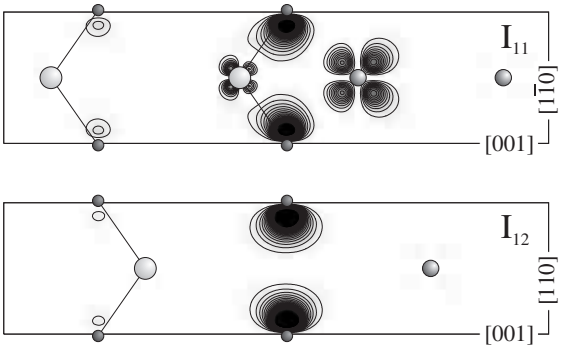

Figure 5.24: Contour plot of the interface states I_{11} and I_{12} of the Au/GaN(001) contact (geometry B) at the $\mathbf{\Gamma}$ point of the BZ. Contour spacing is $1 \cdot 10^{-2} e/a_0^3$.

In Fig. 5.24, we show two localized interface states, I_{11} and I_{12}, with energy in the semiconductor band gap. Both states exhibit large contributions of the GaN bridge bond surface state. I_{11} consists additionally of d-orbital contributions of the outermost Ga and Au atoms. The electron bands corresponding to these two interface states reveal, that these states are localized along the path **Γ-J**. At the **J** point, I_{11} corresponds to the state I_4 and at **J′**, I_{12} is represented by the state I_8. The localization of bridge bond GaN surface states occurs also at the configuration B of the Al/GaN(001) contact. This shows that the bridge bond GaN surface state is stabilized as localized state in the case that a metal atom is positioned in front of the outermost Ga atom. Considering the equilibrium interface morphology, the interface state formed with the help of the bridge bond surface state interacts with metal surface states, as shown for example in Fig. 5.18 and Fig. 5.19.

Finally, we present in Fig. 5.25 the contour plots of interface states at the **K** point of the BZ. Therein, I_{13} shows one of the GaN surface states, related to Ga $3d$ and N $2s$ orbitals. I_{14} is formed as a bonding-like state resulting from N $2p$ and Ga $4p$ as well as Au $5d$ orbitals. I_{15} and I_{16} have large contributions from Au surface states. The localized bridge bond surface state occurs at the **K** point as interface state I_{17} and thus, it is localized over the whole **Γ-J-K** path in the Brillouin zone. In contrast to the localization of the GaN bridge bond surface state, the GaN dangling bond surface state interacts strongly with Au bulk and surface states and therefore it is not localized as it is shown in the lower right-hand panel of Fig. 5.25.

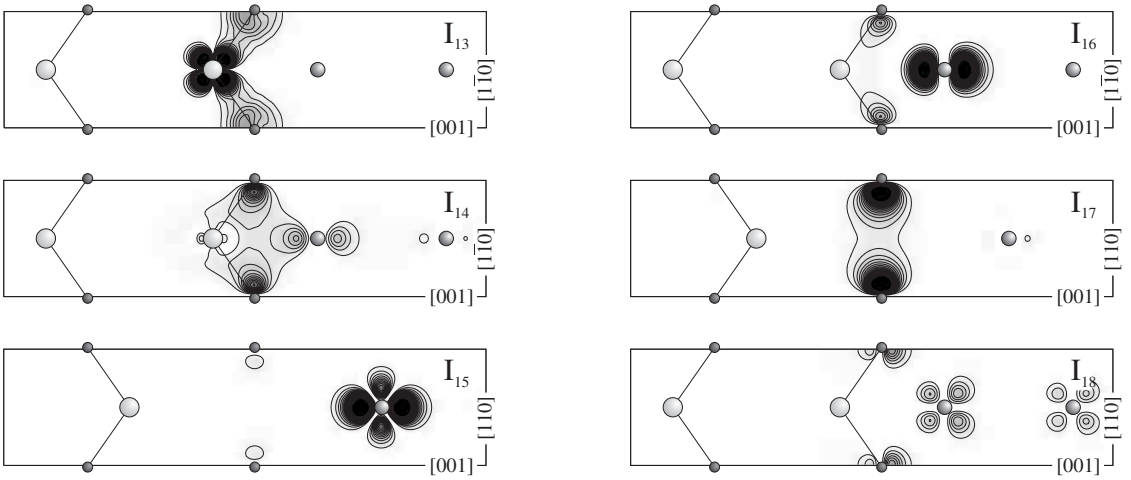

Figure 5.25: Contour plot of the interface states I_{13} up to I_{18} of the Au/GaN(001) contact (geometry B) at the **K** point of the BZ. Contour spacing is $1 \cdot 10^{-2} e/a_0^3$.

Compared to the results for geometry B of the Al/GaN contact it turns out that the Au/GaN junctions exhibit more localized interface states due to Au surface states. In order to understand better the Au bulk and surface contributions to the electronic properties of the interface, we discuss in the following section its surface states both without and with a compressive strain along the growth direction.

5.3.2 The Au(001) surface under strain

Au is softer than Al and it can therefore be expected that its electronic structure is not affected by compressive strains as much as that of Al. In Fig. 5.26, we present the electron band structure in the 2D-BZ of an Au(001) slab together with the projected Au bulk band structure. The left-hand panel shows the results for the equilibrium geometry, the right-hand panel shows the band structure of the slab in the same geometry, i.e. with applied compressive strain, used for the Au/GaN(001) interface. Both surface calculations have been performed using slabs containing 21 layers of Au atoms, amounting to 231 valence electrons per supercell. An energy cutoff of 80 Ry and a (8,8,1) MP grid was used. The Fermi level was calculated using a Gaussian electronic-level broadening scheme with a standard deviation of 0.01 Ry. The bulk simulations for the projected band structure were performed with a (16,16,16) MP grid and E_{cut} = 40 Ry.

The energy range from E_F -10 eV up to E_F -2 eV of the band structures are dominated by 5*d* bands while *s* like bands occur around the Fermi level and at higher energy. We note in this context, that due to the significant spatial overlap of *d* and *s* orbitals, a strict distinction between *d* and *s* bands is not possible. The states are much hybridized with varying *d*- and *s*-like contributions.

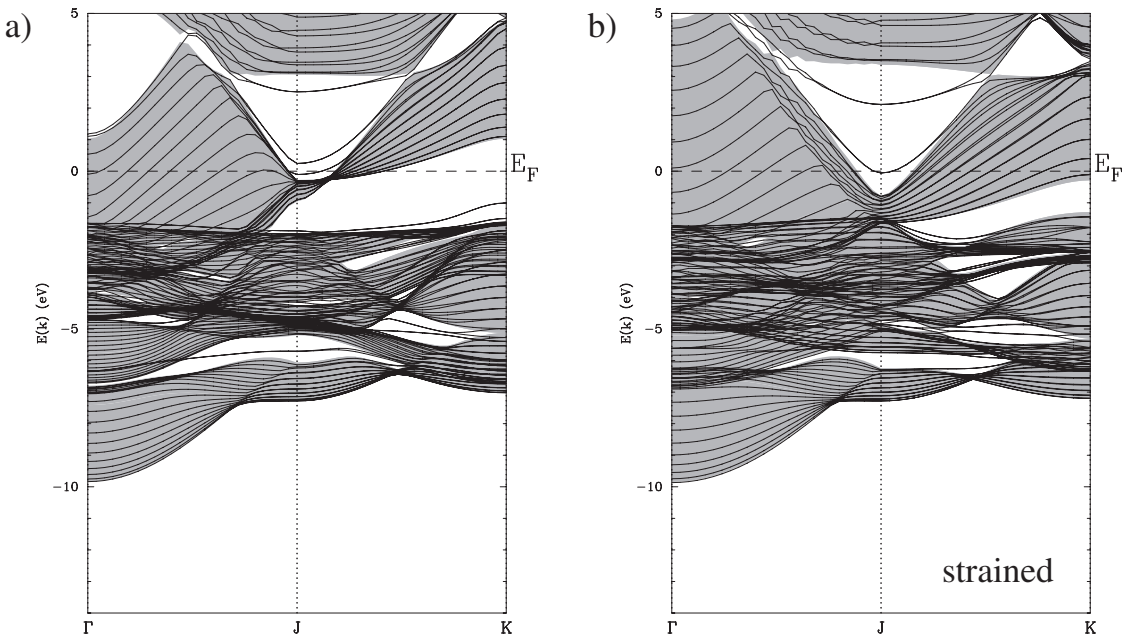

Figure 5.26: Projected band structures of epitaxial bulk Au along high-symmetry lines of the surface BZ. **a)** shows the unstrained, equilibrium geometry. The solid lines show the band structure of 21 layer Au slab calculation. **b)** represents the highly strained geometry used for the Au/GaN(001) interface.

Around the **J** point of the BZ a large stomach gap with a triangular shape occurs from slightly below E_F up to E_F + 3 eV. Therein several surface state bands not degenerate with projected bulk states appear. Several surface states are also present in the lower part of the band structure. In the equilibrium geometry, the borders of the large stomach gap along the path **J**-**K** cross the Fermi level. At around E_F - 2 eV, a surface state is present over the whole BZ.

In the situation of applied strain shown in the right-hand panel of Fig. 5.26, the *s*-like bands are spread out in energy. In particular, along the line **J**-**K** the size of the stomach gap between *s* and *d* bands is reduced and the Fermi level is degenerate with bulk states. The lower-energy *d*-like bands are weakly affected by the applied strain. The surface states in the stomach gap centered at the **J** point are equally weakly affected by the strain. Considering their energy position around the Fermi level, these surface state play an important role in the formation of the interface states discussed in the previous section.

5.3.3 Discussion

We have investigated the electronic structure of Au/GaN(001) interfaces for two atomic geometries. For both interface configurations, numerous localized and resonant interface states occur. Comparing the two interface geometries A and B, the same trends as for the Al/GaN(001) junction are observed: going from A to B, the equilibrium interfacial distance is increased and as consequence, the SBH is decreased. While interface states at low energy are weakly affected by the atomic interface configuration, the interface states in the semiconductor optical gap are different for the two geometries. Only in configuration B, the interface state attributed to the GaN bridge bond surface state does not interact with the metal and remains localized over the whole BZ. Furthermore, the intermetallic bonding like interface states does exclusively occur when the interfacial metal atom is placed in front of the outermost semiconductor cation.

Comparing the Au(001)surface band structure with those of the two Au/GaN(001) interfaces, it turns out that Au surface states around the **J** point interact with GaN surface states forming the interface states I_5, I_8 and I_9 for the configuration A (see Fig. 5.16) and I_4-I_6, I_9 and I_{10} for the interface geometry B (see Fig. 5.21). In the latter case, I_6 is close enough to the GaN conduction band and therefore the intermetallic interface state already identified for the Al/GaAs, Al/AlAs and Al/GaN(configuration B) contacts is formed as shown in Fig. 5.22. As in the case of Al/GaN, its energy is well above the Fermi level. Thus, this state cannot contribute to the transport properties of the Au/GaN interface.

From the occurrence of intermetallic bonding-like interface states also at the Au/GaN junction we conclude that its formation mechanism is very general. However, these states occur at high energies above the Fermi level. As a consequence, they are unoccupied and do not contribute to transport properties of the contact. Furthermore it has to be noted, that these states do not occur for the equilibrium interface geometry A since the facing metal atoms are too far from the outermost Ga atom.

5.4 The Cu/GaN(001) interface

The results for Al/GaN(001) and Au/GaN(001) cannot be confirmed easily with those obtained for Al/GaAs(001) and Al/AlAs(001) junctions since the interfaces have different geometry. In this context, it would be interesting to find a metal with a lattice constant as close as possible to $a_{GaN}/\sqrt{2} = 3.17$ Å. An ideal candidate could be W with a lattice constant of 3.16 Å, but it is technological very difficult to handle. Experimental contacts to GaN are normally realized with Au, Ag, Pt and several alloys using Ti ($a = 2.95$ Å), Ni ($a = 3.52$ Å), Al ($a = 4.05$ Å) and V ($a = 3.03$ Å) [32–36]. Using alloys is a common technique in order to adjust the lattice constant and to tune the work function of the metallic part of the contact.

We propose alternatively Cu to realize a contact to cubic GaN(001) using the same interface geometry used for Al/GaAs. Cu has the experimental lattice constant $a_{Cu} = 3.61$ Å [183], which is closer to $a_{GaN}/\sqrt{2}$ than to a_{GaN}.

In our calculations, we use a pseudopotential for Cu with the parameters shown in Fig. 5.1. Therein, we treat the closed $3d$ electron shell as valence electrons since a treatment of these electrons as frozen core states leads to inaccurate results. Using this pseudopotential for Cu, we obtain an LDA-value 3.57 Å for the lattice constant. Thus, the lattice mismatch between Cu and GaN is about 13% which is larger than the lattice mismatch between Al and GaN or Au and GaN. The applied strain is accommodated with an expansion along the growth direction. By performing total energy minimizations as a function of $a_\perp$, we obtain $a_\perp = 4.10$ Å for the Cu orthogonal lattice constant, when $a_\parallel$ is fixed to the value of $a_{\mathrm{GaN}}/\sqrt{2}$.

We model the interface with a slab geometry using a supercell containing 13 atomic layers of GaN and 7 atomic layers of Cu with a total number of 27 atoms and 267 valence electrons per supercell. The Cu fcc lattice is rotated by 45° around the [001] growth axis with respect to the cubic lattice of GaN (see Fig. 5.27).

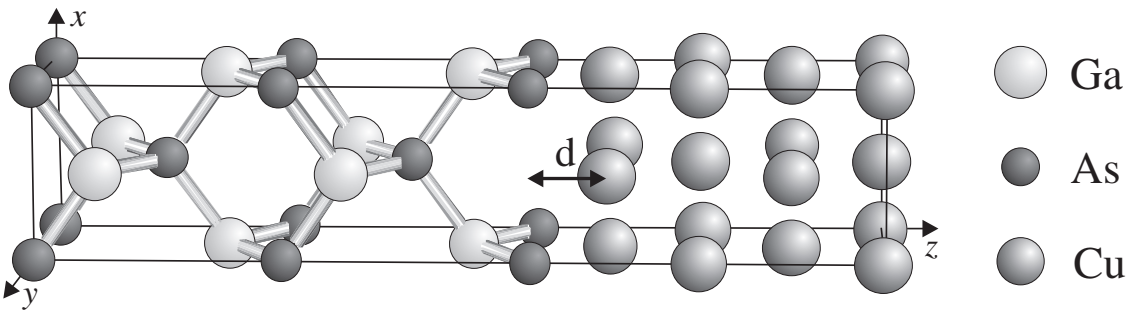

Figure 5.27: Atomic structure of the abrupt, N-terminated Cu/GaN(001) interface.

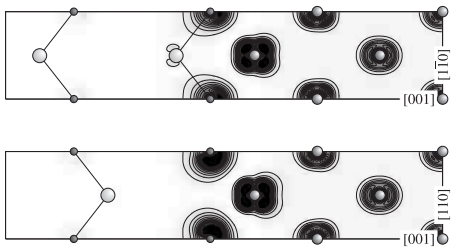

Figure 5.28: Contour plot in the two border planes of the integrated probability density of all electronic states with energy in the range [E_F- 1 eV, E_F +1 eV]. Contour spacing is $2 \cdot 10^{-1} e/a_0^3$.

The equilibrium interfacial distance is $d_0 = 1.45$ Å and the equilibrium supercell volume is $\Omega_0 = 1932\ a_0^3$. In the following, we carry out the same analysis of the electron structure at the interface as for the other systems. In Fig. 5.28, the contour plots of the electron density corresponding to all electronic states with energy in the range [E_F - 1 eV, E_F + 1 eV] amounting to 12.0 electrons per supercell are shown. The calculation was performed with a cutoff energy of 80 Ry and a (10,10,1) MP grid.

The probability density exhibits *s*-like maxima around the interfacial N atoms as well as *d*-like maximum values at the outermost Cu atoms. In the bulk-like region of the metal, the density is very similar to that of the Au/GaN(001) interface, indicating that the Cu 3*d* orbitals influence the electron structure near the Fermi energy in the same way as it was observed for the Au 5*d* bands. As for the two other metal contacts to GaN no intermetallic bonding-like structure occurs in this energy range between the outermost Ga and the interfacial Cu atoms.

The interface band structure is shown in Fig. 5.29. Therein, solid lines represent the numerical results of the Cu/GaN superlattice. The light and dark grey shaded areas show to projected bulk states of Cu and GaN, respectively. It turns out, that the interface band structure at energy corresponding to the lower part of the GaN valence band is comparable to those of the Al/GaN and Au/GaN contacts. Stomach gaps of the projected band structure in the semiconductor optical gap occur around the **Γ** and the **K** point, but not at the **J** point. The energy positions of several selected interface states are indicated with circles.

As in the previous sections, we discuss briefly the structure of the interface states indicated in Fig. 5.29. We start with states at the **J** point, shown in Fig. 5.30. I_1 and I_2 represent GaN surface states as we have already found for the Al/GaN and Au/GaN junctions. I_3 is a bonding interface state between N p_y and Cu *d* orbitals. It exhibits a structure similar to that of I_6 at the Au/GaN(geometry A) contact. I_4 has very high energy (E_F + 4.2 eV) and is degenerate with Cu and GaN bulk states. Thus it is not well localized and it should not play a role in the transport properties of the junction since it is unoccupied. In order to better identify its structure, the contour spacing has been reduced by a factor of five. However, this state is remarkable since it has intermetallic bonding-like nature.

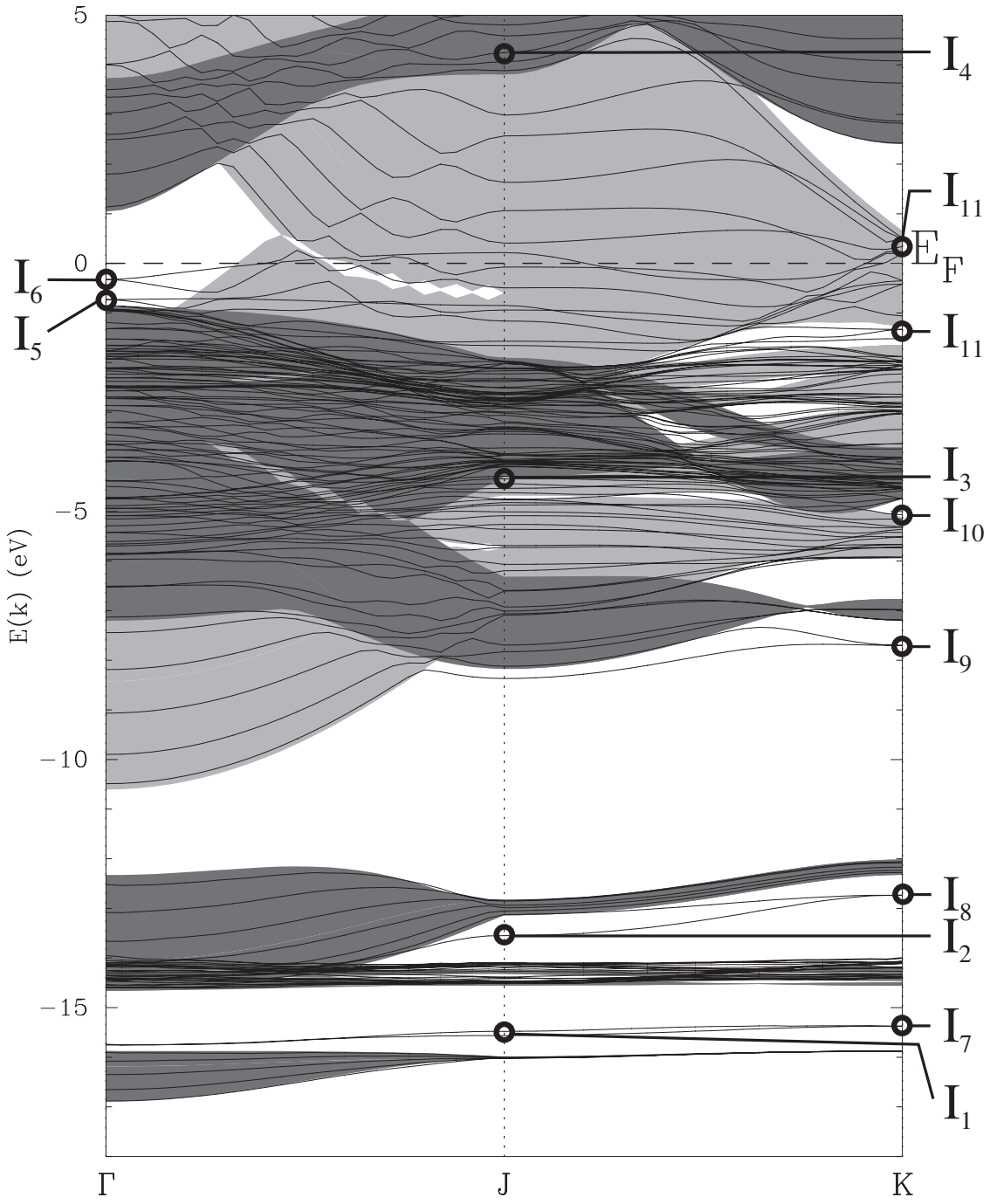

Figure 5.29: Electron band structure of the Cu/GaN(001) interface. The projected band structures of bulk GaN and Cu are shown as dark grey and light grey areas, respectively. Circles indicate the energy position of interface states discussed in the following figures .

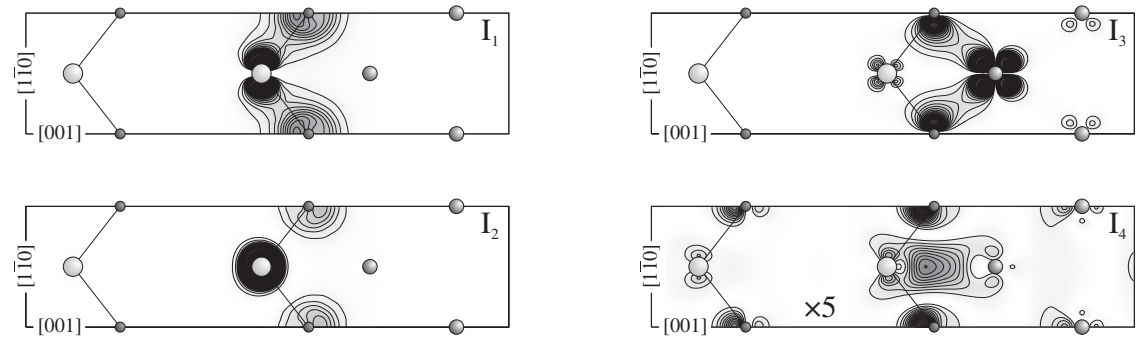

Figure 5.30: Contour plot of the interface states I_1 up to I_4 of the Cu/GaN(001) contact at the **J** point of the BZ. Contour spacing is $1 \cdot 10^{-2} e/a_0^3$ for I_1 up to I_3 and $2 \cdot 10^{-3} e/a_0^3$ for I_4

In Fig. 5.31, we present the contour plots of the two interface state bands in the stomach gap at **Γ** above the semiconductor valence band maximum. I_5 is a Cu surface state formed by 3*d* orbitals. It is shown in the *xy* diagonal plane passing through the interfacial Cu atoms since its wavefunction has nodes in the *x* and *y* planes. I_6 corresponds to an anti-bonding interface state between the GaN bridge bond surface state and a Cu surface state. It corresponds to state I_{11} of the Au/GaN(geometry B).

At the **K** point of the BZ, the interface states are very similar to those observed at the Au/GaN junction. The contour plots of their probability density are shown in Fig. 5.32. I_7 and I_8 correspond to GaN surface states formed by N *s* and Ga *d* orbitals. I_7 is the bonding state while I_8 is the anti-bonding one. I_9 is the bonding interface state formed by Ga *d*, N *p* and Cu *d* orbitals. This state occurs also at the Au/GaN(geometry B) interface (see I_{14} in Fig. 5.25). I_{10} and I_{11} are interface states with large contributions of the GaN dangling bond and bridge bond surface states, respectively. Both states exhibit also contributions of Cu 3*d* orbitals. Finally, I_{12} is an interface state mostly related to a Cu surface state.

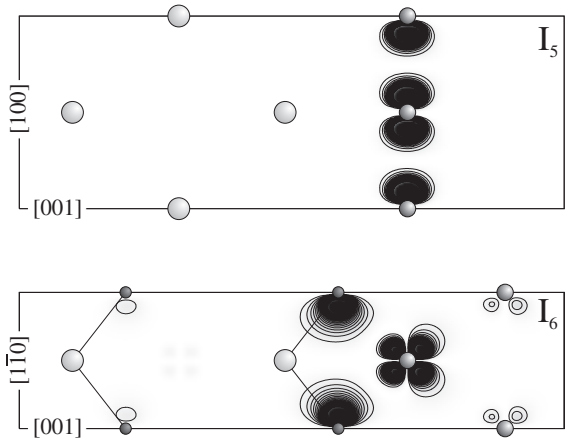

Figure 5.31: Contour plot of the interface states I_5 and I_6 at the **Γ** point of the BZ. I_6 is shown in the [100] GaN crystal plane passing through the interfacial Cu atoms, i.e. in the *xy* diagonal plane with an offset of a half supercell in the *x* direction. Contour spacing is $1 \cdot 10^{-2} e/a_0^3$.

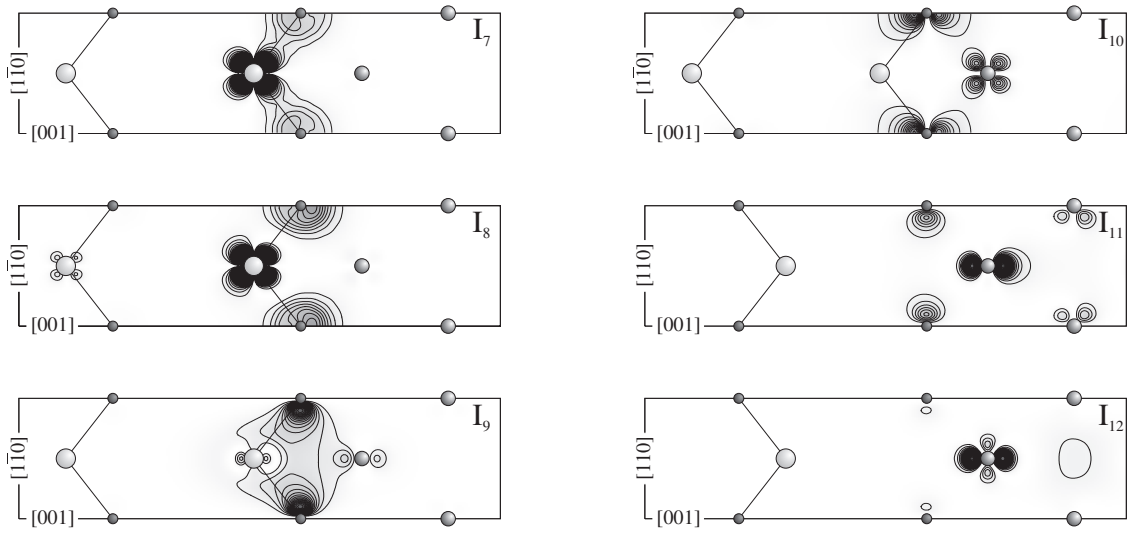

Figure 5.32: Contour plot of the interface states I_7 up to I_{12} at the **K** point of the BZ. Contour spacing is $1 \cdot 10^{-2} e/a_0^3$.

Since the electronic structure of this interface is very similar to that of Au/GaN, we investigate in the following section the electronic structures of bulk Cu and of the Cu(001) surface in order to compare them with those of bulk Au and of the Au(001) surface.

5.4.1 The Cu(001) surface under strain

In Fig. 5.33, we present the electron band structure in the 2D-BZ of a Cu(001) slab together with the projected Cu bulk band structure. In order to compare these results with those of Au, we consider the (1×1) configuration with one atom per layer. In order to apply these results to the configuration used to model the Cu/GaN interface, the BZ points **J** and **K** have to be identified with **M** and **X** as described in section 3.2.

The left-hand panel of Fig. 5.33 shows the results for the equilibrium geometry, the right-hand panel shows the band structure of the slab in the same atomic geometry with applied compressive strain used to model the Cu/GaN(001) interface. Both surface calculations have been performed using slabs containing 21 layers of Cu atoms, amounting to 231 valence electrons per supercell. An energy cutoff of 80 Ry and a (10,10,1) MP grid was used. The Fermi level was calculated using a Gaussian electronic-level broadening scheme with a standard deviation of 0.01 Ry. The bulk simulations for the projected band structure were performed with a (16,16,16) MP grid and E_{cut} = 80 Ry.

The band structures in the energy range from E_F - 12 eV up to E_F - 2 eV are dominated by 3d states while s-states occur around the Fermi level and at higher energy. As for Au, a strict distinction between d and s bands is impossible due to the degeneracy in energy between d and s states.

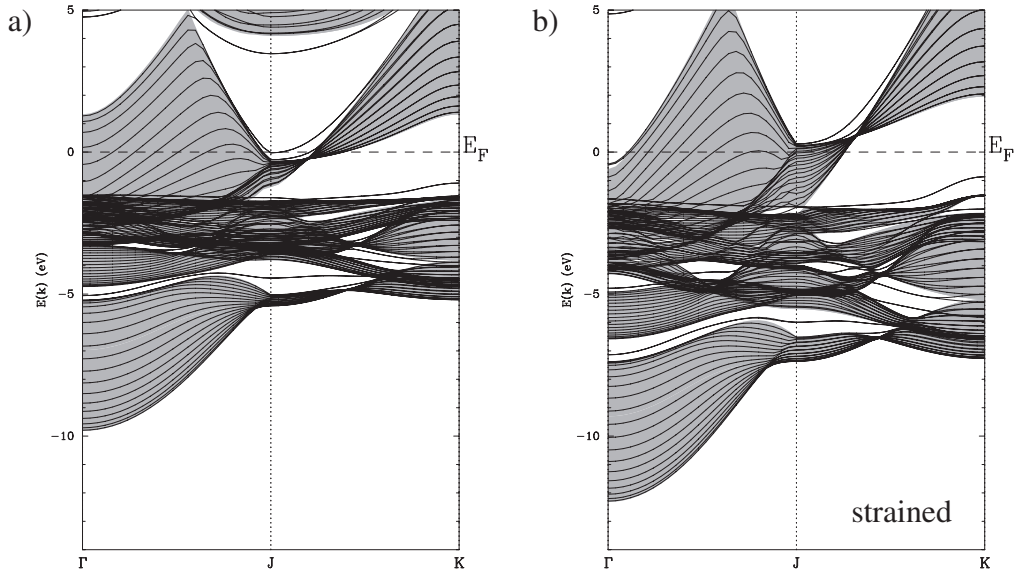

Figure 5.33: Projected band structures of epitaxial bulk Cu along high-symmetry lines of the surface BZ. **a)** shows the unstrained, equilibrium geometry. The solid lines show the band structure of 21 layer Cu slab calculation. **b)** represents the strained geometry used for the Cu/GaN(001) interface.

Around the **J** point of the BZ a large stomach gap with a triangular shape occurs above E_F.Therein several surface states not degenerate with projected bulk states appear. Several surface states occur also in the lower parts of the band structure. In the equilibrium geometry, the borders of the large stomach gap along the path **J**-**K** cross the Fermi level. At around E_F - 2 eV a surface state is present over the whole BZ.

A second energy gap with a parabolic shape occurs around the **Γ** point. The minimum of this gap is at about $E_F + 1$ eV for the equilibrium, unstrained geometry and slightly below E_F for the strained structure.

The electronic structures of Cu and Au, are very similar, especially in the unstrained case. This can be explained by the fact that apart from the different frozen core configurations, valence electron states are similar. Both pseudopotentials bind a closed shell of *d*-electrons and one *s*-electron. Additionally, the effect of strain is consistent: while compressive strain applied to the Au slab raises the minimum of the parabolic gap, the expansive strain lowers the energy minimum of this gap in the case of Cu. The same effect with opposite sign occurs for the *s*-related bands at the Fermi energy along the path **J**-**K**. For Cu, these bands are raised in energy while for Au these bands are lowered in energy.

5.4.2 Discussion

We have investigated the electronic structure of the Cu/GaN(001) interface. Considering the charge density of electron states around the Fermi energy and the structure of interface states, the results are very similar to those obtained for the Au/GaN(001) junctions. This is remarkable since the atomic structure of the two interfaces is different: in the case of Au, the metal atoms continue the Ga fcc sublattice, in the case of Cu, the metal fcc structure is rotated by 45° around the [001] growth axis.

Interface state exhibiting contributions of metal surface states are related to *d*-like atomic orbitals. The interface state I_4 confirms the formation mechanism of the intermetallic bonding-like interface state as a general one. This state occurs in the semiconductor band gap for all interfaces we have investigated whenever a metal atom is placed in front of the outermost semiconductor cation. However, this state occurs at the Cu/GaN junction at very high energies. It is even degenerate with GaN conduction band edge states. It remains to be clarified, why the GaN conduction states are not so repulsive to place the intermetallic bonding-like state below the conduction band edge, as it is the case for the other interfaces.

The similar electronic structure of Cu and Au explains the very similar results for the Au/GaN and the Cu/GaN junctions. It turns out, that the metal *d* valence electrons play an important role in the formation of interface states. Furthermore, it seems that the electronic properties of the metal are more important than the interface geometry: the electronic structures of Cu/GaN and Au/GaN are comparable and the metal pseudopotentials are similar, but the interface morphology is different. The Al/GaN and Au/GaN junctions show considerable differences in the structure of interface states. In this case, the atomic structure at the interface is similar, but the metal pseudopotentials are different.

6 Conclusions

We have carried out a detailed study of the electronic structure of metal contacts to representative cubic III-V semiconductors. We focused especially on the existence, nature and formation mechanisms of interface states and their role in the formation of Schottky barriers. Using state-of-the-art *ab initio* pseudopotential calculations in the framework of the local density approximation to density functional theory, we have calculated the electronic states at abrupt, defect-free, anion-terminated metal/semiconductor junctions. Specifically, we have investigated Al contacts to GaAs(001), AlAs(001) and cubic GaN(001) as well as Al, Au and Cu junctions to N-terminated cubic GaN(001).

For abrupt, ideal metal/semiconductor interfaces without extrinsic defects at the junction and without major differences of the atomic structure and the valencies between the two constituents, one would not have expected strongly localized interface states near the Fermi energy. We have found, on the contrary, localized states and strong resonances at the interface of our systems whose energy is in the semiconductor optical band gap. Careful analysis revealed that this is made possible by the symmetry properties of the relevant electron wavefunctions.

These interface states can be classified into three groups according to their nature: interface states related to surface states of one of the two constituting materials, interface states formed by the interaction between surface states of both the metal and the semiconductor and intermetallic, bonding-like interface states. The latter ones form a strong bond between the interfacial metal atoms and the outermost semiconductor cations. This structure is very remarkable since its bond length is about 3 Å, which is almost two times larger than the typical interatomic bond length in covalent solids. To our knowledge, states having this structure have not been reported previously in the literature.

Calculations of the electronic structure of the junction as a function of the distance between the metal and the semiconductor slabs have allowed us to connect localized and resonant states occurring at the interface with the surface states of the free-standing, unreconstructed surfaces of the two materials. A continuous monitoring of energy levels and wavefunctions of interface state bands as a function of the interfacial distance allowed us to investigate the influence of surface states of the constituting, unreconstructed slabs on the formation of interface states occurring at the intimate contact.

We have identified the mechanism responsible for the formation of the intermetallic, bonding interface state as an interaction between localized states of the isolated metal (001) surface and semiconductor bulk conduction band-edge states, mediated by dangling bond surface states of the isolated, unreconstructed semiconductor (001) surface. The existence of this state, not only for one particular interface but generally also at those junctions fulfilling the condition that atoms on the outermost atomic plane of the metal are placed in front of the outermost semiconductor cation, revealed that its formation mechanism is very robust. In the case of contacts to GaAs and AlAs, this state has energy close to the Fermi level while its energy is largely above E_F for metal/GaN(001) junctions.

Analysis of all states near the Fermi energy, i.e. those contributing mostly to electronic transport across the interface, indicates that the intermetallic bonding-like structure should have a relevant contribution to the macroscopic electronic processes of Al/GaAs and Al/AlAs junctions. At metal/GaN junctions, these states are not expected to contribute to the electronic transport since their energy is much too large with respect to E_F.

Our results for Al contacts to a series of different semiconductors have allowed us to investigate the effect of semiconductor ionicity on the Schottky barrier formation and on the nature and existence of interface states. The comparison of the Schottky barrier heights of the three Al/semiconductor systems indicates that the larger the ionicity and the band gap of the semiconductor the larger is the resulting *p*-type SBH. The electronic structure and nature of surface states of the unreconstructed (001) surfaces of GaAs, AlAs and cubic GaN shows, that the surface state bands in the optical gap region near the Fermi energy are very similar for the three semiconductors. The differences in semiconductor ionicity and band gap energies affect only weakly the nature of surface states close to the optical gap. Direct inspection of interface electron states confirmed that the semiconductor surface states play an equally important role in the formation of interface states for the three semiconductors.

We also investigated the properties of contacts between different metals and GaN. The results for junctions between GaN and Al, Au and Cu show that the SBH depends strongly on the metal work function, indicating that no pinning of the Fermi level occurs at these abrupt, ideal contacts. Concerning the existence and nature of interface states we have shown that Au and Cu surface states related to $3d$ orbitals give rise to a large number of interface states over a wide energy range including E_F.

Considering that our results do not indicate Fermi level pinning at metal contacts to GaN, and taking into account the experimental evidence of Fermi level pinning at metal/$Al_xGa_{1-x}As$ junctions, our numerical results indicate that interface states of the intermetallic, bonding-like kind could play an important role in the positioning of the Fermi level during the interface formation at metal/$Al_xGa_{1-x}As$ interfaces.

References

[1] W. Mönch. *Electronic structure of metal-semiconductor contacts* (Kluwer, Dordrecht, 1990).

[2] R. T. Tung. *Recent advances in Schottky barrier concepts.* Materials Science & Engineering R-Reports, **35**(1-3), 1 (2001).

[3] G. Margaritondo. *Electronic structure of semiconductor heterojunctions* (Kluwer, Dordrecht, 1988).

[4] G. Margaritondo. *Interface states at semiconductor junctions.* Reports on Progress in Physics, **62**(5), 765 (1999).

[5] L. J. Brillson. *Contacts to semiconductors fundamentals and technology* (Noyes Publications, Park Ridge, New Jersey, 1993).

[6] E. H. Rhoderick and R. H. Williams. *Metal-semiconductor contacts* (Clarendon Press, Oxford, 1988), 2nd edition.

[7] E. G. Clarke and A. W. Czanderna. *Optical Transmittance and Microgravimetric Studies of Oxidation of (100) Single-Crystal Films of Copper.* Surface Science, **49**(2), 529 (1975).

[8] L. J. Brillson. *Interaction of Metals with Semiconductor Surfaces.* Applied Surface Science, **11-2**(JUL), 249 (1982).

[9] A. Zangwill and A. C. Redfield. *Structural Selectivity in Aluminum Transition-Metal Alloys.* Journal of Physics F-Metal Physics, **18**(1), 1 (1988).

[10] F. Braun. *Ueber die Stromleitung durch Schwefelmetalle.* Annalen der Physik und Chemie, **153**, 556 (1874).

[11] W. Schottky and W. Deutschmann. *Zum Mechanismus der Richtwirkung von Kupfergleichrichtern.* Physikalische Zeitschrift, **30**, 839 (1929).

[12] E. H. Rhoderick. *Conduction Mechanism in Schottky Diodes.* Journal of Physics D-Applied Physics, **5**(10), 1920 (1972).

[13] A. G. Milnes and D. L. Feucht. *Heterojunctions and metal-semiconductor junctions* (Academic Press, New York, 1972).

[14] F. Capasso and G. Margaritondo (editors). *Heterojunction band discontinuities physics and device applications* (North-Holland, Amsterdam, 1987).

[15] E. H. Rhoderick. *Levines Model of Schottky Barriers.* Journal of Applied Physics, **46**(6), 2809 (1975).

[16] H. Kroemer. *Heterostructure Devices - a Device Physicist Looks at Interfaces.* Surface Science, **132**(1-3), 543 (1983).

[17] N. Newman, M. Vanschilfgaarde, T. Kendelwicz, M. D. Williams, and W. E. Spicer. *Electrical Study of Schottky Barriers on Atomically Clean GaAs(110) Surfaces.* Physical Review B, **33**(2), 1146 (1986).

[18] J. R. Waldrop. *Electrical-Properties of Ideal Metal Contacts to GaAs - Schottky-Barrier Height.* Journal of Vacuum Science & Technology B, **2**(3), 445 (1984).

[19] M. Prietsch. *Ballistic-Electron-Emission Microscopy (BEEM) - Studies of Metal-Semiconductor Interfaces with Nanometer Resolution.* Physics Reports-Review Section of Physics Letters, **253**(4), 164 (1995).

[20] W. J. Kaiser and L. D. Bell. *Direct Investigation of Subsurface Interface Electronic-Structure by Ballistic-Electron-Emission Microscopy.* Physical Review Letters, **60**(14), 1406 (1988).

[21] L. D. Bell, W. J. Kaiser, M. H. Hecht, and F. J. Grunthaner. *Direct Control and Characterization of a Schottky-Barrier by Scanning Tunneling Microscopy.* Applied Physics Letters, **52**(4), 278 (1988).

[22] L. J. Brillson. *Surfaces and Interfaces: Atomic-Scale Structure, Band Bendeing and Band Offsets.* In *Handbook on semiconductors* (edited by T. S. Moss), volume 1, pages 281–417 (North-Holland, Amsterdam, 1992), completely revised and enlarged edition.

[23] J. R. Waldrop. *Schottky-Barrier Height of Ideal Metal Contacts to GaAs.* Applied Physics Letters, **44**(10), 1002 (1984).

[24] C. Barret and J. Massies. *On the Dependence of Schottky-Barrier Height and Interface States Upon Initial Semiconductor Surface Parameters in GaAs (001)/Al Junctions.* Journal of Vacuum Science & Technology B, **1**(3), 819 (1983).

[25] Y. A. Goldberg and Tsarenko.Bv. *Investigation of Relaxation of Capacitance of Surface-Barrier Structures and Determination of Parameters of Impurity Atoms in N-Type GaAs.* Soviet Physics Semiconductors-USSR, **5**(9), 1553 (1972).

[26] Y. A. Goldberg, Tsarenko.Bv, Y. P. Yakovlev, and T. Y. Rafiev. *Surface-Barrier Structures of Metal and N-Type $Ga_{1-x}Al_xAs$, and their Energy-Band Diagram.* Soviet Physics Semiconductors-USSR, **6**(3), 398 (1972).

[27] J. S. Best. *Schottky-Barrier Height of Au on n-$Ga_{1-x}Al_xAs$ as a Function of AlAs Content.* Applied Physics Letters, **34**(8), 522 (1979).

[28] K. Okamoto, C. E. C. Wood, and L. F. Eastman. *Schottky-Barrier Heights of Molecular-Beam Epitaxial Metal-AlGaAs Structures.* Applied Physics Letters, **38**(8), 636 (1981).

[29] L. J. Brillson, M. L. Slade, R. E. Viturro, M. K. Kelly, N. Tache, G. Margaritondo, J. M. Woodall, P. D. Kirchner, G. D. Pettit, and S. L. Wright. *Absence of Fermi Level Pinning at Metal-$In_xGa_{1-x}As$ (100) Interfaces.* Applied Physics Letters, **48**(21), 1458 (1986).

[30] K. Kajiyama, Mizushim.Y, and S. Sakata. *Schottky-Barrier Height of n-$In_xGa_{1-x}As$ Diodes.* Applied Physics Letters, **23**(8), 458 (1973).

[31] K. Kajiyama, S. Sakata, and O. Ochi. *Barrier Height of HF-GaAs Diode.* Journal of Applied Physics, **46**(7), 3221 (1975).

[32] T. U. Kampen and W. Mönch. *Metal contacts on α-GaN.* Mrs Internet Journal of Nitride Semiconductor Research [http://nsr.mij.mrs.org/], **1**(1-46), art. no. 41 (1996).

[33] A. C. Schmitz, A. T. Ping, M. A. Khan, Q. Chen, J. W. Yang, and I. Adesida. *Metal contacts to n-type GaN.* Journal of Electronic Materials, **27**(4), 255 (1998).

[34] Q. Z. Liu and S. S. Lau. *A review of the metal-GaN contact technology.* Solid-State Electronics, **42**(5), 677 (1998).

[35] J. S. Foresi and T. D. Moustakas. *Metal Contacts to Gallium Nitride.* Applied Physics Letters, **62**(22), 2859 (1993).

[36] S. J. Pearton, J. C. Zolper, R. J. Shul, and F. Ren. *GaN: Processing, defects, and devices.* Journal of Applied Physics, **86**(1), 1 (1999).

[37] W. Schottky. *Halbleitertheorie der Sperrschicht.* Naturwissenschaften, **26**(52), 843 (1938).

[38] N. F. Mott. *Note on the contact between a metal and an insulator or semi-conductor.* Proceedings of the Cambridge Philosophical Society, **34**, 568 (1938).

[39] B. Davydov. *The rectifying action of semiconductors.* Technical Physics of the USSR, **5**, 87 (1938).

[40] B. Davydov. *On the contact resistance of semi-conductors.* Journal of Physics, **1**(2), 167 (1939).

[41] S. Kurtin, T. C. Mcgill, and C. A. Mead. *Fundamental Transition in Electronic Nature of Solids.* Physical Review Letters, **22**(26), 1433 (1969).

[42] M. Schlüter. *Chemical Trends in Metal-Semiconductor Barrier Heights.* Physical Review B, **17**(12), 5044 (1978).

[43] J. Bardeen. *Surface States and Rectification at a Metal Semi-Conductor Contact.* Physical Review, **71**(10), 717 (1947).

[44] I. Y. Tamm. *Über eine mögliche Art der Elektronenbindung an Kristalloberflächen.* Physikalische Zeitschrift der Sowjetunionen, **1**, 733 (1932).

[45] I. Y. Tamm. *Über eine mögliche Art der Elektronenbindung an Kristalloberflächen.* Zeitschrift für Physik, **76**, 849 (1932).

[46] W. Shockley. *On the surface States Associated with a periodic potential.* Physical Review, **56**, 317323 (1939).

[47] A. M. Cowley and S. M. Sze. *Surface States and Barrier Height of Metal-Semiconductor Systems.* Journal of Applied Physics, **36**(10), 3212 (1965).

[48] V. Heine. *Theory of Surface States.* Physical Review, **138**(6A), 1689 (1965).

[49] F. Yndurain. *Density of States and Barrier Height of Metal-Si Contacts.* Journal of Physics Part C Solid State Physics, **4**(17), 2849 (1971).

[50] E. Louis, F. Yndurain, and F. Flores. *Metal-Semiconductor Junction for (110) Surfaces of Zincblende Compounds.* Physical Review B, **13**(10), 4408 (1976).

[51] F. Flores and C. Tejedor. *On the Formation of Semiconductor Interfaces.* Journal of Physics C-Solid State Physics, **20**(2), 145 (1987).

[52] F. Flores, A. Munoz, and J. C. Duran. *Semiconductor Interface Formation - the Role of the Induced Density of Interface States.* Applied Surface Science, **41-2**, 144 (1989).

[53] F. Flores and J. Ortega. *Semiconductor Interface Formation - Theoretical Aspects.* Applied Surface Science, **56-8**, 301 (1992).

[54] J. Tersoff. *Schottky-Barrier Heights and the Continuum of Gap States.* Physical Review Letters, **52**(6), 465 (1984).

[55] W. E. Spicer, P. W. Chye, P. R. Skeath, C. Y. Su, and I. Lindau. *New and Unified Model for Schottky-Barrier and III-V Insulator Interface States Formation.* Journal of Vacuum Science & Technology, **16**(5), 1422 (1979).

[56] H. H. Wieder. *Perspectives on III-V-Compound MIS Structures.* Journal of Vacuum Science & Technology, **15**(4), 1498 (1978).

[57] R. H. Williams, R. R. Varma, W. E. Spear, and P. G. Lecomber. *Fermi Level Position in Doped Amorphous Silicon.* Journal of Physics C-Solid State Physics, **12**(5), L209 (1979).

[58] W. E. Spicer, Z. Lilientalweber, E. Weber, N. Newman, T. Kendelewicz, R. Cao, C. Mccants, P. Mahowald, K. Miyano, and I. Lindau. *The Advanced Unified Defect Model for Schottky-Barrier Formation.* Journal of Vacuum Science & Technology B, **6**(4), 1245 (1988).

[59] H. Hasegawa and H. Ohno. *Unified Disorder Induced Gap State Model for Insulator-Semiconductor and Metal-Semiconductor Interfaces*. Journal of Vacuum Science & Technology B, **4**(4), 1130 (1986).

[60] J. L. Freeouf and J. M. Woodall. *Schottky Barriers - an Effective Work Function Model*. Applied Physics Letters, **39**(9), 727 (1981).

[61] J. L. Freeouf, M. Aono, F. J. Himpsel, and D. E. Eastman. *A Study of Schottky-Barrier Formation for Ga-Si(111)-(2x1) and Sb-Si(111)-(2x1) Interfaces*. Journal of Vacuum Science & Technology, **19**(3), 681 (1981).

[62] J. M. Woodall and J. L. Freeouf. *Summary Abstract: Are they really Schottky barriers after all?* Journal of Vacuum Science & Technology, **21**(2), 574 (1982).

[63] R. T. Tung. *Chemical bonding and Fermi level pinning at metal-semiconductor interfaces*. Physical Review Letters, **84**(26), 6078 (2000).

[64] R. T. Tung. *Formation of an electric dipole at metal-semiconductor interfaces*. Physical Review B, **6420**(20) (2001).

[65] J. Ihm, S. G. Louie, and M. L. Cohen. *Electronic-Structure of Ge and Diamond Schottky Barriers*. Physical Review B, **18**(8), 4172 (1978).

[66] J. Ihm, A. Zunger, and M. L. Cohen. *Momentum-Space Formalism for the Total Energy of Solids*. Journal of Physics C-Solid State Physics, **12**(21), 4409 (1979).

[67] J. Ihm and M. L. Cohen. *Self-Consistent Pseudopotential Calculations of the Equilibrium Properties of Bulk and Surface Si*. Solid State Communications, **29**(10), 711 (1979).

[68] J. Ihm and M. L. Cohen. *Self-Consistent Calculation of the Electronic-Structure of the (110) GaAs-Znse Interface*. Physical Review B, **20**(2), 729 (1979).

[69] S. G. Louie and M. L. Cohen. *Self-Consistent Pseudopotential Calculation for a Metal-Semiconductor Interface*. Physical Review Letters, **35**(13), 866 (1975).

[70] S. G. Louie. *Pseudopotential Calculations and Theory of Metal-Semiconductor Interfaces*. Bulletin of the American Physical Society, **21**(3), 377 (1976).

[71] S. G. Louie and M. L. Cohen. *Electronic-Structure of a Metal-Semiconductor Interface*. Physical Review B, **13**(6), 2461 (1976).

[72] S. G. Louie, J. R. Chelikowsky, and M. L. Cohen. *Ionicity and Theory of Schottky Barriers*. Physical Review B, **15**(4), 2154 (1977).

[73] S. B. Zhang, M. L. Cohen, and S. G. Louie. *Interface Potential Changes and Schottky Barriers*. Physical Review B, **32**(6), 3955 (1985).

[74] S. B. Zhang, M. L. Cohen, and S. G. Louie. *Structural and Electronic-Properties of the Al-GaAs(110) Interface*. Physical Review B, **34**(2), 768 (1986).

[75] S. B. Zhang, D. Tománek, S. G. Louie, M. L. Cohen, and M. S. Hybertsen. *Quasiparticle Calculation of Valence Band Offset of AlAs-GaAs(001).* Solid State Communications, **66**(6), 585 (1988).

[76] R. G. Dandrea and C. B. Duke. *Interfacial Atomic Composition and Schottky-Barrier Heights at the Al/GaAs(001) Interface.* Journal of Vacuum Science & Technology B, **11**(4), 1553 (1993).

[77] R. G. Dandrea and C. B. Duke. *Calculation of the Schottky-Barrier Height at the Al/GaAs(001) Heterojunction - Effect of Interfacial Atomic Relaxations.* Journal of Vacuum Science & Technology a-Vacuum Surfaces and Films, **11**(4), 848 (1993).

[78] J. Bardi, N. Binggeli, and A. Baldereschi. *Structural and compositional dependences of the Schottky barrier in $Al/Ga_{1-x}Al_xAs(100)$ and (110) junctions.* Physical Review B, **59**(12), 8054 (1999).

[79] A. Ruini, R. Resta, and S. Baroni. *Effects of interface morphology on Schottky-barrier heights: A case study on Al/GaAs(001).* Physical Review B, **56**(23), 14921 (1997).

[80] R. J. Needs, J. P. A. Charlesworth, and R. W. Godby. *1st-Principles Study of the Effects of Interface Structure on the Schottky-Barrier Height of the Al-GaAs(110) Interface.* Europhysics Letters, **25**(1), 31 (1994).

[81] M. van Schilfgaarde, E. R. Weber, and N. Newman. *Pressure-Dependence of III-V Schottky Barriers - a Critical Test of Theories for Fermi-Level Pinning.* Physical Review Letters, **73**(4), 581 (1994).

[82] W. E. Pickett, S. G. Louie, and M. L. Cohen. *Ge-Gaas (110) Interface - Self-Consistent Calculation of Interface States and Electronic-Structure.* Physical Review Letters, **39**(2), 109 (1977).

[83] W. E. Pickett, S. G. Louie, and M. L. Cohen. *Self-Consistent Calculations of Interface States and Electronic-Structure of (110) Interfaces of Ge-GaAs and AlAs-GaAs.* Physical Review B, **17**(2), 815 (1978).

[84] I. P. Batra, E. Tekman, and S. Ciraci. *Theory of Schottky-Barrier and Metallization.* Progress in Surface Science, **36**(4), 289 (1991).

[85] S. Ciraci and I. P. Batra. *Bonding and Electronic-Structure of the GaAs(110)-Al Interface.* Solid State Communications, **51**(1), 43 (1984).

[86] S. Ciraci, A. Baratoff, and I. P. Batra. *Fermi-Level Pinning in an Al-Ge Metal-Semiconductor Junction.* Physical Review B, **43**(9), 7046 (1991).

[87] J. Bardi, N. Binggeli, and A. Baldereschi. *Existence of localized interface states in metal/GaAs(100) junctions: Au versus Al contacts.* Physical Review B, **61**(8), 5416 (2000).

[88] G. P. Das, P. Blöchl, O. K. Andersen, N. E. Christensen, and O. Gunnarsson. *Electronic-Structure and Schottky-Barrier Heights of (111) $NiSi_2$/Si A-Type and B-Type Interfaces.* Physical Review Letters, **63**(11), 1168 (1989).

[89] H. Fujitani and S. Asano. *Schottky-Barrier Height and Electronic-Structure of the Si Interface with Metal Silicides - $CoSi_2$, $NiSi_2$, and YSi_2.* Physical Review B, **50**(12), 8681 (1994).

[90] S. Picozzi, A. Continenza, S. Massidda, and A. J. Freeman. *Structural and electronic properties of ideal nitride/Al interfaces.* Physical Review B, **57**(8), 4849 (1998).

[91] S. Picozzi, A. Continenza, S. Massidda, A. J. Freeman, and N. Newman. *Influence of the exchange reaction on the electronic structure of GaN/Al junctions.* Physical Review B, **58**(12), 7906 (1998).

[92] S. Picozzi, A. Continenza, and A. J. Freeman. *Surface states and Fermi-level pinning at clean and Al covered GaN surfaces.* Physical Review B, **59**(3), 1609 (1999).

[93] S. Picozzi, A. Continenza, G. Satta, S. Massidda, and A. J. Freeman. *Metal-induced gap states and Schottky barrier heights at nonreactive GaN/noble-metal interfaces.* Physical Review B, **61**(24), 16736 (2000).

[94] S. Picozzi, A. Continenza, S. Massidda, and A. J. Freeman. *Schottky barrier height in GaN/Al junctions: an ab-initio study.* Physica Status Solidi a-Applied Research, **190**(1), 257 (2002).

[95] S. Picozzi, G. Profeta, A. Continenza, S. Massidda, and A. J. Freeman. *Role of structural relaxations and chemical substitutions on piezoelectric fields and potential lineup in GaN/Al junctions.* Physical Review B, **65**(16) (2002).

[96] E. K. U. Gross and R. M. Dreizler. *Density functional theory an approach to the quantum many-body problem* (Springer, Berlin, 1990).

[97] W. Kohn. *Highlights of Condensed-Matter Theory.* In *International School of Physics "Enrico Fermi"* (edited by F. Bassani, F. Fumi, and P. Tosi), pages 1–15 (North-Holland, Amsterdam, Varenna on Lake Como, Villa Monastero, 28 June - 16 July 1983, 1985).

[98] R. G. Parr and W. Yang. *Density-functional theory of atoms and molecules* (Oxford University Press, New York, 1989).

[99] R. O. Jones and O. Gunnarsson. *The Density Functional Formalism, Its Applications and Prospects.* Reviews of Modern Physics, **61**(3), 689 (1989).

[100] W. E. Pickett. *Pseudopotential Methods in Condensed Matter Applications.* Computer Physics Reports, **9**(3), 115 (1989).

[101] M. Born and R. Oppenheimer. *Zur Quantentheorie der Molekeln.* Annalen der Physik, **84**(4), 457 (1927).

[102] P. Hohenberg and W. Kohn. *Inhomogeneous Electron Gas.* Physical Review B, **136**(3B), B864 (1964).

[103] W. Kohn and L. J. Sham. *Quantum Density Oscillations in an Inhomogeneous Electron Gas.* Physical Review, **137**(6A), 1697 (1965).

[104] D. M. Ceperley and B. J. Alder. *Ground-State of the Electron-Gas by a Stochastic Method.* Physical Review Letters, **45**(7), 566 (1980).

[105] J. P. Perdew and A. Zunger. *Self-Interaction Correction to Density-Functional Approximations for Many-Electron Systems.* Physical Review B, **23**(10), 5048 (1981).

[106] B. Holm and U. von Barth. *Fully self-consistent GW self-energy of the electron gas.* Physical Review B, **57**(4), 2108 (1998).

[107] B. Holm. *Total energies from GW calculations.* Physical Review Letters, **83**(4), 788 (1999).

[108] J. P. Perdew. *Accurate Density Functional for the Energy - Real-Space Cutoff of the Gradient Expansion for the Exchange Hole.* Physical Review Letters, **55**(16), 1665 (1985).

[109] J. P. Perdew and Y. Wang. *Accurate and Simple Density Functional for the Electronic Exchange Energy - Generalized Gradient Approximation.* Physical Review B, **33**(12), 8800 (1986).

[110] J. P. Perdew, J. A. Chevary, S. H. Vosko, K. A. Jackson, M. R. Pederson, D. J. Singh, and C. Fiolhais. *Atoms, Molecules, Solids, and Surfaces - Applications of the Generalized Gradient Approximation for Exchange and Correlation.* Physical Review B, **46**(11), 6671 (1992).

[111] F. Bloch. *Über die Quantenmechanik der Elektronen in Kristallgittern.* Zeitschrift für Physik, **52**, 555 (1929).

[112] N. W. Ashcroft and N. D. Mermin. *Solid state physics* (Saunders College, Philadelphia, 1976).

[113] H. Hellmann. *Einführung in die Quantenchemie* (Deuticke, Leipzig, 1937).

[114] R. P. Feynman. *Forces in Molecules.* Physical Review, **56**, 340 (1939).

[115] O. H. Nielsen and R. M. Martin. *Stresses in Semiconductors - Abinitio Calculations on Si, Ge, and Gaas.* Physical Review B, **32**(6), 3792 (1985).

[116] O. H. Nielsen and R. M. Martin. *Quantum-Mechanical Theory of Stress and Force.* Physical Review B, **32**(6), 3780 (1985).

[117] D. R. Hamann, M. Schlüter, and C. Chiang. *Norm-Conserving Pseudopotentials.* Physical Review Letters, **43**(20), 1494 (1979).

[118] G. B. Bachelet, D. R. Hamann, and M. Schlüter. *Pseudopotentials That Work - from H to Pu.* Physical Review B, **26**(8), 4199 (1982).

[119] D. Vanderbilt. *Soft Self-Consistent Pseudopotentials in a Generalized Eigenvalue Formalism.* Physical Review B, **41**(11), 7892 (1990).

[120] V. Fiorentini, M. Methfessel, and M. Scheffler. *Electronic and Structural-Properties of Gan by the Full-Potential Linear Muffin-Tin Orbitals Method - the Role of the D-Electrons.* Physical Review B, **47**(20), 13353 (1993).

[121] A. Garcia and M. L. Cohen. *Effect of Ga 3d States on the Structural-Properties of Gaas and Gap.* Physical Review B, **47**(11), 6751 (1993).

[122] K. Karch, F. Bechstedt, and T. Pletl. *Lattice dynamics of GaN: Effects of 3d electrons.* Physical Review B, **56**(7), 3560 (1997).

[123] R. Miotto, G. P. Srivastava, and A. C. Ferraz. *Effects of gradient and non-linear core corrections on structural and electronic properties of GaN bulk and (001) surfaces.* Physica B-Condensed Matter, **292**(1-2), 97 (2000).

[124] B. Bouhafs, F. Litimein, Z. Dridi, and P. Ruterana. *Theoretical analysis of d electron effects on the electronic properties of wurtzite and zincblende GaN.* Physica Status Solidi B-Basic Research, **236**(1), 61 (2003).

[125] N. Troullier and J. L. Martins. *Efficient Pseudopotentials for Plane-Wave Calculations.* Physical Review B, **43**(3), 1993 (1991).

[126] N. Troullier and J. L. Martins. *Efficient Pseudopotentials for Plane-Wave Calculations .2. Operators for Fast Iterative Diagonalization.* Physical Review B, **43**(11), 8861 (1991).

[127] L. Kleinman and D. M. Bylander. *Efficacious Form for Model Pseudopotentials.* Physical Review Letters, **48**(20), 1425 (1982).

[128] X. Gonze, P. Kackell, and M. Scheffler. *Ghost States for Separable, Norm-Conserving, Abinitio Pseudopotentials.* Physical Review B, **41**(17), 12264 (1990).

[129] X. Gonze, R. Stumpf, and M. Scheffler. *Analysis of Separable Potentials.* Physical Review B, **44**(16), 8503 (1991).

[130] H. J. Monkhorst and J. D. Pack. *Special Points for Brillouin-Zone Integrations.* Physical Review B, **13**(12), 5188 (1976).

[131] A. Baldereschi. *Mean-Value Point in Brillouin Zone.* Physical Review B, **7**(12), 5212 (1973).

[132] D. J. Chadi and M. L. Cohen. *Special Points in Brillouin Zone.* Physical Review B, **8**(12), 5747 (1973).

[133] S. Froyen. *Brillouin-Zone Integration by Fourier Quadrature - Special Points for Superlattice and Supercell Calculations.* Physical Review B, **39**(5), 3168 (1989).

[134] C. L. Fu and K. M. Ho. *First-Principles Calculation of the Equilibrium Ground-State Properties of Transition-Metals - Applications to Nb and Mo.* Physical Review B, **28**(10), 5480 (1983).

[135] J. P. Perdew, R. G. Parr, M. Levy, and J. L. Balduz. *Density-Functional Theory for Fractional Particle Number - Derivative Discontinuities of the Energy.* Physical Review Letters, **49**(23), 1691 (1982).

[136] M. Peressi, N. Binggeli, and A. Baldereschi. *Band engineering at interfaces: theory and numerical experiments.* Journal of Physics D-Applied Physics, **31**(11), 1273 (1998). See also references therein.

[137] S. Baroni, R. Resta, A. Baldereschi, and M. Peressi. *Spectroscopy of semiconductor microstructures.* In *NATO Advanced Research Workshop on Spectroscopy of Semiconductor Microstructures* (edited by G. Fasol, A. Fasolino, and P. Luigi), page 251 (Plenum Press, New York, Venice, May 9-13, 1989, 1989).

[138] A. Baldereschi, M. Peressi, S. Baroni, and R. Resta. *Semiconductor Superlattices and Interfaces.* In *International School of Physics "Enrico Fermi"* (edited by A. Stella and L. Miglio), page 59 (North-Holland, Amsterdam, Varenna on Lake Como, Villa Monastero, 25 June - 5 July 1991, 1993).

[139] L. Kleinman. *Comment on the average potential of a Wigner solid.* Physical Review B, **24**(12), 7412 (1981).

[140] T. Maxisch, N. Binggeli, and A. Baldereschi. *Intermetallic bonds and midgap interface states at epitaxial Al/GaAs(001) junctions.* Physical Review B, **67**(12), 125315 (2003).

[141] J. Bardi, N. Binggeli, and A. Baldereschi. *Pressure and alloy-composition dependence of $Al/Ga_{1-x}Al_xAs(100)$ Schottky barriers.* Physical Review B, **54**(16), 11102 (1996).

[142] A. Y. Cho and P. D. Dernier. *Single-Crystal-Aluminum Schottky-Barrier Diodes Prepared by Molecular-Beam Epitaxy (MBE) on GaAs.* Journal of Applied Physics, **49**(6), 3328 (1978).

[143] G. Landgren, R. Ludeke, and C. Serrano. *Epitaxial Al Films on GaAs(100) Surfaces.* Journal of Crystal Growth, **60**(2), 393 (1982).

[144] J. C. Woicik, J. G. Pellegrino, S. H. Southworth, P. S. Shaw, B. A. Karlin, C. E. Bouldin, and K. E. Miyano. *Accommodation of Strain in Ultrathin InAs/GaAs Films.* Physical Review B, **52**(4), R2281 (1995).

[145] J. Hornstra and W. J. Bartels. *Determination of Lattice-Constant of Epitaxial Layers of III-V Compounds.* Journal of Crystal Growth, **44**(5), 513 (1978).

[146] G. F. Koster. *Properties of the thirty-two point groups* (M.I.T. Press, Cambridge, Massachusetts, 1966), second printing, december 1966 edition.

[147] S. L. Altmann and P. Herzig. *Point-group theory tables* (Clarendon, Oxford, 1994).

[148] J. Tersoff. *Schottky Barriers and Semiconductor Band Structures*. Physical Review B, **32**(10), 6968 (1985).

[149] J. Tersoff. *Recent Models of Schottky-Barrier Formation*. Journal of Vacuum Science & Technology B, **3**(4), 1157 (1985).

[150] J. Tersoff. *Calculation of Schottky-Barrier Heights from Semiconductor Band Structures*. Surface Science, **168**(1-3), 275 (1986).

[151] J. Tersoff. *Reference Levels for Heterojunctions and Schottky Barriers*. Physical Review Letters, **56**(6), 675 (1986).

[152] J. Tersoff and W. A. Harrison. *Transition-Metal Impurities in Semiconductors - Their Connection with Band Lineups and Schottky Barriers*. Physical Review Letters, **58**(22), 2367 (1987).

[153] T. J. Drummond. *Schottky barriers on GaAs: Screened pinning at defect levels*. Physical Review B, **59**(12), 8182 (1999).

[154] C. Berthod, J. Bardi, N. Binggeli, and A. Baldereschi. *Schottky barrier tuning at Al/GaAs(100) junctions*. Journal of Vacuum Science & Technology B, **14**(4), 3000 (1996).

[155] A. Zangwill. *Physics at surfaces* (Cambridge University Press, Cambridge, 1996), reprinted edition.

[156] E. Caruthers, L. Kleinman, and G. P. Alldredge. *Energy-Bands for (001) Surface of Aluminum*. Physical Review B, **8**(10), 4570 (1973).

[157] E. Caruthers, L. Kleinman, and G. P. Alldredge. *Effects of Potential on Surface States*. Physical Review B, **10**(4), 1252 (1974).

[158] J. A. Appelbaum, G. A. Baraff, and D. R. Hamann. *Theoretical-Study of GaAs (100) Surface*. Journal of Vacuum Science & Technology, **13**(4), 751 (1976).

[159] J. A. Appelbaum, G. A. Baraff, and D. R. Hamann. *GaAs(100) - Its Spectrum, Effective Charge, and Reconstruction Patterns*. Physical Review B, **14**(4), 1623 (1976).

[160] I. Ivanov and J. Pollmann. *Microscopic Approach to the Quantum Size Effect in Super-Lattices*. Solid State Communications, **32**(10), 869 (1979).

[161] I. Ivanov, A. Mazur, and J. Pollmann. *Ideal (111), (110) and (100) Surfaces of Si, Ge and Gaas - Comparison of Their Electronic-Structure*. Surface Science, **92**(2-3), 365 (1980).

[162] O. Madelung (editor). *Physics of Group IV Elements and III-V Compounds*, volume 17a of *Landolt-Börnstein: Semiconductors* (Springer-Verlag, Berlin, 1982).

[163] T. Maxisch, A. Baldereschi, and N. Binggeli. *Midgap interface states at epitaxial Al/AlAs(001) heterojunctions*. Solid State Communications, **126**(5), 265 (2003).

[164] Y. S. Hiraoka and M. Mashita. *Ab-Initio Study on the As-Stabilized Surface-Structure in AlAs Molecular-Beam Epitaxy*. Journal of Crystal Growth, **150**(1-4), 163 (1995).

[165] T. Ito. *A theoretical investigation of the epitaxial relationship of Al/AlAs(001)*. Japanese Journal of Applied Physics Part 1-Regular Papers Short Notes & Review Papers, **35**(6A), 3376 (1996).

[166] T. Maxisch and A. Baldereschi. *Interface states at metal contacts to cubic GaN*. to be submitted.

[167] E. S. Hellman, D. N. E. Buchanan, D. Wiesmann, and I. Brener. *Growth of Ga-face and N-face GaN films using ZnO substrates*. Mrs Internet Journal of Nitride Semiconductor Research, **1**(1-46), art. no. (1996).

[168] E. S. Hellman, Z. LilientalWeber, and D. N. E. Buchanan. *Epitaxial growth and orientation of GaN on (100)γ-$LiAlO_2$*. Mrs Internet Journal of Nitride Semiconductor Research, **2**(27-31), art. no. (1997).

[169] E. S. Hellman. *The polarity of GaN: A critical review*. Mrs Internet Journal of Nitride Semiconductor Research, **3**(11) (1998).

[170] L. Liu and J. H. Edgar. *Substrates for gallium nitride epitaxy*. Materials Science & Engineering R-Reports, **37**(3), 61 (2002).

[171] J. H. Edgar (editor). *Properties of group III nitrides* (INSPEC, London, 1994).

[172] V. Bougrov, M. E. Levinshtein, S. L. Rumyantsev, and A. Zubrilov. *Gallium Nitride (GaN)*. In *Properties of advanced semiconductor materials GaN, AIN, InN, BN, SiC, SiGe* (edited by M. Levinshtein, S. Rumyantsev, and M. Shur) (John Wiley & Sons, New York, 2001).

[173] W. R. L. Lambrecht, B. Segall, S. Strite, G. Martin, A. Agarwal, H. Morkoc, and A. Rockett. *X-Ray Photoelectron-Spectroscopy and Theory of the Valence-Band and Semicore Ga 3d States in GaN*. Physical Review B, **50**(19), 14155 (1994).

[174] A. Filippetti and N. A. Spaldin. *Self-interaction-corrected pseudopotential scheme for magnetic and strongly-correlated systems*. Physical Review B, **67**(12) (2003).

[175] B. Stankiewicz and L. Jurczyszyn. *Electronic structure of thin films of zinc-blende GaN(001): LCAO calculation*. Vacuum, **54**(1-4), 155 (1999).

[176] D. Schikora, M. Hankeln, D. J. As, K. Lischka, T. Litz, A. Waag, T. Buhrow, and F. Henneberger. *Epitaxial growth and optical transitions of cubic GaN films.* Physical Review B, **54**(12), R8381 (1996).

[177] A. D. Bykhovski and M. S. Shur. *Surface reconstruction of zinc-blende GaN.* Applied Physics Letters, **69**(16), 2397 (1996).

[178] O. Brandt, H. Yang, B. Jenichen, Y. Suzuki, L. Daweritz, and K. H. Ploog. *Surface Reconstructions of Zincblende Gan/Gaas(001) in Plasma-Assisted Molecular-Beam Epitaxy.* Physical Review B, **52**(4), R2253 (1995).

[179] H. Yang, O. Brandt, and K. Ploog. *MBE growth of cubic GaN on GaAs substrates.* Physica Status Solidi B-Basic Research, **194**(1), 109 (1996).

[180] H. Yang, O. Brandt, M. Wassermeier, J. Behrend, H. P. Schonherr, and K. H. Ploog. *Evaluation of the surface stoichiometry during molecular beam epitaxy of cubic GaN on (001) GaAs.* Applied Physics Letters, **68**(2), 244 (1996).

[181] M. Wassermeier, A. Yamada, H. Yang, O. Brandt, J. Behrend, and K. H. Ploog. *Atomic structure of the surface reconstructions of zincblende GaN(001).* Surface Science, **385**(1), 178 (1997).

[182] H. J. F. Jansen and A. J. Freeman. *Total-Energy Full-Potential Linearized Augmented-Plane-Wave Method for Bulk Solids - Electronic and Structural-Properties of Tungsten.* Physical Review B, **30**(2), 561 (1984).

[183] M. Winter. *WebElements [http://www.webelements.com/].*

Curriculum Vitæ

Surname	**Maxisch**
First name	**Thomas**
Born	January 15, 1974
in	Kassel, Germany
Nationality	German

1999–2003	PhD thesis at the Institut de théorie des phénomènes physiques, Faculté des sciences de base, EPFL, Lausanne. *Ab initio study of interface states at metal contacts to III-V semiconductors.*
October 1999	Diploma thesis in physics at the physics department of the, Philipps-University of Marburg, Germany. *Theory of the electron-phonon coupling in semiconductor microcavities.*
June 1993	German General High School Diploma

List of publications

D. Karaiskaj, T. Maxisch, C. Ellmers, H. J. Kolbe, *et al. Linewidths in a semiconductor microcavity with variable strength of normal-mode coupling.* Physical Review B, **59**(21), 13525 (1999).

M. Hofmann, D. Karaiskaj, C. Ellmers, T. Maxisch, *et al. Normal-mode linewidths in a semiconductor microcavity with various cavity qualities.* Physica Status Solidi(**a**), **178**(1), 179 (2000).

T. Maxisch, N. Binggeli, and A. Baldereschi. *Intermetallic bonds and midgap interface states at epitaxial Al/GaAs(001) junctions.* Physical Review B, **67**(12), 125315 (2003).

T. Maxisch, A. Baldereschi, and N. Binggeli. *Midgap interface states at epitaxial Al/AlAs(001) heterojunctions.* Solid State Communications **126**(5), 265 (2003).

T. Maxisch and A. Baldereschi. *Interface states at metal contacts to cubic GaN*, to be submitted.